DEVELOPMENT OF CAPILLARY ELECTROPHORETIC-BASED TECHNIQUES TO ANALYZE DOXORUBICIN IN TISSUES, CELLS AND SUBCELLULAR FRACTIONS

A DISSERTATION
SUBMITTED TO THE FACULTY OF THE GRADUATE SCHOOL
OF THE UNIVERSITY OF MINNESOTA
BY

Yaohua Wang

IN PARTIAL FULFILLMENT OF THE REQUIREMENTS
FOR THE DEGREE OF
DOCTOR OF PHILOSOPHY

EDGAR A. ARRIAGA, ADVISER

September, 2010

Acknowledgements

I would like to thank my parents, Zhaolong Wang and Xuqin Dong, for their love, understanding and support in every step I take in my life. During my 6-year Ph.D. study, I was only with them for less than 60 days. They never complain and always encourage me to press on toward my dreams. Without them, I would never have the encouragement and perseverance to finish my Ph.D. study. I would like to thank my husband, Qiang Gao, who stands by me all the time during these 6 years. Without him, no one could share my happiness and sorrow, and my life would be colorless.

I would like to thank my advisor, Dr. Edgar Arriaga for shaping me to be a scientist during my Ph.D. study. When I feel desperate in research, he can always help me to find hope. When I have problems, he never tells me what to do but discusses and brain-storms the problems with me. The most important thing I learned through my Ph.D. is the way to do research. His care and encouragement always make the tough Ph.D. research a little bit easier. I also would like to thank all the group members, past and present, for their advice, support and friendship. I would like to thank Angie Eder and Yun Chen for guiding me to get familiar with my research projects. Thank Chad Satori for proof-reading my thesis and Joe Katzenmeyer for helping me with HPLC experiments.

I would like to thank all my COM coworkers, Glenn Kenadjian, Karen Beach, Adrienne and Paul Volk, *etc*. I cannot list all the names as too many people pouring their care and blessings on me. Without their encouragement and prayer, I could never go

through the hardest time in my Ph.D. study and job hunting. I would like to thank my dear friend Qian Yu, although she is in China, her care is always with me during my Ph.D. study.

Lastly, I would like to thank Merck Research Laboratories for providing me *Merck Research Laboratories Fellowship in Analytical/Physical Chemistry* during the year of 2008-2009.

Dedication

This Thesis is dedicated to my parents, Zhaolong Wang and Xuqin Dong, and my husband Qiang Gao.

Abstract

Doxorubicin (DOX) is a widely used anti-cancer drug. It is hypothesized that the efficacy and toxicity of DOX is related to its distribution and metabolism. Capillary electrophoresis (CE) including its variants such as micellar electrokinetic chromatography (MEKC) is becoming a popular method in bioanalysis due to its high sensitivity and separation efficiency, small sample size requirements, simple sample preparation procedures, versatility in sampling and short separation times.

The goal of this thesis is to take advantage of these features and develop CE-based methods to investigate the metabolism, subcellular distribution and localization of DOX in biological samples after DOX treatments.

A direct sampling technique was developed to quantify DOX at or near the tumor site in hepatocellular carcinoma tissues after chemoembolization. This technique allows for sampling small volume of tissues (<10 pL) selectively from adjacent tumor and non-tumor regions with high spatial resolution (100 μm) and reproducibility. Using this technique coupled with MEKC-LIF (laser-induced fluorescence detection), DOX was detected and quantified, in both tumor and non-tumor regions in resected human livers.

A MEKC method was developed to monitor the incorporation, transformation and subcellular metabolism of a DOX prodrug, *N*-L-leucyl-doxorubicin (LeuDOX), which is expected to have higher efficacy and lower toxicity. It successfully separated LeuDOX from DOX and its major metabolite, doxorubicinol (DOXol). The metabolism of

LeuDOX in four subcellular fractions of human uterine sarcoma cells suggested that LeuDOX is mainly activated to DOX in the lysosome-enriched fraction which contains hydrolytic enzymes.

Metabolism of DOX in isolated subcellular fractions from young and old rat livers was investigated by MEKC-LIF, suggesting that this technique is adequate to investigate the effect of aging on the metabolism of DOX at the subcellular level. The study showed that the young rat liver is more metabolic active than that of the old rat.

In subcellular drug analysis, the purity of the subcellular fractions limits the determination of the subcellular localization of metabolites. Organelles with high purity and biological function are necessary to refine the understanding of DOX metabolism in a specific organelle type. An immunoisolation method based on the use of an antibody specific to a peroxisomal membrane protein was developed to isolate peroxisomes with low levels of contaminating mitochondria and lysosomes. The metabolism of DOX and a model compound, BODIPY fatty acid analog, showed possible peroxisomal biotransformation of these xenobiotics.

The techniques and methodologies developed in the dissertation work would be the basis of future developments including assessing the function of new prodrugs at the cellular and subcellular levels, profiling subcellular specific metabolism and monitoring drug distribution and metabolism in tissue cross-sections. These measurements are necessary to understand the efficacy and toxicity of chemotherapy drug treatments in preclinical and clinical studies.

Table of Contents

Acknowledgements……i
Dedication……iii
Abstract ……iv
Table of Contents……vi
List of Tables……x
List of Figures……xii
List of Abbreviation…… xiv

Chapter 1. Thesis Overview……1

Chapter 2. Introduction……6
2.1. Doxorubicin (DOX)……7
2.1.1. Physicochemical properties……7
2.1.2. Clinical applications……9
2.1.3. Mechanism of DOX action……15
2.1.4. Metabolism and subcellular distribution……19
2.2. Analysis of DOX and metabolites……25
2.2.1. Sample preparation……25
2.2.2. Techniques for analysis of DOX and metabolites……31
2.2.3. Detection methods for DOX and metabolites……39

Chapter 3. Direct Sampling from Human Liver Tissue Cross-sections for Electrophoretic Analysis of Doxorubicin……43
3.1. Introduction……44
3.2. Material and methods……47
3.2.1. Chemicals and reagents……47
3.2.2. Preparation of tissue sample and gelatin tissue-mimics……48
3.2.3. Capillary preparation and direct tissue sampling……50
3.2.4. Atomic force microscopy (AFM) of tissue cross-sections after direct sampling……51
3.2.5. MEKC analysis of DOX in directly sampled tissue……51
3.2.6. Determination and quantification of DOX……53
3.2.7. Safety considerations……55
3.3. Results and discussion……55
3.3.1. Assessing the reproducibility of direct tissue sampling……55
3.3.2. Surface topology after sampling……58
3.3.3. Determination of DOX in liver tissue……60

3.3.4. Dox in tumor and non-tumor tissue regions……..……...62
3.4. Conclusions……..……...67

Chapter 4. Monitoring Incorporation, Transformation and Subcellular Distribution of *N*-L-leucyl-doxorubicin in Uterine Sarcoma Cells Using Capillary Electrophoretic Techniques……..……..69
4.1. Introduction……....……70
4.2. Material and methods……..……...…….73
4.2.1. Chemicals and reagents……..…...……73
4.2.2. Synthesis of LeuDOX……..……...…74
4.2.3. Cell culture, IC_{50} value and sample preparation for MEKC analysis…74
4.2.4. CE setup and analysis…….……76
4.2.5. Data acquisition and analysis…….....78
4.3. Results and discussion……..…….……..…79
4.3.1. CTAB based separation system……79
4.3.2. IC_{50} values of DOX and LeuDOX on MES-SA and MES-SA/Dx5 cell lines……...81
4.3.3. Incorporation and transformation of LeuDOX……..……..…82
4.3.4. Subcellular distribution of DOX and LeuDOX……..……..…87
4.4. Conclusions…….……...…89

Chapter 5. Micellar Electrokinetic Chromatography Monitors Doxorubicin Metabolism in Subcellular Fractions of Young Adult and Old Fischer 344 Rat Livers……..….90
5.1. Introduction……...……...91
5.2. Material and methods…...……....94
5.2.1. Chemicals and reagents……...…....95
5.2.2. Preparation of liver subcellular fractions……95
5.2.3. *In vitro* metabolism of DOX……..…....96
5.2.4. MEKC-LIF analysis……...……..….96
5.2.5. Data analysis……...……98
5.3. Results……...……..…....99
5.3.1. Identification of metabolites…….……...99
5.3.2. Effect of cofactors NADPH and Mg^{2+} on enzyme metabolic activity……..…....……102
5.3.3. Metabolism in the MF and PMF of young adult and old rat liver…....103
5.3.4. DOX metabolism in young adult and old as a function of time…….....103
5.4. Discussion……...……....….106
5.4.1. Identification of DOX metabolites in MEKC-LIF……..…...106
5.4.2. Effect of cofactors on the metabolism of DOX……...…….…..107
5.4.3. DOX metabolism in young adult and old rat livers……..…..……107
5.4.4. Purity of subcellular fractions……109

5.5. Conclusions……..……..……109

Chapter 6. Biotransformation of Doxorubicin in Immunoisolated Peroxisomes.....110
6.1. Introduction ……..……..…112
6.2. Material and methods……...……..…115
6.2.1. Chemicals and reagents…….....115
6.2.2. Cell culture and sample preparation…….....117
6.2.3. Immunoisolation of peroxisomes…….....117
6.2.4. Protein quantification and enzyme assays……...……..118
6.2.5. *In vitro* metabolism of B_{12}FA and DOX in isolated peroxisomes…..…120
6.2.6. MEKC analysis of B_{12}FA or DOX *in vitro* metabolites……...……..…120
6.2.7. MEKC data analysis……...……...122
6.3. Results and discussion……..……...…….....123
6.3.1. Purity of the immunoisolated peroxisomes……...……123
6.3.2. MEKC of BODIPY fatty acid analogs of different chain length……...124
6.3.3. *In vitro* metabolism of B_{12}FA……...……..126
6.3.4. *In vitro* metabolism of DOX……...…..128
6.4. Conclusions……..……..……131

Chapter 7. Conclusion and Future Work…….....……..132
7.1. Conclusions……..……..……132
7.2. Future work……...……..136
7.2.1 Direct tissue sampling…….....……..……136
7.2.2 Subcellular metabolism……...……140
7.2.3 Capillary electrophoresis (CE) coupled to mass spectrometry (MS)….143

Bibliography……...……146

Appendix A. Supplementary Material to Chapter 3……..…….....162
A1 Elastic moduli of gelatin tissue-mimics.....163
A2 Fluorescence imaging of tissue cross-sections.....……164
A3 MEKC-LIF analysis of tissue extract of a liver without chemo-embolization ……...……...165
A4 Mobility corrections…….……..165
A5 Hematoxylin and eosin (H&E) staining…….166

Appendix B. Supplementary Material to Chapter 4……..…….....168
B1 Synthesis of *N*-L-leucyl-doxorubicin……..……...169
B2 Viability of cells after DOX and LeuDOX treatments……171
B3 Fluorescence spectra of DOX in borate-SDS and CTAB-tricine buffer……..171

B4 LeuDOX transformation in cell culture medium……...…172

Appendix C. Supplementary Material of Chapter 5……..…….....173
C1 Florescence spectrum of DOX and metabolites in BS50-γCD20 buffer……..……174
C2 Mobility correction and comparison…….174
C3 HPLC-LIF-MS analysis of *in vitro* DOX metabolism in PMF of rat livers……...……175
C4 Percent of metabolites and DOX change over time…….....179

Appendix D. Supplementary Material of Chapter 6……..…….....180
D1 Metabolism of B_{12}FA in cultured L6 myoblasts……..……..181

List of Tables

Chapter 2. Introduction
2-1. Comparison of the efficacy and toxicity of DOX and LeuDOX 14
2-2. Comparison of AUC_{48h} of DOX and LeuDOX at equimolar doses 15
2-3. Characteristic of enzymes involved in DOX metabolism 20
2-4. Size and density of organelles in sucrose 26
2-5. Subcellular fractions pelleted at different g-forces in differential centrifugation 27
2-6. Enzymes and proteins detected in Western blots used as organelle markers 29

Chapter 3. Direct Sampling from Human Liver Tissue Cross-sections for Electrophoretic Analysis of Doxorubicin
3-1. Reproducibility of DOX in direct samplings from a 5-μm thick gelatin slice as determined by MEKC-LIF 56
3-2. Volume of tissue sampled after direct sampling from a 5-μm thick tissue cross-section determined by AFM 58
3-3. Corrected mobilities and amounts of DOX in tumor and non-tumor regions of a 5 μm thick tissue cross-section 66

Chapter 4. Monitoring Incorporation, Transformation and Subcellular Distribution of *N*-L-leucyl-doxorubicin in Uterine Sarcoma Cells Using Capillary Electrophoretic Techniques.
4-1. Equimolar concentration treatments of DOX and LeuDOX 85
4-2. Equitoxic concentration treatments of DOX and LeuDOX 86
4-3. Subcellular distribution in DOX and LeuDOX treated MES-SA/Dx5 cells 87

Chapter 5. Micellar Electrokinetic Chromatography Monitors Doxorubicin Metabolism in Subcellular Fractions of Young Adult and Old Fischer 344 Rat Livers
5-1. Percent of DOX and metabolites with and without the addition of cofactors 103

Chapter 6. Biotransformation of Doxorubicin in Immunoisolated Peroxisomes
6-1. Catalase, β-hexosaminidase activities and NAO accumulation in retained and unretained fractions 124
6-2. Peak area of $B_{12}FA$ and possible metabolites in retained peroxisomal and unretained fractions 126

6-3. Corrected mobilities of possible metabolites in retained peroxisomal and unretained fractions 131

Chapter 7. Conclusion and Future Work
7-1. Antibodies for immunoisolation of organelles 141

Appendix A. Supplementary Material to Chapter 3
A-1 . Elastic moduli of gelatin tissue-mimics and HCC tissue 163
A-2 . Comparison of calculated mobilities with and without correction 166

Appendix C. Supplementary Material to Chapter 5
C-1. Corrected mobilities and *p*-values of metabolites and standards 175
C-2. Percent of metabolites and DOX in MF and MF at different incubation times 179

List of Figures

Chapter 2. Introduction
2-1. Structure of DOX 8
2-2. Excitation and emission spectra of DOX 8
2-3. Selective activation mechanism of prodrugs 12
2-4. Structure of LeuDOX 14
2-5. Formation of reactive oxygen species via the redox quinone cycle of anthracyclines 17
2-6. Metabolic pathways of DOX 21
2-7. Schematic illustration of capillary electrophoresis setup 33
2-8. Schematic illustration of MEKC separation of neutral analytes with different hydrophobicity 35
2-9. 2D and 3D structures of γ-cyclodextrin 39
2-10. Scheme of a dual channel post-column LIF detection system 42

Chapter 3. Direct Sampling from Human Liver Tissue Cross-sections for Electrophoretic Analysis of Doxorubicin
3-1. Details relevant to direct tissue sampling 50
3-2. Direct sampling from a 5-μm thick gelatin slice 57
3-3. Tappping-mode AFM images of a tissue cross-section after sampling 59
3-4. MEKC-LIF analysis of bulk liver tissue extract 61
3-5. Direct tissue sampling from a tissue cross-section and MEKC-LIF analysis 63
3-6. Direct tissue sampling from the non-tumor and tumor regions of a tissue cross-section and their respective MEKC-LIF analyses 65

Chapter 4. Monitoring Incorporation, Transformation and Subcellular Distribution of *N*-L-leucyl-doxorubicin in Uterine Sarcoma Cells Using Capillary Electrophoretic Techniques.
4-1. Structures of DOX and LeuOX 72
4-2. MEKC separation of DOX, LeuDOX and DOXol 81
4-3. MEKC separation of whole cell lysate in DOX or LeuDOX treatment 84

Chapter 5. Micellar Electrokinetic Chromatography Monitors Doxorubicin Metabolism in Subcellular Fractions of Young Adult and Old Fischer 344 Rat Livers
5-1. Possible metabolic pathways of DOX 99
5-2. Identification metabolites by internal standard addition 101
5-3. Effect of cofactors on the metabolic activity of rat liver 102
5-4. *In vitro* metabolism of DOX in PMF and MF fractions of young and old rat livers

104
5-5. Changes in percent of DOX and metabolites over time in PMF and MF 105

Chapter 6. Biotransformation of Doxorubicin in Immunoisolated Peroxisomes
6-1. Structure of B_{12}FA and DOX 114
6-2. Reaction scheme of β-oxidation of B_{12}FA 124
6-3. Separation and detection of BODIPY fatty acid analogs by MEKC-LIF 125
6-4. *In vitro* metabolism of B_{12}FA in retained peroxisomal and unretained fraction 127
6-5. DOX and products after reacting with H_2O_2 *in vitro* 129
6-6. *In vitro* metabolism of DOX in retained peroxisomal and unretained fractions 130

Chapter 7. Conclusion and Future Work
7-1. Images of a swine liver cross-section after treated with TACE using DOX-eluting beads 138
7-2. *In vitro* metabolism of DOX in liver samples after being frozen for one year at -80 ºC 139
7-3. Proposed microfluidic device designed for subcellular metabolism analysis 142

Appendix A. Supplementary Material to Chapter 3
A-1. Representative stress vs. strain plot of gelatin and HCC tissue 163
A-2. Epifluorescence images of a non-chemoembolized and a chemoembolized tissue cross-sections 164
A-3. MEKC separation of tissue extract without chemoembolization treatment 165
A-4. MEKC separation of three samples taken from a 5-μm thick tissue cross-section for mobility correction 166
A-5. Bright field images of H&E staining of liver tissue cross-sections 167

Appendix B. Supplementary Material to Chapter 4
B-1. Chromatogram and mass spectrum of LeuDOX 170
B-2. Percent survival - drug concentration curve 171
B-3. Emission spectra of DOX in SDS and CTAB buffer 172
B-4. Electropherogram of LeuDOX incubated in cell culture medium 172

Appendix C. Supplementary Material to Chapter 5
C-1. Fluorescence spectra of DOX, DOXol and 7-deoxyDOXone 174
C-2. Mass chromatogram of a liver PMF treated withDOX 177
C-3. DOX biotransformation dynamics in PMF of a young rat liver 178
Appendix D. Supplementary Material to Chapter 6
D-1. Electropherograms of L6 cells incubated with B_{12}FA for different lengths of times 182

List of Abbreviations

7-deoxyDOXolone: 7-dexoy-doxorubicinolone
7-deoxyDOXone: 7-dexoy-doxorubicinone
γ-CD: γ-cyclodextrin
AFM: Atomic force microscopy
$B_{12}F$: BODIPY 500/510 C1C12
CD: cyclodextrin
CE: capillary electrophoresis
CF: cytosolic fraction.
CTAB: cetyl trimethyl ammonium bromide
CYP: cytochrome P450
DOX: doxorubicin
DOXol: doxorubicinol
DOXone: doxorubicinone
EOF: electroosmotic flow
HCC: hepatocellular carcinoma
HDOF: high density organelle enriched fraction
HPLC: high performance liquid chromatography
LeuDOX: *N*-L-leucyl-doxorubicin
LIF: laser-induced fluorescence detection
LDOF: low density organelle enriched fraction
LOD: limit of detection
MEKC: micellar electrokinetic chromatography
MF: mitochondria-enriched fraction
MS: mass spectrometry
NF: nucleus enriched fraction
PMF: post-mitochondria fraction
PMP70: 70 kDa peroxisomal membrane protein
PMT: photomultiplier tube
SDS: sodium dodecyl sulfate
TACE: transcatheter arterial chemoembolization

Chapter 1

Thesis Overview

Nowadays, one fourth of the deaths in United States are due to cancer. In 2009, about 1.5 million new cancer cases and half million deaths were expected in the United States.[1] Different treatments have been developed to fight against cancer, including the use of chemotherapy, radiation therapy, biological therapy and surgery. Chemotherapy is a standard cancer treatment which uses chemical reagents to kill cancer cells. Compared with surgery or radiation therapy, chemotherapy is a more systemic treatment in that the drugs circulate in bloodstream to all parts of the body. For this reason, the main side effect of chemotherapy is that it also affects the body's normal organs or tissues, and causes acute, chronic or permanent damages. Many efforts have been made to increase the efficacy and overcome the side effects of chemotherapy such as discovering new drugs and developing new drug delivery systems. Nowadays, most preclinical and clinical assessments of chemotherapy drugs are based on studying the pharmacokinetics of drugs in body fluids. These clinical assessments cannot reveal drug actions at the target tissues at the cellular and subcellular levels, which are required for successful drug assessments.

In order to analyze chemotherapy drugs within tissues, cells and subcellular compartments, it is necessary to develop analytical methods with high sensitivity and efficiency. High performance liquid chromatography (HPLC) is widely used in pharmaceutical analysis. However, it requires extensive sample preparation procedures and relatively large amounts of sample because of high limit of detection. Thus, this technique cannot be used directly in the analysis of samples with complex matrices, low in abundance and/or limited in availability. Capillary electrophoresis (CE) is a technique that has small sample size requirements, flexible sample introduction modes, high

separation efficiencies and short separation times. The goal of this thesis work was to develop CE-based methodologies and techniques to monitor the distribution and metabolism of chemotherapy drugs within tissues, cells and subcellular fractions. Doxorubicin (DOX) was used as a model because of its prevalence in cancer treatments and its native fluorescence which is compatible with the laser-induced fluorescence (LIF) detection used in this dissertation work.

Chapter 2 of this dissertation provides a detailed background of DOX, including its properties, function mechanisms, metabolism and subcellular distributions as well as different techniques that have been applied to analyze DOX.

Chapter 3 describes the development of a CE-based sampling and separation system to monitor the distribution and metabolism of DOX administrated by chemoembolization. This chapter discusses the development and validation of a new direct tissue sampling technique which allows for sampling small amount of tissues (less than 10 picoliters) selectively with high spatial resolution (100 μm) and reproducibility. This sampling technique coupled with micellar electrokinetic chromatography (MEKC), a variant of CE, was applied to determine the concentrations of DOX in tumor and adjacent non-tumor regions in a hepatocellular carcinoma tissue cross-section.

Chapter 4 describes the development of a cetyl trimethylammonium bromide (CTAB)-based MEKC separation system that is capable of separating a DOX prodrug, *N*-L-leucyl-doxorubicin (LeuDOX), from DOX and its metabolites. This was the first published electrophoretic separation system for DOX prodrugs. This system was applied to investigate the incorporation, transformation and subcellular distribution of LeuDOX in both DOX-sensitive and resistant uterine sarcoma cells. The high ratio of DOX to

LeuDOX found in the lysosome-enriched fraction suggested that LeuDOX activation to DOX may occur in this fraction.

Chapter 5 describes the metabolism of DOX in isolated subcellular fractions i.e., mitochondria-enriched fraction (MF) and post-mitochondria fractions (PMF), of young and old Fischer 344 rat livers. Studying DOX metabolism in isolated subcellular fractions helps to determine the original organelle where a metabolism reaction takes place. MEKC-LIF analysis revealed that both MF and PMF of young rat liver are more metabolically active than the corresponding fractions of the old rat liver.

In subcellular metabolism studies (Chapters 4 and 5), the purity of organelles in the enriched fractions is the one of the major limitations. These fractions have different types of organelles complicating the assignment of a metabolic reaction to a specific organelles type. In order to refine the understanding of DOX metabolism in a specific type of organelle, it is necessary to use highly purified organelles. Chapter 6 introduces an immunoisolation technique to enrich peroxisomes from L6 rat myoblasts using an antibody targeting a peroxisomal membrane protein. The immunoisolated fraction (retained) showed a two-fold enrichment of the peroxisomes and low levels of mitochondria and lysosomes compared with the unretained fraction. These peroxisomes were used to study the biotransfomations of DOX and a fatty acid analog. Two different DOX metabolites were observed in the retained and unretained fractions, while no obvious metabolites of the fatty acid analog were detected, probably due to the comigration of the metabolites and the fatty acid analog, or the low β-oxidation activity of the immunoisolated peroxisomes.

Finally, Chapter 7 provides a perspective on the main findings of this dessertation work and describes future developments of CE-based techniques that include (i) high-throughput in sampling and separation, and (ii) versatility in monitoring both fluorescent and non-fluorescent chemotherapy drugs in tissues, cells and subcellular fractions. With these improvements, the techniques and methodologies developed in this dissertation could be applied to preclinical and clinical studies such as assessing the function of new prodrugs at the cellular and subcellular levels, profiling subcellular specific metabolism and monitoring drug distribution and metabolism in tissue cross-sections. These measurements are ultimately necessary to understand the efficacy and toxicity of chemotherapy drug treatments.

Chapter 2

Introduction

This chapter describes the background of doxorubicin (DOX), including: (i) physicochemical properties, (ii) clinical applications, (iii) mechanisms of action, (iv) metabolism and subcellular distribution, and (v) analytical methods used in analyzing DOX and metabolites in biological samples.

2.1. Doxorubicin (DOX)

2.1.1 Physicochemical properties

DOX is an anthracycline which was first discovered in *Streptomyces Peucetius* in 1969. It has been under clinical trials since the 1970s and has become one of the most widely used chemotherapy drugs.[2, 3] It is especially useful in treating solid tumors such as breast cancer and hematologic malignancies such as leukemia.[3] More often, in treating cancers like uterine sarcoma and hepatocellular carcinoma, DOX is administrated as a "cocktail" with other chemotherapy drugs such as ifosfamide, mitomycin C and cis-platin.[4, 5]

The structure of DOX has two parts: an aglycone ring system and a daunosamine sugar moiety (Figure 2-1). Due to the highly conjugated structure of the aglycone ring, DOX has fluorescence with two maximum emissions at about 550 and 585 nm (Figure 2-2). However, the spectral profile and quantum yield of DOX is highly dependent on its surrounding environment.[6] For example, when intercalating in DNA, its fluorescence is reduced to only 5% of that in the absence of DNA.[7]

The pKa of the amino group of daunosamine moiety is ~7.5 and the pKa of the hydroxyl group on the C11 position is ~9.5, and the calculated pI of DOX to ~8.5.[8] The

aglycone ring system of DOX is highly hydrophobic, allowing it to partition strongly into cellular membranes.[9]

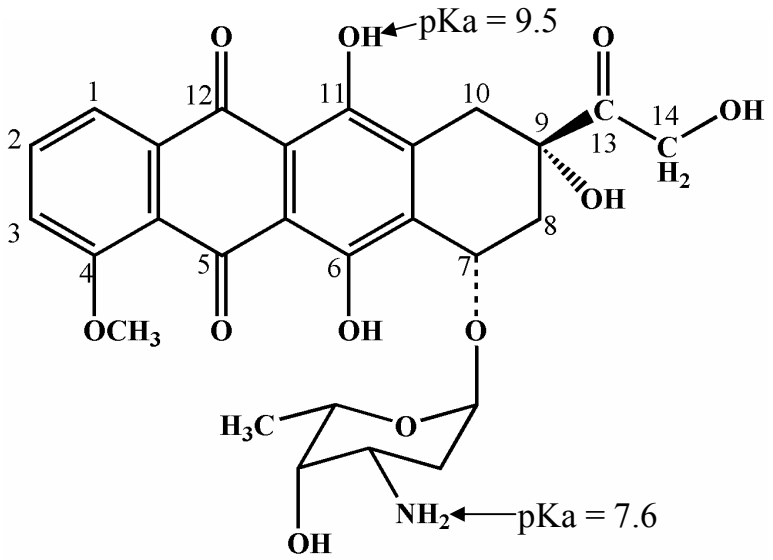

Figure 2-1. Structure of DOX. The pKa of the amino and hydroxyl groups are indicated by arrows.

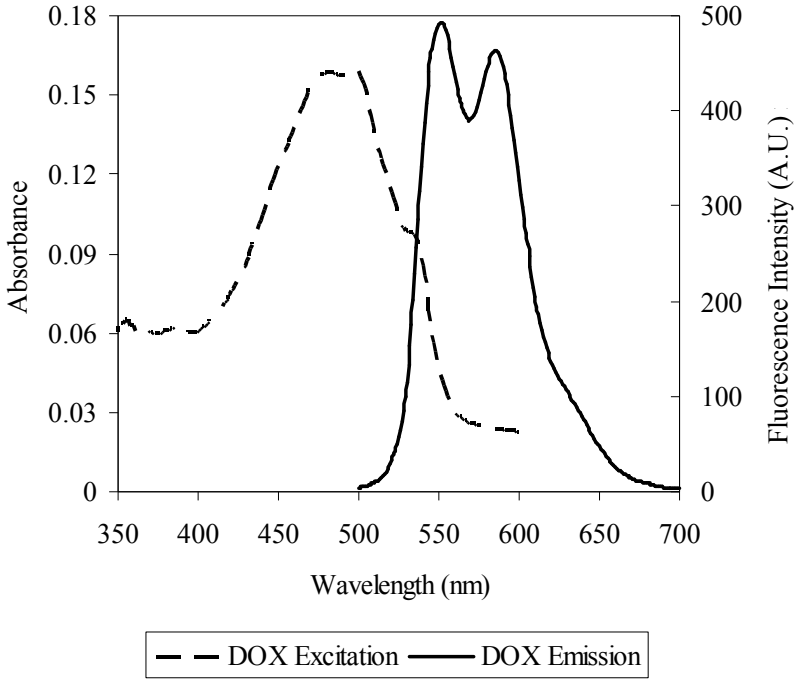

Figure 2-2. Excitation and emission spectra of DOX. The excitation spectrum is represented by solid line; the emission spectrum in dash line was obtained using 488-nm excitation.

2.1.2 Clinical applications

Efficacy and toxicity in cancer treatments

DOX is effective in the treatment of hematological malignancies and cancers localized in solid tissue, but is less effective in treating malignancies in tissues that overexpress the drug efflux protein, P-glycoprotein (PGP) (e.g. brain, colon, kidney)[10]. Similar to other chemotherapy drugs, DOX can cause acute and chronic side effects. Acute side effects such as myelosuppression, nausea and vomiting, hair loss and fatigue are reversible or clinically manageable. DOX is more notorious in its chronic side effect, cardiotoxicity, which is irreversible.[11] For this reason, the lifetime dose a patient may receive per unit body surface area is around 450-550 mg/m^2.[12] Another impediment of using DOX in cancer treatments is the appearance of multi-drug resistance (MDR), in which cancer cells develop broad resistance to a wide variety of chemotherapy drugs.[13] The mechanism of MDR will be discussed in Section 2.1.3 of this chapter.

Tissue distributions

Upon DOX treatment, DOX can be found not only in plasma and tumor tissues but in non-target tissues such as liver, heart and skeletal muscle.[14, 15] Research on the distribution of DOX in rat showed liver exhibited substantially higher levels of DOX (on a per gram of protein basis) than did plasma.[15] DOX also preferentially accumulates in the heart, which is directly related to its cardiotoxicity. The absolute level of DOX in heart is about ten times higher than that observed in skeletal muscle.[15] The plasma and tissue distribution of DOX is highly affected by the drug delivery system and administration method.

DOX delivery systems and administration methods

When DOX was first introduced, bolus intravenous injection was the only mode of administration. To reduce its toxicity to cardiac and other normal tissues while retaining its anti-tumor effects, different drug delivery systems and administration methods have been developed, including fractioned schedule of administration, continuous infusion,[16] transcather arterial chemoembolization (TACE),[17] liposomal delivery[18] and prodrug.[19] Different drug delivery systems produce different tissue, cell and intracellular distributions of DOX, which can affect its efficacy and toxicity. [20, 21] In this thesis work, capillary electrophoretic (CE)-based techniques were developed to study the tissue, cell and subcellular distribution of DOX in two drug delivery systems, i.e., TACE and prodrug.

TACE is a technique which combines embolization and chemotherapy in treating hepatoceullular carcinoma (HCC). To achieve site-specific delivery, chemotherapy drugs such as DOX and mitomycin C are administrated via a catheter through the liver artery which supplies 90% of the blood flow to tumor but only 10% to liver. Meanwhile, embolic agents such as gelfoam are used to create an ischemic effect on the tumor.[22] The combination of chemotherapy and embolization is expected to increase the drug concentration and dwelling time in tumor. Chapter 3 discusses the development of CE-based technique to determine DOX concentrations in both tumor and non-tumor regions of TACE treated liver tissues from patients with HCC.

Prodrugs are non-toxic derivatives of cytotoxic drugs. They need to be activated to exhibit their pharmacological action. The use of prodrugs in chemotherapy has two purposes: (1) to increase the bioavailability of anti-tumor agents so that their

pharmacokinetics can be improved, and/or (2) to increase the selectivity of the drugs for tumor tissues and cells.[23]

In the first case, the prodrugs are preferentially activated relatively slow in the blood or liver, thereby preventing acute toxic effects due to high peak concentrations of the anti-tumor drug.[24] In the second case, the prodrugs are designed to be selectively activated to regenerate the toxic parent drugs at the targeted site (Figure 2-3). Upon reaching tumor tissues and cells, these prodrugs are cleaved by enzymes, such as prostate-specific antigen, glucuronidase, and generic proteases, thereby releasing the parent drug.[23] Further prodrug selectivity may be obtained if the drug is designed to bind to a molecule that recognizes tumor-associated factors, such as hypoxia, tumor-associated enzymes and receptors.[25] Compared with parent drugs, prodrugs are more site-specific, efficient and less toxic to normal tissues and cells. For DOX prodrugs, the modification is usually at the free amino group of the daunosamine moiety.

Nowadays there are mainly two strategies of designing prodrugs, monotherapy and two-step therapy.[26] Monotherapy uses prodrugs that are designed for direct recognition of tumor-associated factors, such as hypoxia, tumor-associated enzymes and receptors. First, oxygen deficiency in the core of solid tumors leads to enhanced activity of reducing enzymes, such as nitroreductases. Second, some enzymes are activated or present in elevated levels in tumor tissues. For example, plasmin, the enzyme that is associated with the invasion and metastatic activity of tumor cells is activated from plasminogen locally at or near the tumor cell surface.[27] Finally, tumor-selective expression of receptors can be exploited for the delivery of anti-tumor agents. At present, a number of receptors used in monotherapy are receptors that are required for angiogenesis.[25]

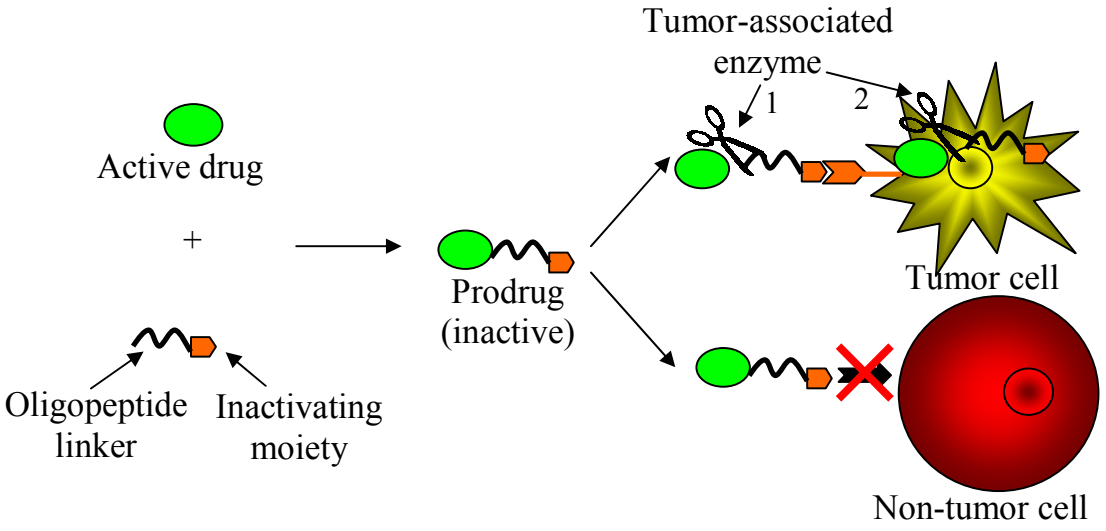

Figure 2-3. Selective activation mechanism of prodrugs. The toxic anti-cancer drug is linked to an inactivating moiety via a short linker, e.g., oligopeptide. Upon reaching the tumor site, the linker is cleaved off by tumor-associated enzymes (1) extracellularly or (2) intracellularly, releasing the active anti-cancer drug.

If a prodrug is inefficiently activated by human enzymes, a two-step therapy is needed. In a two-step therapy, first an enzyme is directed to or expressed at the tumor site, and then a prodrug that is a substrate for the localized enzyme is administrated. For example, in antibody-directed enzyme prodrug therapy (ADEPT), the enzyme is directed by an antibody against a tumor antigen through an antibody-enzyme conjugate.[26] If the enzyme is encoded by a gene, it is called gene-directed enzyme prodrug therapy (GDEPT).[28] There are some limitations involved in two-step therapy. For instance, the antibody-enzyme conjugate does not always localize in tumor site to the desired extent since the tumor may express a limited number of antigens.[25] Moreover, in two-step therapies, both steps must proceed satisfactorily in order to get efficient treatment, which makes it less practical and economical than monotherapies.

Different types of DOX prodrugs have been designed to increase its efficacy and reduce its cardiotoxicity. These prodrugs can be activated by lysosomal enzymes (e.g., cathepsin),[29] prostate-specific antigen (PSA),[30] matrix metalloproteinase (MMP)[31] and lugumain[32]. These enzymes are reported to have elevated expression level and activity in tumors either extracellularly or intracellularly. Other DOX prodrugs are designed to target receptors expressed on tumor cells such as α_v integrins or to facilitate drug transportation across cell membrane.[33] Polymer-DOX prodrugs are also designed as high molecular weight of the polymer carrier could result in the accumulation of the conjugates in solid tumors due to the enhanced permeation and retention (EPR) effect.[34]

The first and simplest DOX prodrug is *N*-L-leucyl-doxorubicin (LeuDOX) (Figure 2-4) which was designed in early 1980s.[35] It is has L-leucine conjugated to the amino group of the daunosamine moiety of DOX. LeuDOX is used as a prodrug over other *N*-amino acid DOX derivatives because of i) its greater hydrophobicity which enhances its accumulation in subcutaneous tissues, and ii) its sensitivity toward enzymatic hydrolysis to release DOX.[36, 37] The hydrolytic enzymes involved, such as cathepsin B and D, have elevated expression level in tumors, [38] leading to preferentially accumulation of DOX in tumor tissues over normal ones.

Preclinical and Phase I trials showed that LeuDOX has higher efficacy at equitoxic doses, a dose that induces equal toxic effect (e.g., lethality). At equimolar dose, LeuDOX has at least 3-4 fold lower overall toxicity, especially cardiotoxicity compared with DOX (Table 2-1).[39, 40]

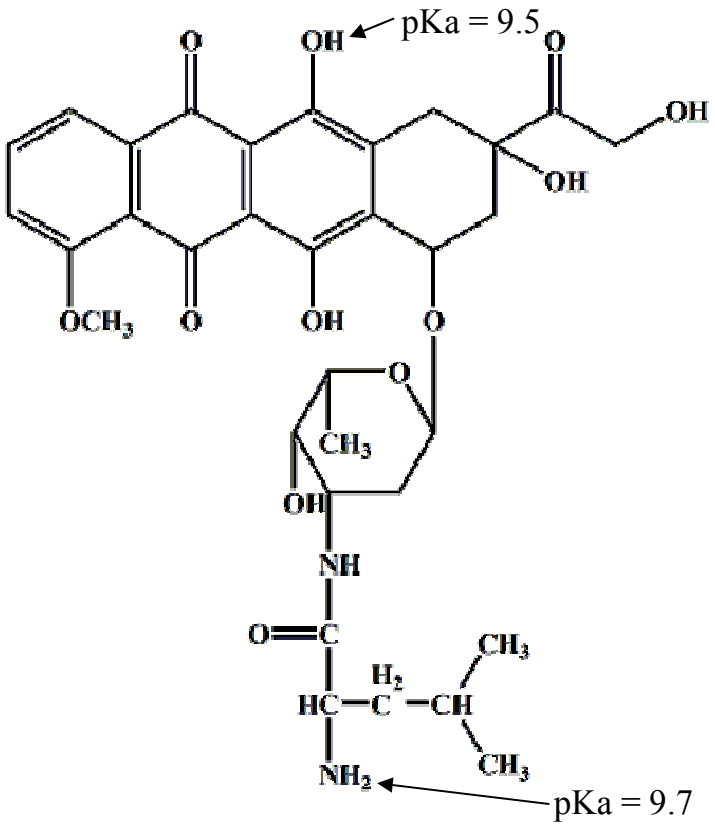

Figure 2-4. Structure of LeuDOX. The pKa of the amino group and hydroxyl group are indicated by arrows.

Table 2-1. Comparison of the efficacy and toxicity of DOX and LeuDOX

	LD_{50} (mg/kg/day)[35]	MTD (mg/kg)[39, 40]	Efficacy[40]
DOX	14.4	8	7/16
LeuDOX	46.7	28	10/16

LD_{50}**:** a dose that induces 50% lethality in mice after 30 days of observation; MTD: Maximum tolerated dose in Phase I trial. Efficacy (at equitoxic dose): in a breast and lung tumor study, 7 out 16 of the tumor lines respond to DOX and 10 of 16 respond to LeuDOX.

In prodrug therapies, accumulation and biotransformation of prodrugs are two important steps. The decreased cardiotoxicity of LeuDOX may be either due to the low uptake of this prodrug by cardiac muscle or due to the limited biotransformation of LeuDOX to active DOX. A pharmacokinetics study of LeuDOX in cardiac tissue of

tumor-bearing BALB/c mice showed that the decreased cardiotoxicity of LeuDOX is due to the lower accumulation of this prodrug and the resulting DOX in heart, as evaluated by the areas under the concentration-time curves (AUC) (Table 2-2).[41] The biotransformation is not the limiting step since about 90% of LeuDOX was transformed to DOX. However, in this study, it cannot determine whether the DOX was transformed from LeuDOX in the heart or transformed from LeuDOX somewhere else and accumulated in the heart. In addition to this limitation, pharmacokinetics studies of LeuDOX in plasma (in both human and animal models) and tissues (in animal model) are not informative at the cellular and subcellular levels. It is still unclear whether the reduced toxicity of LeuDOX is due to the lower cellular uptake or a limited biotransformation of the prodrug in the cell. It is also unclear in which subcellular environment LeuDOX is transformed to DOX. Chapter 4 discusses the incorporation, transformation and subcellular localization of LeuDOX in MES-SA uterine sarcoma cell line and its DOX-resistant variant, MES-SA/Dx5 cell line to answer these questions.

Table 2-2. Comparison of AUC_{48h}* of DOX and LeuDOX at equimolar doses

	Plasma ($nmol \cdot ml^{-1} \cdot min$)		Heart ($nmol \cdot g^{-1} \cdot min$)		Tumor ($nmol \cdot g^{-1} \cdot min$)	
Dose (17.2 $\mu mol/m^2$)	DOX	LeuDOX	DOX	LeuDOX	DOX	LeuDOX
DOX	205	-	14064	-	8997	-
LeuDOX	51	221	4262	443	1466	153

* AUC_{48h}: AUC of the first 48 h after drug treatments.

2.1.3 Mechanism of DOX action

Mechanism of DOX anti-tumor activity

Several mechanisms are involved in DOX anti-tumor activity, including topoisomerase IIα (Top IIα) poisoning, DNA intercalation and free radical production.

Top IIα poisoning: Top IIα is an enzyme that regulates the topologic structures of DNA. It is essential in many functions of DNA during cell growth, including transcription, replication, and chromosome segregation.[42] DOX acts as a Top IIα poison.[43] Once intercalating into DNA in cell nucleus, DOX forms a stable ternary complex with DNA and Top IIα, perturbing the religation step of Top IIα, causing DNA breaks and eventually leading to cell death.[44] This is the best-known mechanism of DOX action.

DNA intercalation: DOX is rapidly taken up into the nucleus of cells where it binds with high affinity to DNA. DOX intercalates between the base pairs of double strand DNA by forming a covalent bond with guanine of one strand of DNA via a methylene linkage and a strong noncovalent bond with the other strand of DNA.[45] After intercalation, DOX inhibits the replication, transcription and translation processes of DNA and induces cell death.

Free radical production: In the presence of oxoreductive enzymes such as cytochrome P450 reductase and NADH dehydrogenase, the addition of a free electron converts the quinone part of DOX to a semiquinone free radical. In the presence of oxygen, the oxidation of the semiquinone free radical yields the superoxide radical. The antioxidant enzyme superoxide dismutase further catalyzes the conversion of the superoxide radical to hydrogen peroxide which can subsequently lead to the formation of hydroxyl radicals (Figure 2-5).[46, 47] The latter can react with polyunsaturated fatty acids yielding lipid hydroperoxide, thereby, initiating a lipidradical chain reaction and

oxidative damage to cell membranes.[11] Free radical formation appears to be a major cause of DOX-induced cardiotoxicity and cell apoptosis.[48]

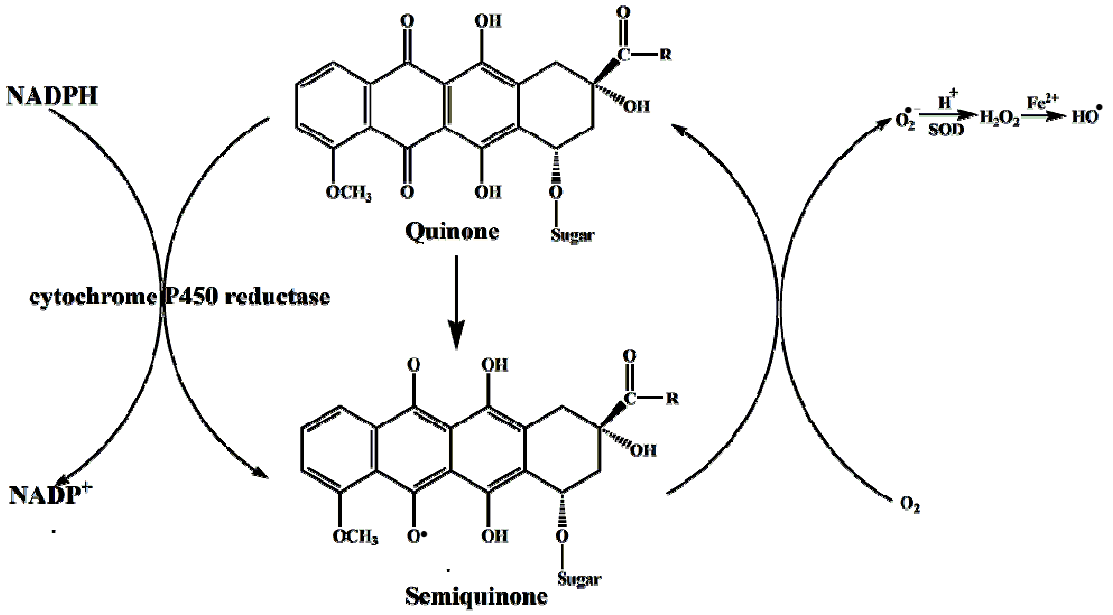

Figure 2-5. Formation of reactive oxygen species via the redox quinone cycle of anthracyclines. NADP: nicotinamide adenine dinucleotide phosphate, SOD: superoxide dismutase.

Multi-drug resistance (MDR)

MDR is a phenomenon that cancer cells develop broad resistance to a wide variety of chemotherapy drugs. The mechanism of multi-drug resistance of a cell line may be multifactorial.[49] The resistance can be caused by decreased influx or increased efflux of the drugs. It can also arise in the cancer cell itself due to genetic and epigenetic alterations that affect drug sensitivity.

ATP-dependent transporters: MDR may associate with the over-expression of adenosine triphosphate-binding cassette (ABC) transporters, P-glycoprotein (PGP). PGP is a broad-spectrum multidrug efflux pump that has 12 transmembrane regions and two ATP-binding sites. The transmembrane regions bind hydrophobic drug substrates that are

either neutral or positively charged.[50] Multidrug-resistance-associated protein 1 (MRP1 or ABCC1) is another type of transporter. MRP1 is similar to PGP in structure, with the exception of an amino-terminal extension that contains five membrane spanning domains attached to a PGP-like core. It recognizes neutral and anionic hydrophobic compounds, and transports glutathione and other conjugates of these drugs.[13] ABC transporters are usually over-expressed in brain, testis, liver, gastrointestinal tract and kidney. In multi-drug resistance cells, PGP expression increases at different subcellular regions, including plasma membrane, cytoplasm, nucleus and mitochondria.[51, 52]

The over-expression of PGP is the major MDR mechanism of a DOX resistant uterine sarcoma cell line (MES-SA/Dx5) which is used as a cell model in this thesis work.[53, 54] MES-SA/Dx5 was produced by culturing MES-SA cells in the presence of increasing concentrations of DOX. It is 100-fold more resistant to DOX than the MES-SA cell line. It is also cross-resistant to a number of chemotherapeutic drugs including daunorubicin, dactinomycin, vincristine, taxol and colchicine.[55]

Lysosomal sequestration: DOX is a weak base that exists to a significant extent in the unionized state at biological pH (pH = 7.4). In cytosol, it can passively diffuse across the lysosomal lipid bilayer and enter the luminal domain. Once inside the lysosome, the low pH environment (pH = 4 - 5) favors protonation of DOX. In this ionized state, DOX is relatively membrane impermeable and unable to diffuse back. Lysosomal sequestration significantly decreases the level of DOX that can reach and accumulate in nucleus where there DOX targets, DNA and Topo IIα, are present. This sequestration has the potential of reducing the sensitivity of the cells to DOX.[56] It appears that in the MES-SA/Dx5 cell line used in the thesis, the vesicular accumulation of DOX is less pronounced than in the

MES-SA cell line, which implies that lysosomal sequestration is not a cause of MES-SA/Dx5 multidrug resistance.[57]

Top IIα catalytic activity: The expression level of Top IIα is different in different stages of a cell cycle. Its expression level is low in quiescent cells, increases in the M phase when nuclear and cytoplasmic division occurs, and decreases in the G1 phase when cells increase in size, produce RNA and synthesize proteins.[58] Since Top IIα forms a cleavable complex with DNA and DOX which leads to cell death, the decrease in its expression level or catalytic activity is also associated with MDR.[59,62]

Effect of DOX prodrugs on multi-drug resistance: DOX prodrugs have been reported to overcome MDR. It is reported that DOX conjugated to a monoclonal antibody or a cell-penetrating peptide can bypass PGP efflux and results in higher intracellular concentration of DOX in DOX-resistant cells.[60, 61] However, only one report appears to discuss the effect of LeuDOX on DOX-resistant cells.[62] The study showed that LeuDox is incorporated to cells to a lesser degree than DOX in both DOX-sensitive and resistant cell lines, which suggested that LeuDOX cannot overcome MDR. Chapter 4 discusses the incorporation, transformation and subcellular metabolism of LeuDOX in DOX-sensitive and resistant uterine sarcoma cell lines to further study the effect of LeuDOX on DOX-resistant cells.

2.1.4 Metabolism and subcellular distribution

Metabolic pathways of DOX

DOX can be metabolized to different metabolites (doxorubicinol (DOXol), doxorubicinone (DOXone), 7-deoxydoxorubicinone (7-deoxyDOXone), *etc.*) in different

organs such as liver and heart through a series of Phase I and Phase II reactions, including carbonyl reduction, reductive glycosidic cleavage, hydrolytic glycosidic cleavage, *etc.* (Figure 2-6).[63, 64] DOXol is formed by NADPH-dependent aldo-keto reductase reducing the carbonyl group in the side chain of the tetracyclic ring of DOX. Both DOX and DOXol undergo quinone reduction, catalyzed by microsoma1 NADPH-cytochrome *c* reductase, to the inactive metabolites 7-deoxyDOXone and 7-deoxydoxorubicinol-aglycone (7-deoxyDOXolone). DOX and metabolites are further transformed into glucuronide or sulfate conjugates by uridine diphosphate glucuronosyltransferase (UDPGT) and sulfotransferase, respectively.[11]

Although the major subcellular location of phase I and phase II enzymes involved in DOX metabolism are known (Table 2-3),[65] some enzymes may appear in multiple subcellular compartments. For instances, CYP3A, a subfamily of cytochrome P450 that might be involved in the metabolism of DOX,[66] is found in mitochondria, lysosomes, peroxisomes and plasma membrane.[67] Investigating the subcellular metabolism of DOX could help to identify the subcellular localization of the enzymes. Chapter 5 discusses the subcellular metabolism of DOX and the possible enzymes involved in young and old rat livers.

Table 2-3. Characteristic of enzymes involved in DOX metabolism

	Enzymes	Reaction	Cofactor	Location
Phase I	Cytochromes P450	Oxidation/Reduction	NADPH	ER
	Reductase	Reduction		Cytosol
Phase II	UDP-glucuronosyltransferases	Transferase	UDPGA	ER
	Sulfotransferases	Transferase	PAPS	Cytosol

ER: endoplasmic reticulum; NADPH: nicotinamide adenine dinucleotide phosphate; UDP: uridine 5' diphosphate; UDPGA: uridine diphosphate glucuronic acid; PAPS: 3'-phosphoadenosine-5'-phosphosulfate.

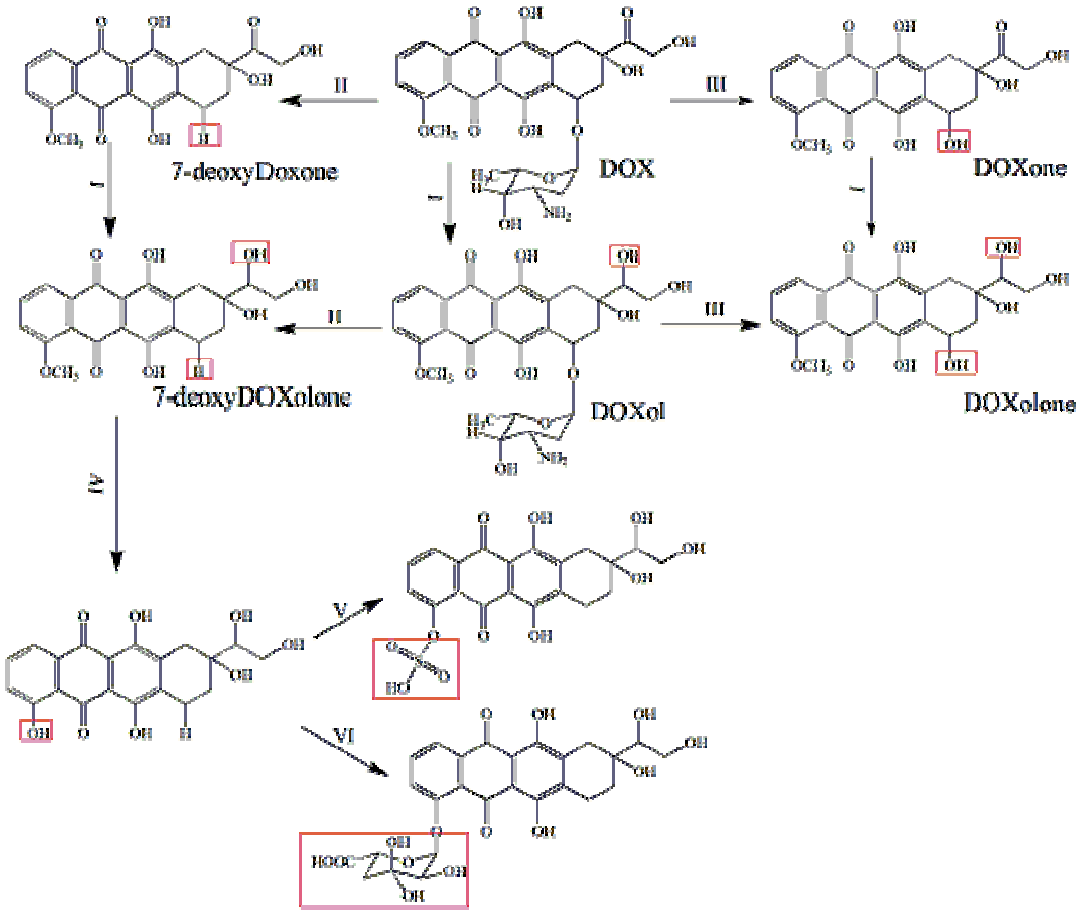

Figure 2-6. Metabolic pathways of DOX. Squares indicate the chemical sites of reaction: (I) carbonyl reduction by NADPH-dependent aldo-keto reductase, (II) reductase-type deglycosidation by NADPH-cytochrome *c* reductase, (III) hydrolase-type deglycosidation by glycosidase, (IV) demethylation by cytochrome P450, (V) sulfation by sulfotransferase, and (VI) glucuronidation by uridine diphosphate glucuronosyltransferases.

Functions of DOX metabolites

Different metabolites of DOX may have different pharmacological activities. They usually have lower anti-tumor efficacy than the parent anthracycline, DOX. One possible reason is that the formation of the ternary complex with DNA and Top IIα of these metabolites (i.e., DOXol and aglycone) is less stable.[68] Metabolites may also be responsible for the side effects of DOX. DOXol appears to alter iron homeostasis thus

leading to chronic cardiotoxicity.[63] For this reason, the metabolites can be used as an indicator of the efficacy and toxicity of a specific drug delivery system.

Subcellular distribution of DOX and metabolites

After treatment, DOX reaches different organelles in the cell where it may play different roles. As mentioned above, in the *nucleus*, DOX forms a ternary complex with DNA and Topo IIα, thereby arresting DNA synthesis and resulting in cell death. DOX in the *mitochondrion* interrupts electron transfer, leading to the production of reactive oxygen species (ROS).[69] When DOX enters acidic organelles such as the *lysosome*, DOX becomes protonated and is sequestrated in this organelle.[70] Nobody has investigated the accumulation and metabolism of DOX in the *peroxisome*, the organelle that contributes to several crucial metabolic processes such as β-oxidation of fatty acids[71, 72] and metabolism of ROS.[73] Besides mitochondria, peroxisomes also produce ROS.[74] DOX is susceptible to be oxidized and degraded by reactive oxygen species such as H_2O_2 in the presence of peroxidase.[75] Such a process may serve as a salvage pathway for diminishing the levels and toxicity of anthracyclines in cardiomyocytes.[76] However, the metabolism of anthracyclines in peroxisomes is largely unknown compared to other organelles such as microsomes and mitochondria. Chapter 6 discusses the preparation of highly enriched peroxisomes and provides initial evidence of peroxisomal transformation of DOX.

Relationship of metabolic activity and aging

A number of drug metabolism studies in rats have shown an age-related decline in the metabolism and clearance of drugs such as phenacetin, chlorzoxazone and

triazolam.[77] Colombo and coworkers showed that the lethal dose of DOX was two-fold higher in young rats (6 weeks) than in old (24 months) rats.[78] Their studies also revealed different pharmacokinetics and metabolic profile in the old and young rats. Peak levels of DOX and its AUC in plasma and in several tissues of old rats were 1.5 to 2-fold higher in the old than in the young rats. Regarding metabolite production, old rat livers appear to produce higher percent of DOXone.[78] Human studies of chemotherapy drugs also showed similar altered pharmacokinetics and metabolic profile in old patients.[79] A study of daunorubicin, an anthrancycline with similar structure as DOX, showed that AUC of daunorubicinol, one of the major metabolites of daunorubicin, increases by 2-4 times in patients over 60 year old compared to younger patients.[80] Since daunorubicinol is associated with cardiotoxicity,[81] this result suggested that the altered metabolism in old patients may compromise the pharmacotherapy of the elderly. In agreement, the treatment with DOX, accelerates cardiotoxicity in old relative to young patients.[82] Therefore, understanding the altered metabolism of DOX in the elderly would help to administrate proper dose and avoid adverse effects.

Other studies on the effect of aging on drug-metabolizing enzymes reveal conflicting results, i.e., the total enzyme content and/or activity may or may not be affected by aging.[83, 84] Some results showed no relationship between age and the content and/or activities of various cytochrome P450 (CYP450) enzymes in human liver microsomes,[85] while others showed aging related decline in total CYP450 content and some CYP450 activities (e.g., CYP3A and CYP2E1).[86] To reveal the changing in CYP450 activities at the genetic level, in last ten years, DNA array technology has been applied to study the aging-induced changes in gene expression. A study of 3000 genes in the male rat liver

found 47 unique transcripts that were affected by aging. Among them, 29 are involved in drug or intermediary metabolism.[87] For example, the gene expressions of NADPH CYP450 oxidoreductase and CYP2C7 are increased, while the expression of CYP3A2 reduced with aging.[87]

Since the results of aging induced changes of enzyme activities are controversial, studying changes of metabolic profile in animal models such as rat livers is a valuable approach to identify metabolic pathways and enzymes that are affected by aging. To investigate the effect of aging on the metabolic activity of rat livers at the subcellular level, Chapter 5 discusses the metabolism of DOX in subcellular fractions of young and old rat livers.

DOX metabolism in vivo and in vitro

Xenobiotic metabolism can be studied *in vivo* and *in vitro*. *In vivo* metabolism studies using animals or humans are more systematic and clinically relevant, but they are costly and time-consuming. The human studies are generally impractical. *In vitro* metabolism studies which use cells, tissues, enzymes or subcellular fractions complement the *in vivo* studies because they help understanding human drug metabolism and potential toxicity in advance. Advantages of using *in vitro* systems include the ability to isolate processes such as phase I metabolism from phase II metabolism, and to compare metabolism across several species. However, caution should be taken to extrapolate *in vitro* results to *in vivo*. First, the *in vitro* systems lack the *in vivo* organization, and depending on the system, cofactors and supporting structures. In addition, chemical delivery and removal processes of *in vivo* system may be altered in the *in vivo* system.[88]

In vitro metabolism in isolated subcellular fractions is widely used in drug discovery and preclinical drug development.[89] Compared to the use of whole cells, it simplifies the system and makes it easy to identify the original organelle where the metabolism occurs. It also helps to discover enzymes in different organelles other than cytochrome P450s that are usually located in microsomes. On the other hand, subcellular system may contain enzymes that are labile and require addition of cofactors for optimal activity.[89] Therefore, the reaction system and cofactors should be chosen carefully in subcellular *in vitro* metabolism. Chapter 5 discusses the use of subcellular fractions from young and old rat livers to study the metabolism of DOX

2.2. Analysis of DOX and metabolites

2.2.1 Sample preparation

The first step in the analysis of DOX and metabolites is sample preparation. When choosing an appropriate sample preparation method, parameters that should be considered include sample size and composition, the compatibility with the downstream analytical techniques as well as the expected outcome of the experiments.

Subcellular fractionation

In the studies of subcellular metabolism of DOX, the subcellular fractionation step is critical. Highly pure and functional organelles are required to study the metabolism in a specific organelle type. Organelles can be prepared using different subcellular fractionation methods which can be classified into centrifugation or non-centrifugation methods.

Centrifugation methods separate organelles based on the differences in size and density of the organelles. In a centrifugal field, the sedimentation velocity (v) of a particle is based on its size and shape as well as the density and viscosity of medium

$$v = \frac{d^2(\rho_o - \rho_m)}{18\mu} g \qquad \text{(Equation 2-1)}$$

where d is the diameter of particle; ρ_o and ρ_m are the density of organelle and medium, respectively; g is the gravitational field and μ is the viscosity of medium. The sizes and densities of common organelles are summarized in Table 2-4.

Table 2-4. Size and density of organelles in sucrose

Organelle	Size (μm)	Density in sucrose (g/ml)[90]
Nucleus	10-20	>1.32
Mitochondria	0.4-2.5	1.19
Lysosomes	0.4-0.8	1.21
Peroxisomes		1.23
Plasma membranes	NA	1.13-1.18

Differential centrifugation which is primarily based on the size of organelles is the simplest method to enrich different subcellular fractions. Based on Equation 2-1, organelles with bigger size (i.e., d^2) have higher sedimentation velocity and can be pelleted at lower centrifugal forces. On the other hand, organelles with smaller size need higher centrifugal forces to be pelleted (Table 2-5). The major limitation of differential centrifugation is that the purity of the resulting fractions is low. Organelles overlapping in size can hardly be separated by this technique. For instance, the low density organelle fraction contains mitochondria, lysosomes and peroxisomes.

Table 2-5. Subcellular fractions pelleted at different g-forces in differential centrifugation

g-force	Subcellular fraction	Organelles
600	Nuclear-enriched fraction	Nuclei, unbroken cells, cell debris
4,000	High density organelle fraction	Most mitochondria, some lysosmes and peroxisomes
15,000	Low density organelle fraction	Most lysosomes and peroxisomes, some mitochonria
100,000		Ribosomes and microsomes
Supernatant from 100,000g	Cytosol	Soluble fraction and cytoplasm

Density gradient centrifugation is a method to obtain more pure subcellular fractions based on their density (Table 2-4). Organelles are layered over a column of density gradient medium in which the medium concentration increases progressively from top to bottom. Based on Equation 2-1, during centrifugation, organelles reach a region in the medium with density equal to that of the organelles ($\rho_o = \rho_m$), the sedimentation velocity becomes zero. Thus organelles with different densities form bands in the gradient. Sucrose is the most widely used density gradient medium, but it is viscous at high density and exerts high osmotic pressure onto organelles. Ficoll (a high molecular weight polymer of sucrose and epichlorhydrin) and Percoll (small silica particles coated with polyvinylpyrrolidone) are density gradient media that alleviate this problem as they are non-permeant.[90] Density perturbation is used to change the density of one type of organelles so that organelles with overlap in size and density can be separated. For instance, the density of organelles involved in endocytotic pathways such as lysosome and endosome can be changed by feeding cells with Triton WR-1339, a detergent, or latex beads.[91] The drawback of the density perturbation method is that the perturbation material used may affect organelle function. The long centrifugation time (from 1 to 16

hours) is another limitation of density gradient centrifugation method, which may also impair the function of the organelles.

Non-centrifugation methods include electrophoretic methods and immunoisolation. Electrophoretic methods such as free flow electrophoresis (FFE) that separates organelles based on the unique charge densities on their surfaces have been developed to enrich mitochondria,[92] lysosmes[93] and peroxisomes.[94] Immunoisolation, which utilizes antibodies targeting cytoplasmic region of organelle-specific surface proteins, is another method to obtain organelles with high purity. For instance, anti-TOM22 antibody[95] and anti-PMP70 antibody[96] have been used to isolate mitochondria and peroxisomes, respectively, from cell and tissue homogenates. Chapter 6 will discuss the immunoisolation of peroxisomes with anti-PMP70 antibody from L6 rat myoblasts.

To assess the purity and functionality of subcellular fractions, enzyme assays and Western blots are the most common methods of choice.

Enzyme assays determine either the consumption of a substrate or production of a product as a function of time in an enzymatic reaction. The change of substrate/product concentration can be monitored by change in absorbance or fluorescence, or measured by calorimetric, chemiluminescent, light scattering, chromatographic or radiometric methods. There are two types of enzyme assays, continuous and stop assays. In continuous assays, the change of substrate/product concentration is monitored several times over a period of time; in discontinuous assays, the enzymatic reaction is first stopped after a period of time and before determines the concentration of substrate/product. Continuous assays are more convenient and straight-forward, but if samples contain particles (e.g., organelles in subcellular fractionation samples), settling of these particles over time causes changes in

absorbance and light scattering.[97] If this is the case, stop assays are a better choice. In enzyme assays, the rate of substrate consumption/product formation may decrease due to the depletion of substrate or approach to equilibrium. In this case, to accurately measure the enzyme activity, it is important to measure the initial, linear rate of the reaction.[97]

In subcellular fractionation, the purity and enrichment of a preparation are measured by the specific activity of enzymes that are localized exclusively in a given organelle type. Specific activity is expressed as the activity of an enzyme per milligram of total protein in a sample ($\mu mol \cdot min^{-1} \cdot mg^{-1}$). Some organelle specific enzyme markers are listed in Table 2-6. The enrichment of an organelle preparation can be determined by the specific activity of the enzyme maker in the preparation divided by its specific activity in the homogenate; the purity can be assessed by the absence of the enzyme maker in organelles other than the target organelle.

Wstern blot is a method to detect specifically the proteins of interest among a mixture of proteins in cell or tissue samples. It uses gel electrophoresis, usually SDS polyacrylamide gel electrophoresis, to separate proteins in the sample. The proteins are then transferred to a membrane (typically nitrocellulose or PVDF), where the protein of interest is probed by its specific antibody and a secondary antibody with a conjugated fluorophore or enzyme.[98] Western blots can be used to compare the relative abundance of a specific protein in different samples, e.g., different organelle preparations, but it is not useful to assess the function or activity of such proteins.

Table 2-6. Enzymes and proteins detected in western blots used as organelle markers

Subcellular fraction	Enzyme assays	Western blot
Mitochondrion	Succinate dehydrogenase[99]	Mitofilin[100]
Lysosome	β-hexosaminidase[101]	LAMP-1[102]
Peroxisome	Catalase[99]	PMP70[103]

Direct sampling

Techniques developed to directly sample and analyze biomolecules in cells or tissues have the advantages of (1) avoiding extensive sample preparation and thus prevent sample loss, and (2) preserving the spatial distribution information of the biomolecules in the sample.

Xenobiotic or endogenous metabolites in a single cell can be analyzed directly by capillary electrophoresis (CE) or mass spectrometry (MS).[104, 105]

In the case of tissue samples which are more clinically relevant, direct sampling and analysis can provide *in situ* data. MALDI (matrix-assisted laser desorption/ ionization)-MS has been developed to sample and map the distribution of drugs and metabolites in mouse or rat tissues with a spatial resolution from one to several hundred micrometers.[106, 107] One of the drawbacks of this direct analysis method is that the background signal from the MALDI matrix interferes with the detection of drugs and metabolites with low molecular weights. With the recent developments in MS/MS and high resolution MS analyzers (e.g., Fourier transform mass spectrometry), this problem is alleviated by focusing on the ions of interest.[108] The other drawback of the MALDI-MS method is that it is not quantitative because of the discrepancies in the ionization efficiency of drugs and their metabolites due to their different structures, abundances and tissue environments.

Another technique that allows the direct sampling from tissues with high resolution is laser-capture microdissection (LCM). This technique uses a laser to selectively remove a small region of interest from a tissue (e.g., 3-μm diameter circle)[109] for subsequent DNA, RNA or protein analyses.[110] This sampling method is seldom used to analyze drug

metabolites, probably because a large number of cells must be collected to make low abundant metabolites detectable. For example, 20-30 LCM samples ranging in diameters from 10 to 25 μm and 6 μm in thickness are needed for one HPLC-MS analysis of a prodrug and its metabolites.[111]

Direct sampling from a rat bain using a capillary has also been reported.[112] The direct sampling followed by on-line pre-concentration, in-capillary derivatization and CE analysis was used to analyze taurine in a rat brain. Unlike microdialysis which only samples the fluid in the extracellular space of tissues, this method samples both intra- and extra-cellular taurine. While site-specific, the method is not quantitative because the volume of tissue sampled cannot be easily controlled. Chapter 3 discusses the development, validation and application of a direct tissue sampling technique that uses a capillary. This technique provides high spatial resolution and quantitative reproducibility.

2.2.2. Techniques for analysis of DOX and metabolites

Both spectroscopic-based (e.g., fluorescence microscopy) and separation-based (e.g., HPLC and CE) techniques have been developed to analyze DOX and metabolites in biological samples.

Fluorescence microscopy

Fluorescence microscopy is the most commonly used method to study the subcellular distributions of DOX due to the drug's native fluorescence. Colocalization of DOX and specific fluorescence organelle markers revealed that DOX accumulates in nuclei,[113, 114] mitochondria,[69, 114] lysosomes,[115] Golgi apparatus,[6, 114] cytoplasm[113] and the microtubule network[113]. Microscopy has the advantage that it can monitor changes over time and

avoids sample loss during preparation. However, fluorescence microscopy cannot distinguish DOX and its metabolites when they colocalize. Moreover, the fluorescent properties of DOX depend on its subcellular environment.[6] For example, when intercalated with DNA, the fluorescence intensity of DOX is only 5% of that of free DOX.[7] Thus, fluorescence microscopy cannot quantitative DOX and metabolites easily in various subcellular enviroments.

High performance liquid chromatography (HPLC)

HPLC is a widely used separation technique in pharmaceutical analysis. In HPLC analytes are separated based on their partition between the mobile phase and the column's stationary phase. There are quite a few reports on the separation of DOX, prodrugs (e.g., LeuDOX),[116] and metabolites such as DOXol, DOXone in body fluids and tissues using HPLC.[117, 118] The most recently reported LOD of DOX and DOXol is 9.6 feptomoles.[119]

The limitations of HPLC include (1) extensive sample preparation, (2) high limit of detection, and (3) large sample amount requirements. In biological samples such as tissue, plasma and urine, the presence of components in the matrix including DNA, lipids and proteins can mask the detection of analytes of interest. Usually, a sample extraction step is necessary. However, this step is not only time-consuming, but also causes the loss of the analytes of interest. [120] In HPLC, relatively large sample volume is usually required (greater than 50 μl), to detect drugs and metabolites in low abundance. This can be a limitation of HPLC in analyzing samples available in small quantities.

Capillary electrophoresis (CE) and derivatives

CE is a powerful method to separate a diverse array of analytes in a narrow bore capillary (e.g., 50 μm I.D.) (Figure 2-7). The small volume of sample (~10 nanoliters) is injected into the capillary from a sample vial electrokinetically or hydrodynamically. After replacing the sample vial with the buffer reservoir, analytes are separated under an electric field (e.g., 400 V/cm) in the capillary. Analytes are then detected by a variety of techniques such as UV and fluorescence measured through the capillary (on-column detection) or immediately after they migrate out of the capillary (post column detection).

Compared with other separation methods including HPLC, CE requires smaller amount of analytes (nanoliters), has higher separation efficiency and provides rapid separation. With LIF detection, the LOD can be as low as one zeptomole (10^{-21} mole).[121] These features make CE a preferred method in the analysis of samples available in small amounts and analytes in low abundance (e.g., DOX metabolites in subcellular fractions).

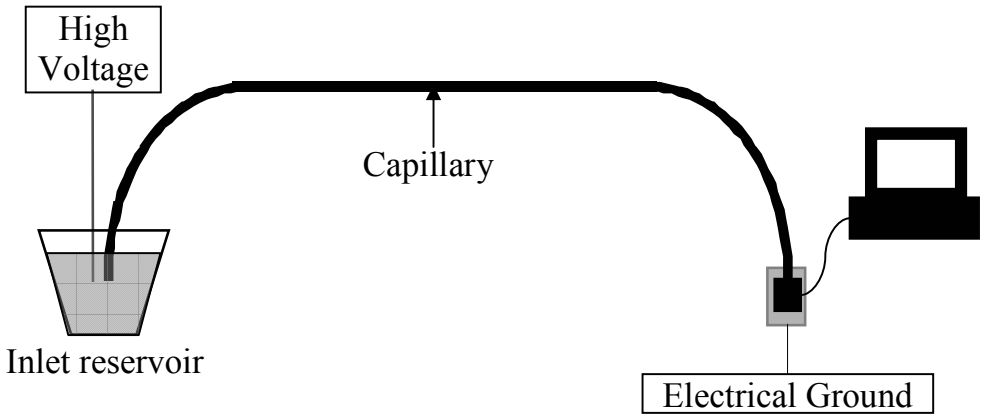

Figure 2-7. Schematic illustration of a capillary electrophoresis setup

The principle of CE is that analytes are separated based on their size-to-charge ratio. In CE, the electrophoretic mobility of a charged molecule is the ratio of the electric force to its frictional drag through the medium. The electrophoretic mobility (μ_e) can be approximated from the Debye-Huckel-Henry theory:

$$\mu_e = \frac{q}{6\pi\eta r} \qquad \text{(Equation 2-2)}$$

where q and r are the ion charge and radius of the species, respectively, and η is the solution viscosity.

The apparent mobility (μ_{app}) of an analyte is the sum of its electrophoretic mobility and the mobility of electroosmotic flow (EOF) (μ_{EOF}).

$$\mu_{app} = \mu_e + \mu_{EOF} \qquad \text{(Equation 2-3)}$$

EOF is caused by the ionized silanol groups (SiO^-) on the capillary wall at pH above 2.3. The ionized silanol groups attract cationic species in the buffer and form a double layer that has a positive charge density. The double layer closer to the surface of capillary wall is the Stern layer composed of inner Helmholtz plan (IHP) and outer Helmholtz plane (OHP). Between the OHP and the bulk solution, there is the diffuse layer in which cation concentrations diminishes until it reaches that of the bulk solution. Under an electric field, the diffuse cations in the double layer migrate to the cathode carrying water of hydration with it, which forms EOF.[122] EOF carries all molecules both charged and neutral toward the cathode. In CE, neutral compounds cannot be separated as their electrophoretic mobility is zero so that their apparent mobility is equal to that of EOF.

Micellar electrokinetic chromatography (MEKC), a variant of CE, is used to separate neutral compounds in addition to charged ones. In MEKC, the separation buffer contains a surfactant such as sodium dodecyl sulfate (SDS). At a concentration higher than its

critical micelle concentration (CMC), the surfactant forms micelles, which have their hydrophilic head regions in contact with surrounding aqueous phase and hydrophobic tail regions located in the center of the micelles (Figure 2-8). The CMC is strongly affected by the type of buffer electrolyte, buffer pH and electrolyte additives. For example, the CMC of SDS is 5.29 mM in 5 mM borate buffer at pH = 9.2 and 4.6 m*M* in 10 mM phosphate-20 mM borate buffer at pH 6.8.[123]

In MEKC separations, analytes distribute between micelles and the separation buffer according to their hydrophobicity. The capacity factor *k'* is given by the ratio of the moles of analyte in the micelle (n_{mc}) to those in the aqueous phase (n_a).

$$k' = \frac{n_{mc}}{n_0} \qquad \text{(Equation 2-4)}$$

Water insoluble neutral compounds partition into the hydrophobic core of the micelles and spend longer time in them; inversely, water soluble ones barely partition into the micelles and spend shorter time in them (Figure 2-8). Since micelles migrate in the opposite direction of the EOF, compounds spend less time in micelles migrate out of the capillary first and those spend more time migrate out later.

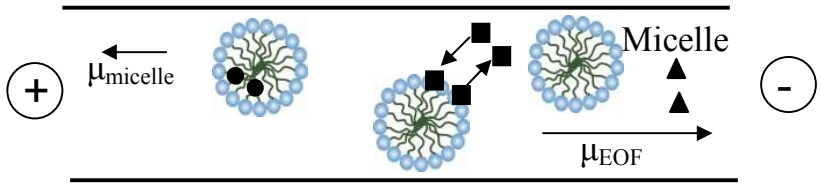

Figure 2-8. Schematic illustration of MEKC separation of neutral analytes with different hydrophobicity. Water soluble analytes (showed in triangle) do not partition into the micelles and migrate at the same velocity as EOF; Hydrophobic analytes (circle) that completely partition into the micelles migrate at the same velocity as the micelles; analytes that partially partition into the micelles have intermediate migration time.

The migration time (t_R) can be calculated as

$$t_R = \left(\frac{1+k'}{1+\left(\frac{t_0}{t_{mc}}\right)k'}\right)t_0 \qquad \text{(Equation 2-5)}$$

where k' is the capacity factor, t_0 and t_{mc} are the migration times of an EOF marker and micelle, respectively. According to Equation 2-5, if a compound like methanol is totally soluble in water ($k' = 0$), its migration time is equal to that of EOF ($t_R = t_0$). On the other hand, if a compound like Sudan III is totally incorporated into the micelles ($k' = \infty$), its migration time is equal to that of micelle ($t_R = t_{mc}$). Any compound with intermediate hydrophobicity will have a migration time between t_0 and t_R.

For charged compounds, they also have electrostatic interactions with micelles. If their charges are opposite to that of micelles, they interact strongly with the micelles due to electrostatic attraction; if they have the same charge as the micelle, electrostatic repulsion occurs. Therefore, the migration behavior of a charged compound is affected by factors include EOF, electrophoretic mobility of micelle, electrophoretic mobility of the charged compound, and capacity factor of the compound.[122]

Optimization MEKC separation conditions: The resolution of a pair of neutral analytes 1 and 2 (analyte 2 being the late-eluting compound) in MEKC is derived as previously decribed[124]

$$R_s = \frac{N^{1/2}}{4}\left(\frac{\alpha-1}{\alpha}\right)\left(\frac{k'_2}{1+k_2'}\right)\left(\frac{1-t_0/t_{mc}}{1+\left(t_0/t_{mc}\right)k'_1}\right) \qquad \text{(Equation 2-6)}$$

where N is the theoretical plate number, α is the separation selectivity defined as k'_2/k'_1.

One of the factors that affect the resolution of MEKC is selectivity (α). It can be manipulated by choosing appropriate buffer, surfactants and additives.

The pH and type of electrolyte of the buffer are important parameters, especially for charged species. The optimum pH can be easily found by performing various seprations using buffers with different pH. On the other hand, at same pH, different ionic species may have different effects on the separation of analytes by specific interactions with the analytes. For example, borate can form complexes with a number of compounds such as carbonhydrates that have *cis*-diols.[125] The concentration of the buffer is another practical parameter to consider. The use of moderately high ionic strength buffers can suppress ionic interactions between charged analytes and ionized silanol groups on the capillary wall. However increasing the ionic strength also decreases EOF and hence increases the separation time.[122] The upper limit of the ionic strength of buffers is restricted by Joule heating, which is a phenomenon when an electrical current passes through a conductor (i.e., buffer in CE) and generates heat. Joule heating affects the efficiency and reproducibity of the separating through affecting the EOF, retention and diffusion of analytes.[126]

Selection of a surfactant is another important parameter to consider in designing MEKC separations. The length of the hydrophobic alkyl-chain, the electric charge, and the structure of the hydrophobic group of a surfactant molecule affect the MEKC performance. Cation surfactants such as cetyl trimethylammonium bromide (CTAB) are used in some separation systems to selectively separate analytes and reduce the adsorption of cation analytes to the capillary wall. CTAB converts cathodic EOF in fused silica capillaries into anodic EOF. The magnitude of the reversed EOF depends on the composition and ionic strength of separation buffer, but largely independent of pH and the concentration of CTAB.[127] Chapter 4 describes a CTAB-based MEKC system to

separate DOX and its prodrug, LeuDOX, which cannot be separated by an SDS-based MEKC system.

Additives such as organic solvents and cyclodextrins (CDs) can be added to improve the resolution of an MEKC separation. Addition of organic solvents helps to adjust the capacity factor and modify the separation selectivity. Organic solvents are added to solubilize analytes (e.g., lipids) whose solubility is low in aqueous phase. It should be noted the addition of organic solvents in MEKC will reduce EOF, change CMC, and the micelle size.

CDs are commonly used as chiral selectors are also used to modify selectivity in MECK.[128] CDs are a family of cyclic oligosaccharides that present a hydrophilic exterior and a hydrophobic cavity. Four types of CDs: α, β, γ and δ which contain six, seven, eight and nine glucose units, respectively are commonly used in MEKC. Figure 2-9 shows the 2D and 3D structure of γ-CD. The number of glucose units determines the size of the cavity. Cavity diameters are 0.57 nm, 0.78 and 0.95 nm for α-, β- and γ-CD, respectively.[129] In the presence of micelles, CDs are not incorporated into micelles, but affect the distribution of analytes between micelles and the nonmicellar phase. Analytes with size compatible to that of the cavities of CDs can enter the cavities and their incorporation into micelles is decreased.[130] In this way, highly hydrophobic compounds tend to be totally incorporated into micelles but have different affinity to CDs can be separated. Since CDs are electrically neutral, they migrate at the velocity of EOF. Analytes that spend most of their time in the cavity of CDs elute faster than those that spend most of their time in micelles.

Since the extent of an analyte included in CDs is dependent on its ability to fit into

the CD cavities, cavity size is the primary factor to be considered when choosing a CD type. Previous work on the interaction of DOX and CDs showed that DOX is tightly bound with γ-CD, less tightly bound with β-CD, and no bound with α-CD.[128] Therefore, γ-CD is the best choice in separating DOX and metabolites. DOX and its major metabolite DOXol are successfully separated by adding γ-CD into borate-SDS MEKC buffer.[131] These two compounds are only different in one OH group and cannot be separated with buffers that only contain borate and SDS. Chapters 4, 5 and 6 all describe the use of γ-CD as an additive in the separation of DOX and metabolites as well as fatty acid analogs.

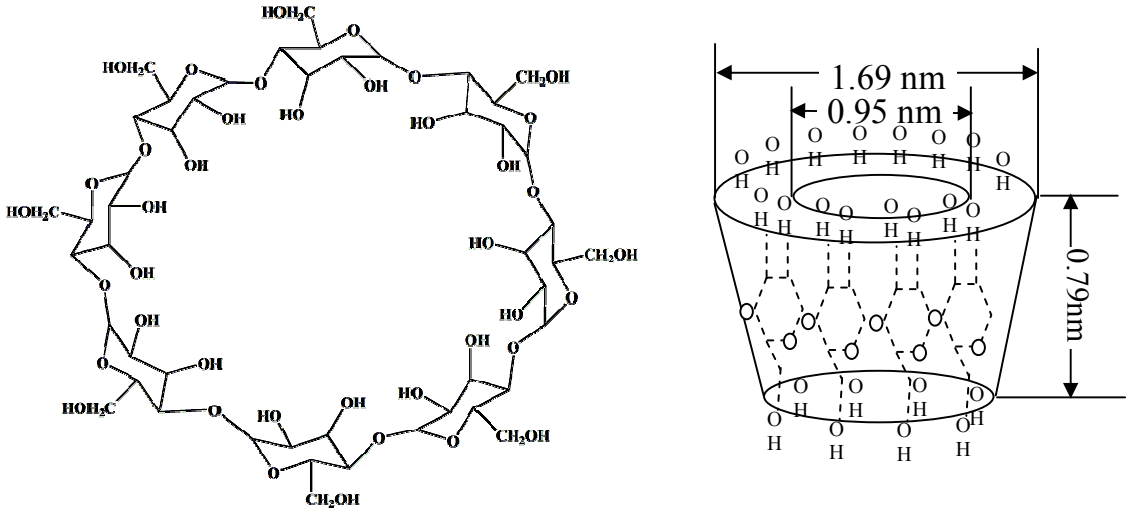

Figure 2-9. 2D and 3D structure of γ-cyclodextrin

2.2.3 Detection methods for DOX and metabolites

UV absorbance, LIF and MS are the most widely used detection methods that are compatible with CE separation modes.

UV absorbance is the most common means of detection since the large majority of compounds absorb light in the UV region. Therefore no chemical modification of the

sample is needed. The major limitation of UV absorbance detection is its low sensitivity. Typical LODs of DOX in CE with UV absorbance detection are in the range of 10^{-5} to 10^{-6} M. Special equipment (e.g., Z-cell and the bubble cell) may improve the LOD of UV detection, but they may cause the loss of separation resolution.[132] Moreover, biological molecules in the sample matrices such as proteins also have UV absorbance and interfere with the detection of analytes.

MS is an information-rich detection method because it provides structural information of the analytes. However, there are also some challenges in MS coupling with the typical CE modes. For example, the MEKC buffer has nonvolatile salts and surfactants which cause ionization suppression of the analytes and clogging of the ionization tip.[133] The sensitivity of MS is another bottleneck of CE-MS. CE is performed in a narrow capillary under a high electric field. The flow rate is low and the amount of analytes is small,[134] which requires high sensitivity. Preconcentration before CE separation, and/or using mass analyzers that have greater sensitivity such as ion trap, Fourier transform ion cyclotron resonance and orbitrap could help meet this requirement.[134]

Laser-induced fluorescence (LIF) detection is one of the most sensitive detection modes in CE with LODs ranging from 10^{-17} to 10^{-21} mole.[135] The limitation of this detection method is that a derivatization step is needed for non-fluorescent analytes. Since DOX and its metabolites are fluorescent, no derivatization is needed. Considering the pros and cons of the detection methods mentioned above, LIF is used in this thesis work. In LIF detectors, analyte molecules absorb light from the laser used for excitation

and a fraction of the excited molecules emit light at a different wavelength upon returning to the ground state. Figure 2-10 illustrates the scheme of a post-column LIF detection system, which is designed to reduce the scattering light generated at the air-capillary and capillary-sample interfaces. Following excitation, the scattering light is dramatically removed with a 505 nm long-pass filter and a pinhole which isolates the illuminated sample region while rejecting light scattered from the cuvette walls. The fluorescence from the sample is then selected by a band pass filter and converted into an electrical signal by a photomultiplier tube (PMT). To reduce further the interference from the excitation laser, the fluorescence photons are collected at a 90 degree angle with respect to the direction of the excitation laser. By using a dichroic mirror in the optical system, two fluorophores can be detected simultaneously in two separate PMTs. For example, if the dichroic mirror with long-pass characteristics, fluorescence wavelengths longer than the cut-off value will pass and be detected in PMT1 and fluorescence wavelengths shorter than the cut-off value will be reflected at 90ºand be detected in PMT2.

In the analysis of DOX and metabolites, it is important to select appropriate filters to allow the detection of low-abundance metabolites. According to Figure 2-2, the two emission maxima of DOX are around 550 and 580 nm. Therefore, a band-pass filter with the central wavelength at 580 nm is expected to be the best option in transmitting fluorescence. However, such a filter can also transmit water Raman band in the range of 565-599 nm.[136] A previous study showed that a 635 ± 27 nm filter provides the best signal-to-noise ratio among the filters tested (530 ± 25, 580 ± 15 and 635 ± 27 nm);[104] this filter was used in the detection of DOX and metabolites in this thesis work. The dual channel detection systems can also be applied to the analysis of DOX and metabolites by

simultaneous detection of the analytes and an internal standard (e.g., fluorescein) in the sample. The internal standard is used to correct mobility of analytes to increase the reproducibility and thus accuracy in analyte identification.[137] Chapter 3 discusses the use of this mobility correction method to distinguish DOX peaks from endogenous fluorescence species in liver tissue samples. The internal standard can also be used to normalize peak area of analytes in different runs to minimize variation in sample preparation or sampling.

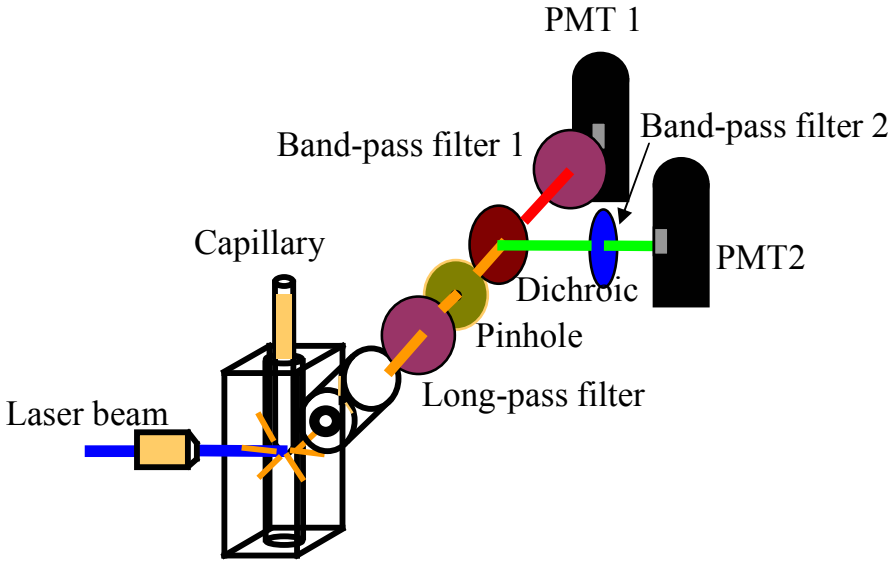

Figure 2-10. Scheme of a dual channel post-column LIF detection system

Chapter 3

Direct Sampling from Human Liver Tissue Cross-sections for Electrophoretic Analysis of Doxorubicin

The work described in this chapter was done in collaboration with Dr. Erik Cressman (Department of Radiology, University of Minnesota). The initial development of the technique was done by Jennifer Hong. We are very grateful to Meiji Seika Kaisha Ltd. for their kind donation of doxorubicin. We thank the Tissue Procurement Facility, Characterization Facility and Tissue Mechanics Laboratory at the University of Minnesota for their instructions in tissue sample preparation, AFM and tissue elastic modulus measurement, respectively.

After chemoembolization of the liver with doxorubicin (DOX), this drug and its metabolites are not homogeneously distributed in this organ. The distribution cannot be easily measured making it difficult to assess how the drug performs in different tissue regions. Here we report a technique for sampling tissue cross-sections that can analyze the contents of micrometer size regions. The tissue cross-sections were from the explanted liver of a hepatocellular carcinoma patient. Samples were directly aspirated from a 5-μm thick tissue cross-section into a 50-μm i.d. capillary where the tissue was solubilized with a separation buffer containing sodium dodecyl sulfate. Upon sample dissolution, DOX and natively fluorescent compounds were separated and detected by micellar electrokinetic chromatography with laser-induced fluorescence detection. Sampling reproducibility and recovery were assessed using 10% (w/v) gelatin as tissue-mimic. Sampling from gelatin slices containing DOX revealed a relative standard deviation of 13%, which was comparable to that of sampling from solution. DOX recovery was 82 ± 16% (n=5). When sampling tumor and non-tumor tissue regions, samples could be taken in the same region 100 μm apart. Atomic force microscopy was used to determine that each sample was 8.4 ± 1.0 pL in volume which made it possible to determine DOX concentrations in the ranges of 0.4 - 1.3 μM and 0.3 - 0.5 μM for the samples taken from tumor and non-tumor regions. The results demonstrated the feasibility of sampling, detection and quantification of DOX in micrometer size regions which could be a useful resource for analyzing the DOX concentration and distribution in highly heterogeneous tissues.

3.1. Introduction

The liver is a highly specialized tissue responsible for many vital functions including the metabolism and clearance of xenobiotics, serum protein synthesis and lipid storage.[138] These multiple functions can be performed by the same organ because of its highly heterogeneous nature manifested by the different liver cell types, matrix compositions, and protein activities.[138] This heterogeneity may complicate the interpretation of the effect of treatment of diseases such as hepatocellular carcinoma (HCC) and the underlying cirrhosis. Thus, techniques that make it possible to measure the tissue properties with high spatial resolution are important for elucidating the mechanisms of these diseases, discovering biomarkers and evaluating treatments.[139, 140] These techniques would be especially helpful for evaluating the efficacy of transcatheter arterial chemoembolization (TACE), a treatment that delivers chemotherapy drugs directly to the tumor site by a catheter via the hepatic artery, and uses embolic agents to create an ischemic effect on the tumor.[22] Since the efficacy of TACE is presumably related to the concentrations of drugs at the tumor site and the adjacent parenchyma, it should be useful to determine these concentrations. These measurements are challenging because drug concentrations are not constant throughout the treated area of the liver. The variations in concentrations may be due to the heterogeneous structure of cancerous and non-cancerous tissue and/or to the method of drug delivery. Among existing techniques, tissue homogenate analysis cannot reveal the concentrations of drugs at the tumor site and the adjacent parenchyma, which are only several micrometers apart. The spatial distribution information is lost as the homogenization process destroys the organization of the sample. Fluorescence microscopy can provide the spatial distribution of a fluorescent drug but it cannot distinguish between drugs, metabolites, and other native components with similar spectroscopic properties.

New techniques have been developed to directly sample and analyze the distribution of biomolecules in target tissues. Reyzer has reported the use of matrix-assisted laser desorption/ionization mass spectrometry (MALDI-MS) to directly analyze and image an anti-tumor drug SCH 226374 in mouse tumor tissue with resolutions of 200 μm in the x-direction and 400 μm in the y-direction.[106] However, the background signal from the MALDI matrix interferes with the detection of drugs and metabolites with low molecular weights. Moreover, the discrepancies in the ionization efficiency of drugs and their metabolites due to their different structures, abundances and tissue environments make this method hardly quantitative.

Another technique that allows the direct sampling from tissues with high resolution is laser-capture microdissection (LCM) which uses a laser to selectively remove a small region of interest from a tissue (e.g., 3-μm diameter circle)[109] for subsequent DNA, RNA or protein analyses. [110] This sampling method is seldom used to analyze drug metabolites, probably because a large number of cells must be collected to make low abundant metabolites detectable. For example, Drexler reported that 20-30 LCM samples need to be combined for one HPLC-MS analysis of a prodrug and its metabolites.[111]

Oguri *et al.* reported a method for analyzing taurine in rat brain by directly sampling from the rat brain using a capillary followed by on-line pre-concentration, in-capillary derivatization and capillary electrophoresis (CE).[112] Unlike microdialysis which only samples the fluid in the extracellular space of tissues, this method samples both intra- and extra-cellular taurine. While site-specific, the method is not quantitative as there is no way to control and calculate the volume of tissue sampled.

In this paper, we report a novel direct tissue analysis method with 100 μm spatial resolution to analyze the tissue distribution of an anti-cancer drug, doxorubicin (DOX), in liver tissue cross-sections after TACE treatment. Using this method, less than 10 picoliters of tissue were directly sampled from either tumor or adjacent non-tumor regions in a liver cross-section using an etched-tip capillary (50 μm I.D. and about 100 μm O.D. after hydrofluoric acid (HF) etching). DOX and other fluorescent species in the sample were subsequently separated and detected using micellar electrokinetic chromatography with laser-induced fluorescence detection (MEKC-LIF), a separation technique that has been used to analyze DOX and its metabolites with a 61 zeptomole limit of detection (LOD) of DOX.[141] Further development of this sampling technique would be highly relevant for evaluating drug distributions and presumably the efficacy of established TACE treatments.

3.2. Material and methods

3.2.1 Chemicals and Reagents

Doxorubicin hydrochloride was a generous gift from Meiji Seika Kaisha Ltd. (Tokyo, Japan). Doxorubicinol was from Qvantas Inc. (Newark, DE). Sodium borate decahydrate, sodium hydroxide (NaOH) and *o*-phosphoric acid were from Fisher Scientific (Fair Lawn, NJ). Sodium dodecyl sulphate (SDS), hydrochloric acid (HCl), hydrofluoric acid (HF), potassium phosphate dibasic, chloroform and isopropanol were from Mallinckrodt (Phillipsburg, NJ). Fluorescein was from Invitrogen (Carlsbad, CA). γ-cyclodextrin (γ-CD) was from TCI America (Portland, OR). Optimal Cutting Temperature compound (O.C.T.) was from Sakura Finetek (Torrance, CA). Dimethyl sulphoxide (DMSO) was

from Honeywell (Muskegon, MI). 10× phosphate-buffer saline (10× PBS containing 1.37 M NaCl, 14.7 mM KH_2PO_4, 78.1 mM Na_2HPO_4, and 26.8 mM KCl) was from EMD Chemicals (Gibbstown, NJ). Methanol and ethanol were from Pharmco-AAPER (Brookfield, CT).

The tissue homogenization buffer consisted of 100 mM phosphate buffer (pH = 3.8) and the MEKC buffer was 10 mM borate and 10 mM SDS (pH = 9.3) (BS-10 buffer) or 50 mM borate, 40 mM SDS and 20 mM γ-CD (pH = 9.3) (BS-CD buffer). All the buffers were made using 18 MΩ water purified from a Millipore water purification system (Millipore, Billerica, MA) and the pH was adjusted with 0.1 M HCl or NaOH.

Stock solutions of DOX, doxorubicinol and fluorescein were prepared in methanol at a concentration of 1×10^{-3} M and kept at -20 ° C until use.

3.2.2 Preparation of tissue sample and gelatin tissue-mimics

After explant, human liver tissue specimens were stored in O.C.T. in a Cryomold (Sakura Fineteck, Torrance, CA) at -80 °C. Cross-sections 5 μm in thickness were obtained by cutting tissue specimens in a cryostat (Leica CM1850, Leica Microsystems, Bannockburn, IL) at -20 °C. The cross-sections were mounted on glass slides (M6146, Cardinal Health, IL) and then frozen at -80 °C; they were brought to room temperature for direct tissue sampling and subsequent MEKC analysis.

For bulk tissue analysis, DOX and its metabolites were extracted using liquid-liquid extraction.[142] A 40 mg tissue sample was homogenized in 200 μl homogenization buffer by 50 strokes in an ice-chilled Dounce homogenizer (0.00025'' clearance, Kontes Glass, Millville, NJ). DOX and its metabolites were extracted using a 200 μl DMSO,

chloroform and isopropanol mixture (1:60:30, v/v/v) and then subjected to centrifugation at 1000g to separate the different phases. The aqueous phase and emulsification were removed, and the organic phase was dried under a nitrogen flow, reconstituted in 200 µl methanol and diluted 25 times in BS-10 buffer prior to MEKC analysis.

Gelatin tissue-mimics containing DOX were made by dissolving different amounts of gelatin powder (type A, MP Biomedicals, Solon, OH) into boiling water to create different concentrations (10%, 15% and 20%, w/v). When adding the gelatin powder, the mixture was stirred with a magnetic stirring bar until all the powder had dissolved. DOX stock solution was then added into the gelatin solution to a final concentration of 10 µM. After the mixture was degassed by sonication and centrifugation (1000g for 10 min), it was poured into a Cryomold and allowed to solidify at 4ºC in a refrigerator for at least 1 h. The gelatin slices (5 µm in thickness) were cut in the same way as the tissue cross-sections and kept at -20 ºC before MEKC analysis.

The elastic moduli of liver tissue and gelatin tissue-mimics (1 cm in length, 0.8 to 1 cm in width and 0.98 to 1.63 mm in thickness) were measured with a Micro Bionix® testing system (MTS Systems, Eden Prairie, MN). The elastic modulus (*E*), defined as the ratio of stress to strain, was calculated as

$$E = \frac{stress}{strain} = \frac{F/A_0}{\Delta L/L_0} \qquad \text{(Equation 3-1)}$$

where F is the force applied to tissue or gelatin, A_0 is the original cross-sectional area through which the force is applied, L_0 is the original length of tissue or gelatin, and ΔL is the change in length when the force is applied. Thus, E can be determined from the slope of the linear region in a stress (F/A_0) versus strain ($\Delta L/L$) plot.

3.2.3 Capillary preparation and direct tissue sampling

The polyimide coating at the injection end of a fused silica capillary (50 µm I.D and 150 µm O.D, Polymicro Technologies, Phoenix, AZ) was burned with a small flame and then the outer wall was etched by immersing the tip of the capillary into HF for 5 min. In order to protect the inner walls of the capillary from etching, water was flushed through the capillary (3 mL/h) with a syringe pump connected at the other end of the capillary. Figure 3-1 shows the tip of a capillary before (A) and after (B) etching.

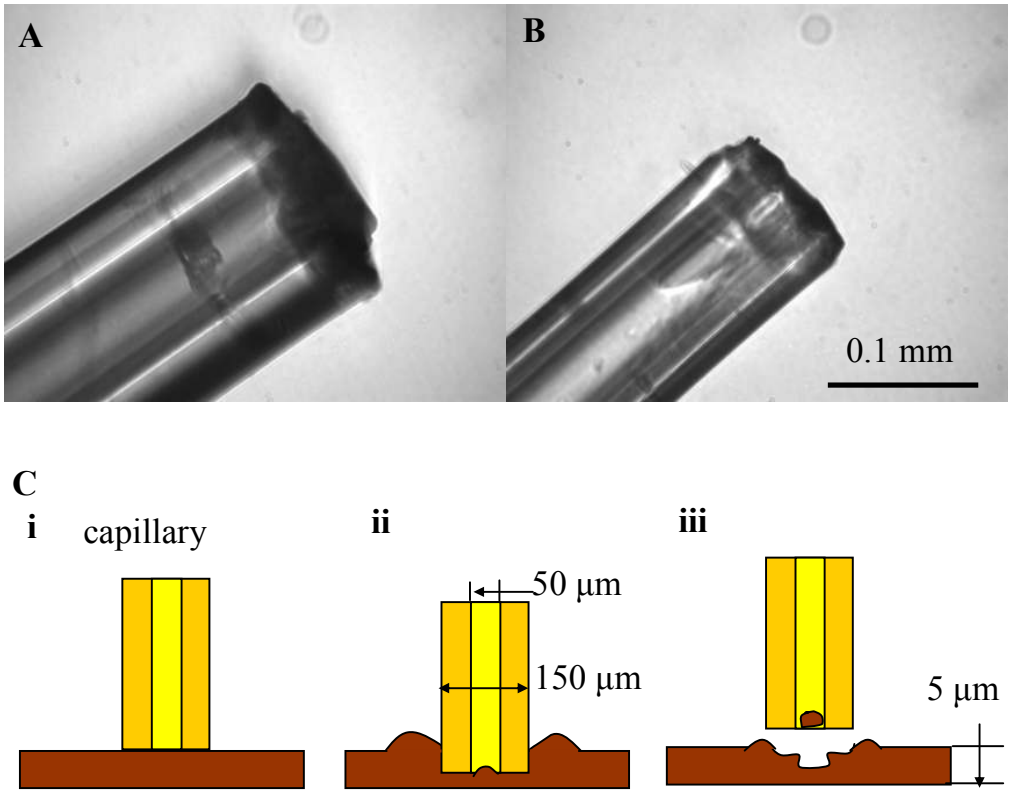

Figure 3-1. Details relevant to direct tissue sampling. The tip of a capillary before (A) and after (B) HF etching. (C) Diagrams illustrating the position of a capillary before (i), at (ii) and after (iii) sampling from a tissue cross-section or gelatin slice.

In order to select the region to be sampled, tissue cross-sections or gelatin slices were observed with a Nikon Eclipse TE300 microscope (Nikon, Huntley, IL) using 10× or 40×

objectives. Figure 3-1C illustrates the steps of direct sampling. First, a capillary was x-y positioned over the spot to be analyzed using a micromanipulation system (MX100L, Soma Scientific, Irvine, CA) as previously described.[143] The capillary was then lowered carefully with a hydraulic micromanipulator (MW1, Soma Scientific) until contact with the tissue cross-section or gelatin slice was detected (Figure 3-1C, i). The capillary was then lowered 5 μm further into the sample (Figure 3-1C, ii) and a negative pressure of 7.6 kPa was applied for 2 s to aspirate the sample into the capillary (Figure 3-1C, iii).

3.2.4 Atomic force microscopy (AFM) of tissue cross-sections after direct sampling

After direct sampling, the surface topology of eight sampled regions on a tissue cross-section was mapped in the tapping mode with a Digital Instruments Nanoscope III Multimode AFM (Digital Instruments (DI), Santa Barbara, CA) to determine the volume of tissue taken in each sampling. The AFM topological image of each sampling spot was processed with Image J software (NIH) to determine the area of the spot and the average intensities of both sampled and neighboring regions. The average intensity (I) was then converted into height (h) using the calibration curve provided by the DI software:

$$I = (33.7 \pm 0.4) \times h - (11.8 \pm 0.3); \quad (R^2 = 0.97) \qquad \text{(Equation 3-2)}$$

The volume of tissue sampled (V) in each spot was calculated as

$$V = A \times \Delta h \qquad \text{(Equation 3-3)}$$

where A is the spot's area and Δh is the average height difference between the sampled and the neighboring regions.

3.2.5 MEKC analysis of DOX in directly sampled tissue

After a tissue sample was aspirated into a capillary, the capillary was brought into the vial containing a fluorescein (internal standard) solution to inject (aspirate) this solution at 7.6 kPa for 2 s. Then the capillary was brought into the vial with BS-CD buffer and MEKC of the tissue sample was performed in a home-built instrument equipped with post-column LIF detection, previously described.[144] The gelatin tissue mimics were sampled and analyzed in the same way as tissue samples, except the separation buffer was BS-10. The SDS in the separation buffers was important as solubilizing agent making it possible to release analytes and other fluorescent compounds that were then separated under a +400 V/cm electric field.

A sheath flow cuvette encased the detectdor end of the capillary. The last 2-mm of this end had the polyimide coating burned off to reduce the background fluorescence caused by this material. As fluorescent analytes migrated out from the capillary, they were excited at 488 nm with an argon ion laser (JDS Uniphase, San Jose, CA). Fluorescence was collected at a 90° angle with respect to the laser beam by a 60× microscope objective (Universe Kogaku, Inc., Oyster Bay, NY). A 505 nm long-pass filter (505 AELP, Omega Optical, Brattleboro, VT) and a 1.4 mm pinhole were used to reduce light scattering. As previously reported, a dual channel fluorescence detector was used.[145] The fluorescence spectral range was split by a 580 nm short-pass dichroic mirror (CP-RR-580, CVI Laser, Albuquerque, NM) and then the fluorescence from DOX was selected by a 635 ± 27.5 nm band-pass filter (XF3015, Omega Optical, Brattleboro, VT) while the fluorescein fluorescence was selected by a 535 ± 17.5 nm band-pass filter (XF3007, Omega Optical, Brattleboro, VT). Fluorescence at these two separate spectral regions was then detected in separate photomultiplier tubes (PMT) (Hamamatsu,

Bridgewater, NJ) biased at 1000 V. The PMT outputs were sampled at 10 Hz and processed with a home-written Labview program (National Instruments, Austin, TX).

Prior to MEKC analysis, the capillary was conditioned with sequential flushes of 0.1 mM NaOH, water, 0.1 mM HCl, water and separation buffer for 30 min each using 150 kPa pressure at the inlet. The same sequence, but running for 2 min each, was carried out between samplings of different tissue regions. The separation buffer was replaced every 2 h with a fresh one to avoid electrolyte depletion and buffer contamination. Prior to sample analysis, the instrument was aligned by maximizing the response of 5×10^{-10} M fluorescein which continuously flowed through the detector while applying a +400 V/cm electric field.

3.2.6 Determination and quantification of DOX

The mobilities of the peaks in the electropherograms of tissue samples taken directly from tissue cross-sections were corrected using the mobility of an internal standard, fluorescein. The corrections were done according to the procedure described by Li, *et al.*[137] that uses the expression

$$t_{corrected,x} = \left[\frac{1}{\hat{t}_x} - \left(\frac{1}{\hat{t}_{fluorescin}} - \frac{1}{t_{fluorescein}} \right) \right]^{-1} \qquad \text{(Equation 3-4)}$$

where $t_{corrected,x}$ is the corrected migration time of an analyte *x* in tissue samples and $\hat{t}_x$ is its observed migration time; $\hat{t}_{fluorescein}$ is the migration time of fluorescein used as an internal standard and $t_{fluorescein}$ is the migration time of fluorescein in the reference run with DOX or doxorubicinol standards. The corrected mobility of the analyte *x* was calculated by

$$\mu_{corrected,x} = \frac{L^2}{V \times t_{corrected,x}} \quad \text{(Equation 3-5)}$$

where L is the length of the capillary, and V is the separation voltage. The corrected mobility of the analyte *x* was compared to that of DOX or doxorubicinol standards. The Student's t test was used to test the null hypothesis "there is no significant difference between the mobilities of DOX or doxorubicinol standards and those of the analytes in the tissue sample" using open-source statistical software "R". The null hypothesis was rejected when the p-value (p) <0.02 (98% confidence level).

The amount of DOX in each tissue sample was determined according to the calibration curve:

$$A_{DOX} = (4.8 \pm 0.1) \times 10^{16} m_{DOX} + (0.028 \pm 0.006) \quad (R^2 = 0.99) \quad \text{(Equation 3-6)}$$

where A_{DOX} is the peak area of DOX and m_{DOX} is the number of moles of DOX injected. The linear range of the curve is from 2.9×10^{-18} to 5.7×10^{-16} mol (corresponding to 5×10^{-10} to 1×10^{-7} M DOX with 5.7 nL sample volume). The LOD (S/N=3) of DOX is estimated to be $(2.00 \pm 0.03) \times 10^{-18}$ mole (n = 3) as determined from the peak intensity resulting from injecting 5.7×10^{-17} mol DOX. Compared to previous reports[141], the LOD in BS-CD buffer is about 30 times higher than in BS-10 buffer because of 1) the addition of γ-CD increases the background noise and 2) the longer DOX migration time in BS-CD buffer that results in broader less-intense DOX peaks.

Doxorubicinol was also detected in some instances. As the integrated fluorescence intensities of DOX and doxorubicinol over the spectral band-pass of the 635 ± 27.5 nm filter were nearly identical (18 fluorescence units (FU) versus 17 FU, respectively),[146] the amounts of doxorubicinol in the tissue samples were also calculated according to Equation 3-6.

The amounts of DOX in the tumor and non-tumor regions of a tissue cross-section were compared using statistic software "R". The null hypothesis "there is no difference in the amounts of DOX between the tumor region and the non-tumor region" was tested using the Student's t test and rejected when $p<0.02$.

3.2.7 Safety considerations

The study using human subjects was approved by the University of Minnesota Institutional Review Board (Study Number: 0508M72944). Protective clothing and surgical gloves were worn when handling liver tissues. All liver specimens were autoclaved before disposal.

3.3. Results and Discussion

3.3.1 Assessing the reproducibility of direct tissue sampling

The reproducibility of the sampling procedure is crucial to quantifying the DOX in each sample taken from tissue cross-sections. To evaluate the reproducibility of this sampling method, samples taken from different spots in a homogenous gelatin slice (5 μm in thickness) containing DOX were analyzed by MEKC-LIF. Gelatin was used as a tissue-mimic because it is the denatured form of collagen, the main component of tissue extracellular matrices, and is the major determinant of tissue mechanical properties.[147] The elastic modulus of a given tissue, a parameter describing the deformation of tissue under stress, determines the ease of sampling the tissue. The elastic moduli of 10%, 15% and 20% gelatin were measured and summarized in Appendix A, Figure A-1 and Table A-1. The elastic modulus of 10% gelatin was found to be close to that of HCC

tissues, so this concentration of gelatin was used to prepare tissue mimics and to assess the reproducibility of direct sampling.

Figure 3-2A shows the image of a 10% gelatin slice after 6 samplings using an etched-tip capillary, and the corresponding electropherograms are shown in Figure 3-2B. The peak areas and amounts of DOX are tabulated in Table 3-1. The darker parts (indicated by arrows in Figure 3-2A) of the sampling spots were the result of the capillary tip deforming the gelatin due to contact during the sampling and were therefore excluded when measuring the areas of the sampling spots. The first sampling (electropherogram not shown) was discarded as an outlier by a Q-test at 99.5% confidence level. This is not surprising since when performing the MEKC analysis of DOX, the capillary wall needs to be conditioned by several injections of DOX standard or sample to improve electropherogram reproducibility.[148] The relative standard deviation (RSD) of the peak areas of DOX in the next 5 samplings (spots 2 to 6) was 13% (Table 3-1), which is comparable to the RSD (11%) of 5 injections of 1×10^{-7} M DOX solution (results not shown), which were intercalated between samplings from the gelatin slice.

Table 3-1. Reproducibility of DOX in direct samplings from a 5-μm thick gelatin slice as determined by MEKC-LIF

	Peak area[1]	DOX amount[2] ($\times 10^{-16}$ mol)	Sampling area (μm^2)[3]
Spot 2	6.07	1.25	1.02×10^4
Spot 3	5.19	1.08	9.96×10^3
Spot 4	6.28	1.30	8.93×10^3
Spot 5	6.14	1.27	9.69×10^3
Spot 6	7.41	1.54	8.56×10^3
Average±SD	6.2±0.8	1.3±0.2	$(9.5\pm0.7)\times10^3$

1. Peak areas were measured from the DOX electropherograms (Figure 3-2B) obtained by MEKC-LIF.
2. DOX amounts were calculated according to Equation 3-6.
3. Sampling areas (demarked regions in Figure 3-2A) were measured by image J.

The reproducibility of direct sampling from a gelatin slice using a normal capillary (150 μm O.D.) is more than twice as low (RSD = 29%, results not shown). This is because the capillary wall compressed or destroyed the gelatin upon contact, which "squeezed" DOX solution out of the gelatin. When this occurred, in addition to the DOX in the gelatin, DOX solution was also introduced into the lumen of the capillary, artificially increasing the intensity of the observed DOX peak. Thus, by etching the tip of a capillary, these detrimental effects were avoided and the reproducibility of the sampled volume improved and was comparable to that of samplings from solution.

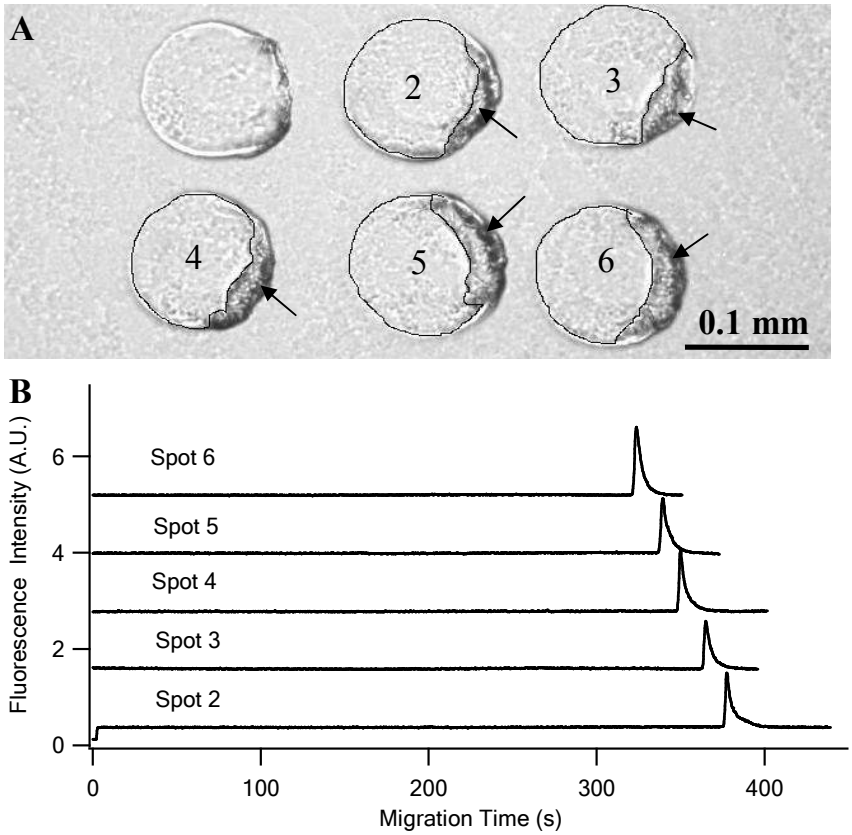

Figure 3-2. Direct sampling from a 5-μm thick gelatin slice. (A) Bright field image of a gelatin slice after six direct samplings. (B) Electropherograms of spots 2-6; those of spots 3-6 are x and y offset for clarity. Gelatin was sampled at 7.6 kPa for 2 s with an etched-tip capillary. Separations were performed in a 48.5 cm long, 50 μm i.d. fused silica capillary at 400 V/cm in BS-10 buffer. Analytes were excited at 488 nm and fluorescence was detected at 635 ± 27.5 nm.

3.3.2 Surface topology after sampling

The surface topologies of tissue cross-sections after sampling were also measured by AFM to determine the volume of tissue sampled in each sampling spot (Figure 3-3). The volumes were calculated according to Equations 3-2 and 3-3. Although the shapes of the holes after sampling were irregular, the RSD of the volumes of tissues sampled was 12% (see Table 3-2), which matches well with the RSD of DOX amount (13%; Table 3-1) detected by MEKC-LIF for samples taken from gelatin slices containing DOX. The difference in sampling volumes mainly comes from the areas of the sample spots (RSD = 12%, Table 3-2), while the RSD of the average thickness of the tissue sampled (4.5%, Table 3-2) is relatively small.

Table 3-2. Volume of tissue sampled after direct sampling from a 5-μm thick tissue cross-section determined by AFM

	Δh (μm)[1]	Sampling area (μm^2)[2]	Average sampling volume (pL)[3]
Spot 1	1.71	4.50×10^3	7.72
Spot 2	1.67	5.43×10^3	9.06
Spot 3	1.59	3.96×10^3	6.28
Spot 4	1.61	5.00×10^3	8.07
Spot 5	1.61	5.61×10^3	9.03
Spot 6	1.76	4.92×10^3	8.64
Spot 7	1.63	5.66×10^3	9.21
Spot 8	1.78	5.11×10^3	9.12
Average±SD	1.67±0.07	$(5.0\pm0.6)\times10^3$	8.4±1.0

1. Δh were calculated using Equation 3-2 from the average intensities of the sampled and neighboring regions measured by Image J.
2. Sampling areas (demarked regions in Figure 3-3) were measured by Image J.
3. Sampling volumes were calculated according to Equation 3-3

Under the conditions described here, the direct sampling technique does not remove the 5-μm thick tissue section. On average, the removed section was 1.67 μm thick (Table 3-2). This means that only 33% of the tissue form the sampled area was removed

(i.e. 8.4 pL). Although it is beyond the scope of this report, the remaining material could be re-sampled for further analyses.

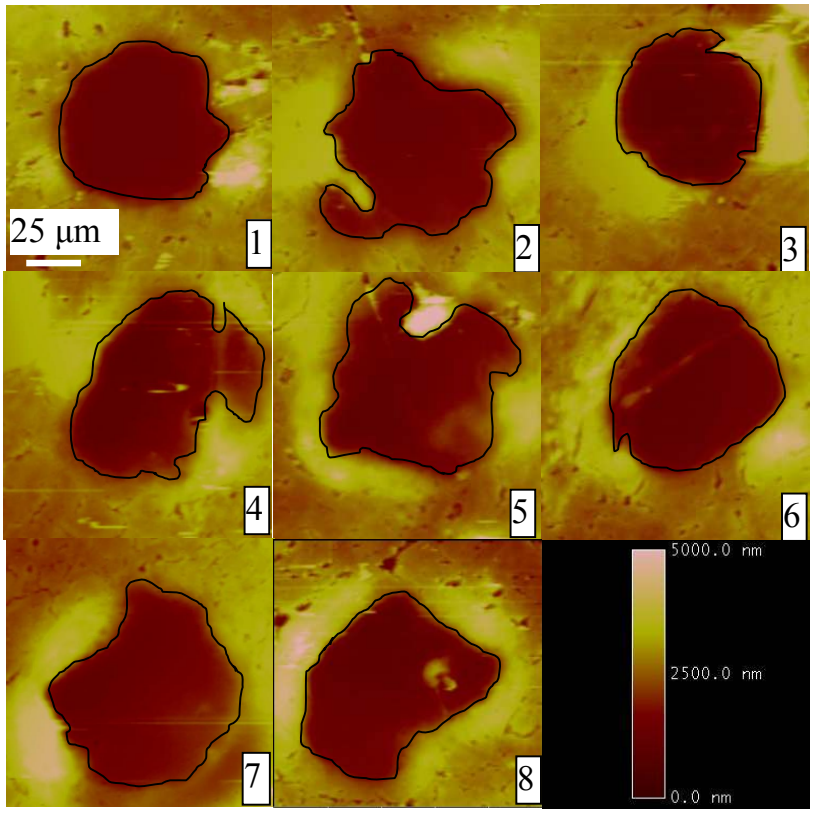

Figure 3-3. Tapping-mode AFM images of a tissue cross-section after sampling. Tissues were sampled from eight regions from a 5-µm thick tissue cross-section at 7.6 kPa for 2 s with an etched-tip capillary. AFM images were obtained with 1 Hz scan rate.

In order to estimate the DOX recovery from a given tissue cross-section we made use of the analysis of gelatin sections. We calculated the total amount of DOX in the volume of sampled gelatin as,

$$Amount\ of\ Dox\ in\ sampled\ gelatin = V \times [DOX] = s \times d \times [DOX] \quad \text{(Equation 3-7)}$$

where V is the volume of the gelatin sampled, $[DOX]$ is the concentration of DOX in gelatin (i.e., 10 µM), s is the sampled area (i.e. average = 9.5×10^3 µm^2, Table 3-2) and d is the thickness of the gelatin removed from the cross-section (i.e. average = 1.67 µm).

Thus, the average amount of DOX in the sampled gelatin volumes is 1.6×10^{-16} moles DOX. From the DOX amounts detected by MEKC-LIF (1.3×10^{-16} moles, Table 3-2), the average recovery of DOX in gelatin is (82 ± 16) % (n = 5).

3.3.3 Determination of DOX in liver tissue

Endogenous fluorescent species in liver specimens (Appendix A, Figure A-2) and DOX fluorescent metabolites may interfere with the determination and quantification of DOX in liver tissue. The BS-10 buffer which is normally used to separate DOX and its metabolites[141] is unable to resolve DOX from its major metabolite, doxorubicinol, and from other endogenous fluorescent species found in the tissue samples (results not shown). We previously reported that a buffer containing 50 mM SDS, 50 mM borate, 20 mM γ-CD is able to separate DOX and doxorubicinol,[149] and this buffer was used as a starting point for selecting a suitable buffer for optimization. By varying the concentrations of SDS, it was found that buffer containing 40 mM SDS, 50 mM borate and 20 mM γ-CD (pH = 9.3) was sufficient to separate DOX, doxorubicinol and endogenous fluorescent species in bulk extracts from a liver administered with DOX via TACE (Figure 3-4, Trace a). Similarly, spiking a tissue extract from an untreated liver confirmed that no endogenous fluorescent species co-migrated with DOX, (Appendix A, Figure A-3).

The ability to distinguish DOX (Peak 3) from doxorubicinol (Peak 2) and other fluorescent species was confirmed by analyzing tissue extract prepared in bulk (Figure 3-4, Trace a), spiking an aliquot of the extract with DOX standard (Figure 3-4, Trace b) or with doxorubicinol standard (Figure 3-4, Trace c) and comparing the

electropherograms obtained before and after spiking. This analysis confirmed that the separation was adequate to distinguish DOX from doxorubicinol (when present) and from other fluorescent species. It is worth noticing that there were two peaks in the doxorubicinol standard (Figure 3-4, Trace c, Peak 2 and 2'), believed to correspond to two stereoisomers,[149] while only one doxorubicinol peak (Figure 3-4, Trace a, Peak 2) was observed in the tissue sample. This suggests the stereospecificity of carbonyl reductase, which is the enzyme that catalyzes the conversion of DOX to doxorubicinol in the liver.[150]

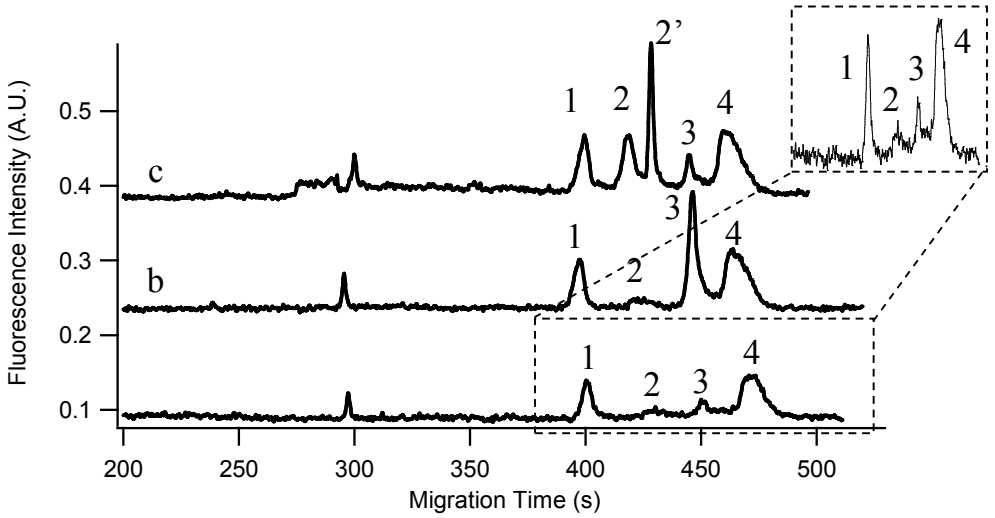

Figure 3-4. MEKC-LIF analysis of bulk liver tissue extract. Trace a: tissue extract only. Trace b: tissue extract spiked with DOX. Trace c: tissue extract spiked with doxorubicinol. Peak 2 and 3 are DOX and doxorubicinol, respectively; Peak 1 and 4 are endogenous fluorescence species in the tissue. Traces b and c are y-axis offset by 0.15 and 0.30 A.U. for clarity. Separations were performed in BS-CD buffer in a 39.2 cm long, 50 μm i.d. fused silica capillary at 400 V/cm after 3 s hydrodynamic injection of sample at 7.6 kPa. Analytes were excited at 488 nm. Detection of fluorescein (internal standard) was at 535 ± 17.5 nm (not shown) and red fluorescence (shown here) was at 635 ± 27.5 nm.

In direct tissue sampling, it is impractical to spike samples with DOX or doxorubicinol standards to determine their peaks in electropherograms. An alternative method is to compare the mobility of a peak to that of DOX and doxorubicinol standards. In this method,

the reproducibility of the mobility is crucial. However, it is known that sample components alter the observed mobilities between runs. Here we used fluorescein as an internal standard (detected in the 535 ± 17.5 nm range) to correct the migration times (Equation 3-4) and consequently correct the observed mobilities (Equation 3-5) of the peaks of the tissue samples (detected in the 635 ± 17.5 nm range). After this correction, the reproducibility of the mobilities of the peaks improved and the Student's t test confirmed that the selected peaks in the tissue sample were DOX (p = 0.82 at 98% confidence level, c.f. Appendix A, Figure A-4 and Table A-2).

3.3.4 DOX in tumor and non-tumor tissue regions

Similar to sampling from gelatin tissue mimics (c.f. Figure 3-2), we monitored direct tissue sampling by bright field microscopy. Figure 3-5 shows a tissue cross-section before (A), during (B) and after sampling (C) and the corresponding electropherogram (D). This procedure was effective for selecting the region to be sampled (Figure 3-5A) and to examine the quality of the region after taking a sample (Figure 3-5C). We then demonstrated that corrections to mobilities were feasible when a sample taken from tissue cross-sections and the internal standard solution were introduced separately into the separation capillary. Green fluorescence peaks are shown in the upper trace and include those of native fluorescent species in the tissue as well as the internal standard, fluorescein. Red fluorescence peaks are shown in the lower trace and include those of DOX and native fluorescent species in the tissue. Mobility correction made it possible to correctly identify the presence of DOX in the sampled tissue regions.

The tumor and non-tumor regions in a tissue cross section were determined based on the tissue morphologies. The vasculature pattern in the non-tumor region was more regular, while the tumor region showed more irregular vasculature as well as extensive necrosis due to DOX treatment. These features are consistent with those observed by enhancement of the differences between the tumor and non-tumor regions after hematoxylin and eosin (H&E) staining (Appendix A, Figure A-5).

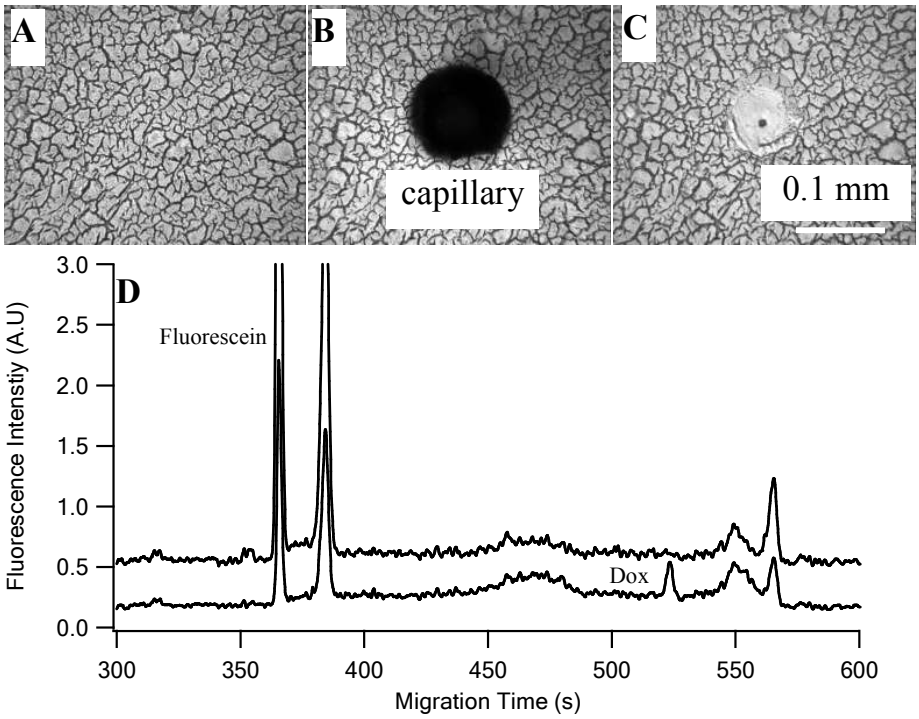

Figure 3-5. Direct tissue sampling from a tissue cross-section and MEKC-LIF analysis. Bright field images of the tissue cross-section before (A), during (B) and after (C) sampling using an etched-tip capillary and the corresponding electropherogram (D). Experimental conditions were the same as in Figure 4 except a 45.7 cm long capillary was used for separations and samples were injected for 2 s.

Sampling in both non-tumor and tumor regions as close as ~ 100 micrometers apart was feasible (Figures 3-6A and 3-6B, respectively). Despite the proximity of the three spots in each sampled region, the electropherogram for each spot was successfully obtained (Figures 3-6C and 3-6D, respectively). The amounts of DOX in each sampling

spot were calculated according to the calibration curve (Equation 3-6) and are summarized in Table 3-3. The amounts of DOX in the tumor region are more widely dispersed than in the non-tumor region, from 3.3 to 10.6 amoles versus 2.7 to 4.3 amoles, respectively (Table 3-3). Assuming that the average volume of the tissue sampled is 8.4 ± 1.0 pL (Table 3-2), the concentrations of DOX in tumor and non-tumor regions are 0.4 to 1.3 μM and 0.3 to 0.5 μM, respectively. Since the sampled volume corresponds to ~ 2 to 3 parenchyma liver cells that have an average volume of 3.8 pL,[151] it is not surprising to observe this variations in the DOX levels in the tumor region, since tumor vasculature heterogeneity and the irregular organization of the cellular environment may lead to such variations, these results point to the importance of measuring drug contents in various tumor regions as it may reveal regions in which the drug does not reach therapeutic levels.

In one of the tumor samples, doxorubicinol was detected with the amount of 2.5×10^{-18} mole. Doxorubicinol is only detected in one of the six samples probably due to its low abundance in the tissue, which may under the LOD of this technique. In bulk analysis, the amount of doxorubicinol was about 41% of that of DOX in the tissue (Figure 3-4). The DOX detected in tissue cross-sections by direct tissue sampling was mostly from 2.7 to 4.3 amole (Table 3-3). If the doxorubicinol was also 41% of that of DOX, it was under the LOD of this method (2.0 amole). Moreover, carbonyl reducatse, the enzyme that catalyzes the conversion of DOX to doxorubicinol may unevenly distribute through out the tissue cross-section, resulting in heterogeneous distribution of doxorubicinol.

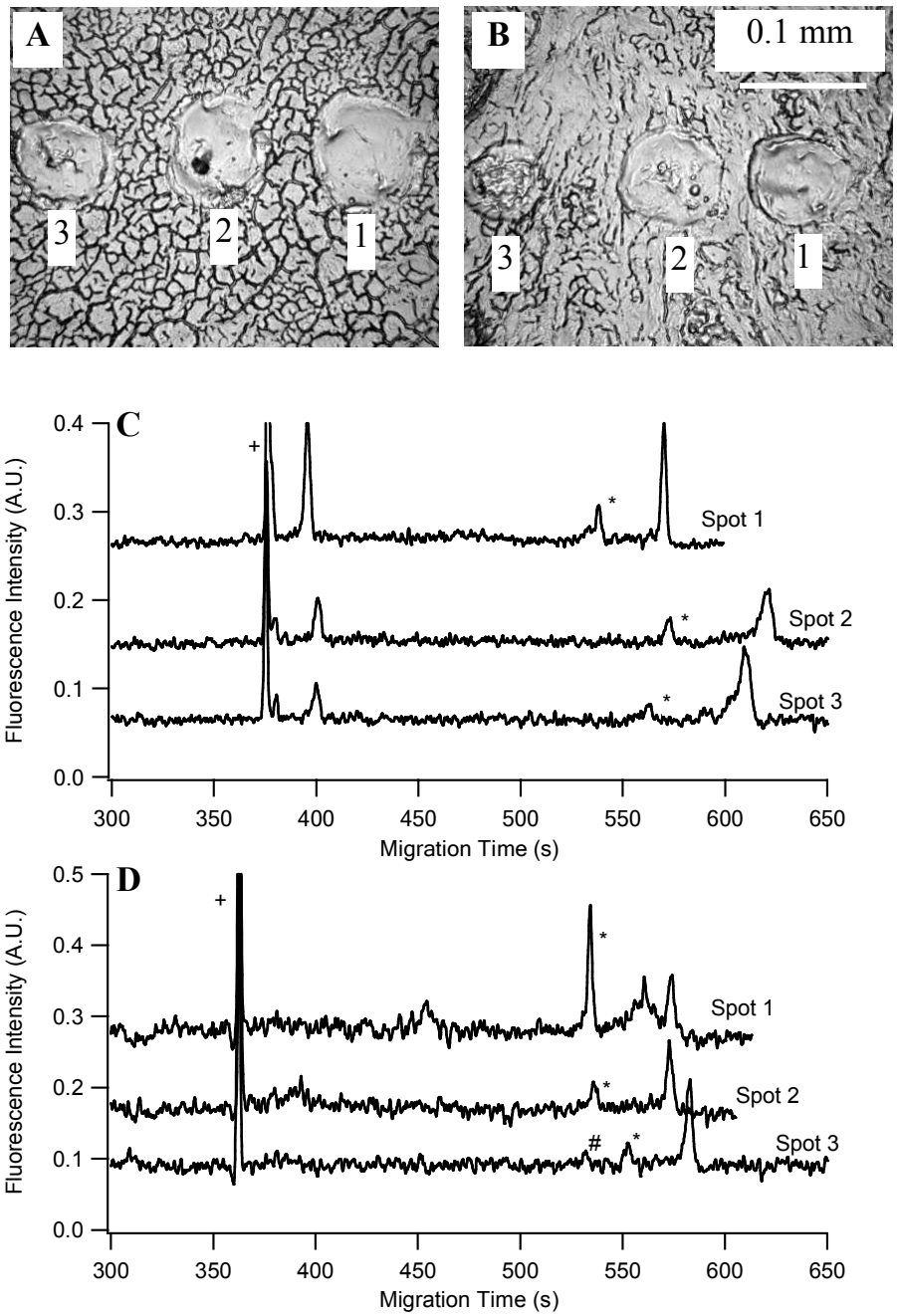

Figure 3-6. Direct tissue sampling from the non-tumor and tumor regions of a tissue cross-section and their respective MEKC-LIF analyses. Bright field images of the tissue cross-section after 3 samplings from non-tumor (A) and tumor (B) regions and corresponding electropherograms (C: non-tumor, D: tumor). The electropherograms of spots 1 and 2 are y-axis offset by 0.2 and 0.1 A.U. For clarity, the traces have been x-axis offset to align the internal standard, fluorescein (labeled with "+"). Peaks labeled with "*" and "#" are assigned to DOX and doxorubicinol after mobility corrections with Equations 3-4 and 3-5. Experimental conditions were as described in Figure 5.

Table 3-3. Corrected mobilities and amounts of DOX in tumor and non-tumor regions of a 5-μm thick tissue cross-section.

	Tumor		Non-tumor	
	DOX		DOX	
	$\mu_{corrected}$[1]	Amount[2]	$\mu_{corrected}$	Amount
Spot 1	2.082	10.6	2.079	4.3
Spot 2	2.098	3.3	2.086	3.3
Spot 3	2.068	4.0	2.097	2.7
Average ± SD	2.08±0.02	6±4	2.09±0.01	3.4±0.8
Standard (n=3)[3]	2.08±0.01	-	2.08±0.01	-

1. The mobility ($\times 10^{-4}$ $cm^2/V \cdot s$) was corrected and calculated according to Equation 3-4 and 3-5.
2. The DOX amount ($\times 10^{-18}$ mole) was calculated from Equation 3-6.
3. Data correspond to the average of triplicate injections; variation is represented as standard deviation.

In an ideal TACE treatment, it is expected that more DOX would accumulate in tumor than in non-tumor region as the drug is delivered to the tumor site directly through a catheter. However, when comparing the DOX amounts in the tumor and non-tumor regions (c.f. Table 3-3), they are not significantly different (p = 0.39 at 98% confidence level). Clearly, direct tissue sampling is promising as a tool to evaluate the distribution of the drug in resected livers, but several future developments are needed: (i) use of focal point drug delivery methods, (ii) knowledge of the distance between the point of drug delivery and the sample taken, and (iii) extensive sampling defined by grid that includes sufficient sample points in both tumor and non-tumor regions. The tissue samples used here were obtained from a liver treated with the segmental arterial delivery of drug, which is too general to provide a focal point for determining the center of drug administration. In the newer drug delivery method, drug-eluting beads, the center of drug administration should be easier to define and address point (i) above. Detailed book keeping of tissue sectioning so that the relative position of a section with respect to the center of drug administration is not routine at tissue procurement facilities, but could be

implemented as needed (c.f. point (ii) above). Lastly, it is difficult to estimate the number of samples that may be needed in a grid to obtain a reliable representation of the spatial drug distribution in tumor and non-tumor regions (point (iii) above). A next practical goal is to define the radial distribution along a line with origin at the point of delivery and that spans both tumor and non-tumor regions. Taking 82 samples in both regions combined (estimated from current data to detect differences in DOX contents between the two regions, power = 0.95, ($\alpha = 0.02$)) would cover 2 cm when relaxing the sampling to 250 μm apart and take about 40 hours of labor. Future developments that improve the throughput may be feasible if using more than one capillary in tandem as reported for simultaneous samplings of single cells.[152,153] Ultimately, these developments may result in practical approaches to investigate drug distributions in the tissues, which in turn could provide a better evaluation of the efficacy of drug treatments.

3.4 Conclusions

Here we demonstrated the feasibility of detecting and quantifying DOX in a 100-μm-diameter region of a tissue cross-section by direct sampling from the cross-section followed by MEKC-LIF analysis. Estimation of the sampled volume by atomic force microscopy, made it possible to calculate DOX concentration in the sampled region. This method has a spatial resolution of about 100 μm, attomole LOD and is reliable as the reproducibility of the sampling method is comparable to that of sampling from solution. The method has great potential as a technology for evaluating the efficacy of TACE treatment and guiding future research to improve such treatment by establishing the tissue distribution map of DOX. This method also has potential applicability for

analyzing other highly heterogeneous tissues such as brain tissue to determine the tissue distribution of other fluorescent biomolecules and xenobiotics.

Chapter 4

Monitoring Incorporation, Transformation and Subcellular Distribution of *N*-$_{L}$-leucyl-doxorubicin in Uterine Sarcoma Cells Using Capillary Electrophoretic Techniques

We are very grateful to Meiji Seika Kaisha Ltd. for their kind donation of doxorubicin. We thank Drs. George Barany, Dan Mullen and Sharon Gazal for their guidance and for providing the equipment needed to synthesize LeuDOX.

Previous reports have demonstrated that *N*-L-leucyl-doxorubicin (LeuDOX) is less toxic than its parent drug, DOX, but the underlying causes of this reduced toxicity have yet to be fully elucidated. In this study, the incorporation of LeuDOX into (i) the MES-SA human uterine sarcoma cell line, and (ii) its DOX resistant counterpart, MES-SA/Dx5 cell line, and the subsequent transformation of LeuDOX into DOX and its subcellular distribution, were investigated by micellar electrokinetic chromatography with laser-induced fluorescence detection (MEKC-LIF).

In both cell lines the cellular uptakes of DOX and LeuDOX were similar at equimolar doses, while the percent transformation of LeuDOX into DOX in MES-SA/Dx5 cells was about twice as great as its transformation in MES-SA cells, which is beneficial for reaching DOX cytotoxic levels in this resistant cell line. When both cells lines were treated with IC_{35} concentrations of either DOX and LeuDOX, the intracellular DOX amounts were six-fold higher in the resistant cell line than in the sensitive cell line, suggesting that other cellular processes play a role in the cytotoxicity of DOX in the resistant cell line.

The amounts and ratios of DOX and LeuDOX in four subcellular fractions of LeuDOX-treated MES-SA/Dx5 cells were also investigated. The highest DOX/LeuDOX ratio (i.e. 2.92) was found in the nuclear fraction, followed by the ratio in the low-density organelle fraction (i.e. 1.92) that contains lysosomes, organelles in which lysosomal hydrolytic enzymes, capthesins, transform LeuDOX into DOX.

4.1 Introduction

Doxorubicin (DOX) (Figure 4-1A) is an anthracycline that has been used as a chemotherapeutic compound since 1969.[154] It is especially useful in treating leukemia, lymphomas and solid tumors such as breast cancer and osteosarcoma.[155] However, its use is often compromised by its major side effect, cardiotoxicity. To reduce DOX cardiotoxicity and improve its therapeutic index, the prodrug, *N*-L-leucyl-Doxorubicin (LeuDOX) (Figure 4-1B) was synthesized in the late 1970s by linking an amino acid, leucine, to the amine group of DOX.[156] LeuDOX can be converted to DOX by lysosomal enzymes such as capthesins.[36] It has been proven that LeuDOX is 3 to 4 times less cardiotoxic than DOX at an equimolar dose[157] and that the maximum tolerated dose (MTD) of LeuDOX in mice is 3.5 times higher than that of DOX.[158] At the MTD, LeuDOX is more effective than DOX in inhibiting xenograft growths.[158, 159]

Although the plasma and tissue pharmacokinetics and pharmacodynamics of LeuDOX have been widely studied,[41, 160, 161] the incorporation of LeuDOX into tumor cells and its transformation into DOX within the tumor cells are still not fully understood. It is not clear whether the reduced toxicity of LeuDOX is due to a lower cellular uptake of the prodrug compared to that of DOX or to the limited transformation of the prodrug into its active form, DOX. Moreover, the destination of LeuDOX within cells, i.e., its subcellular distribution, has not been studied.

Previous studies showed the subcellular distribution of DOX to be strongly associated with different types of toxicity. For example, DOX in the nucleus interacts with DNA and topoisomerase IIα, causing DNA breakage and leading to cell death;[162] DOX in mitochondria produces free radicals and results in mitochondria dysfunction,

which may contribute to cardiac toxicity.[163] Thus, in order to better understand LeuDOX cytotoxicity, the study of its subcellular distribution is indispensable.

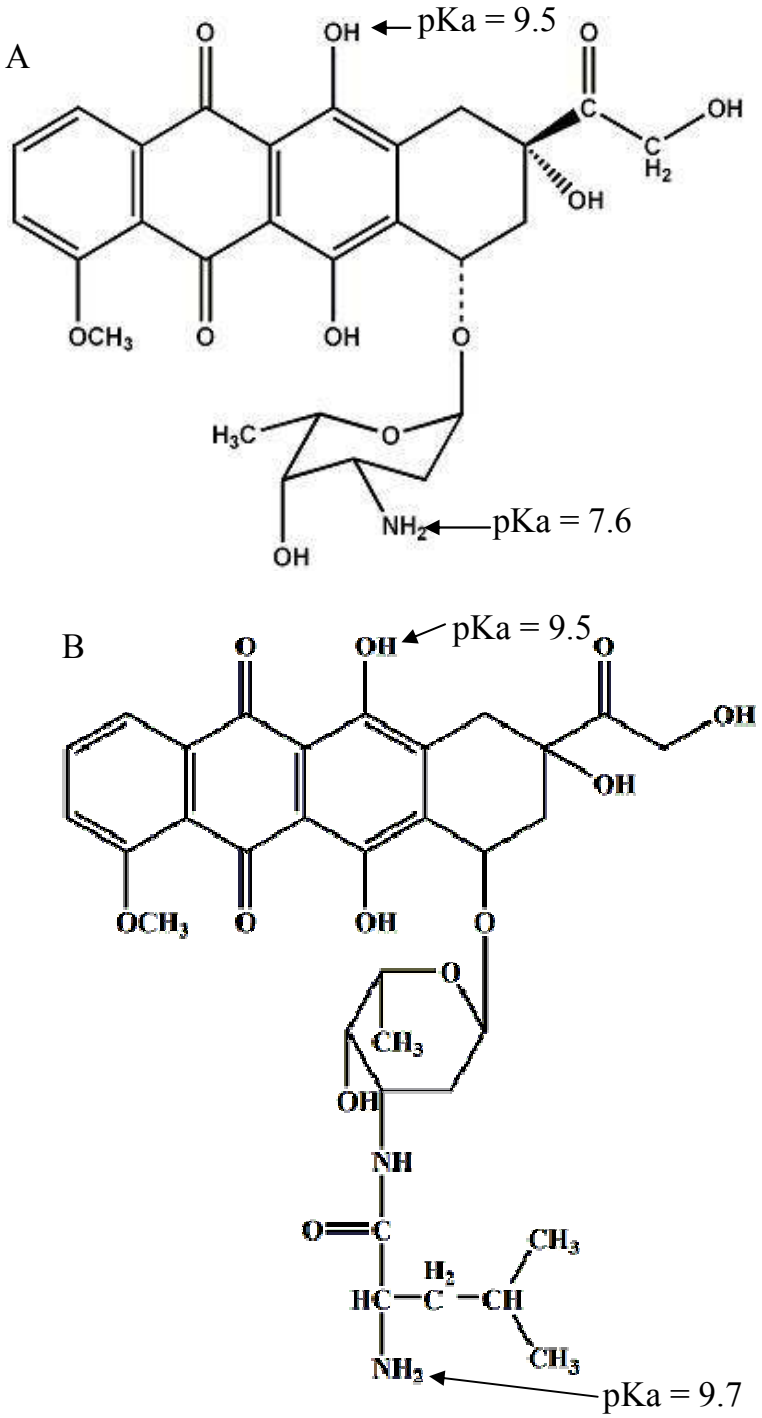

Figure 4-1. Structures of DOX and LeuDOX. The pKa of the amino and hydroxyl groups of Dox and LeuDox are indicted by arrows.

Capillary electrophoresis (CE) with laser-induced fluorescence detection (LIF) has been used to analyze DOX and its metabolites in plasma[164, 165] and cells.[121, 141] This method is especially compatible with subcellular analysis because it requires only nanoliters of samples. In addition, the high sensitivity of LIF detection makes it possible to analyze extremely small amounts (e.g. zeptomoles) of DOX. In this study, we used micellar electrokinetic chromatography (MEKC), a mode of CE, with LIF detection (i.e., MEKC-LIF) for the rapid and sensitive analysis of DOX and LeuDOX in whole cell lysates and subcellular fractions.

The MES-SA human uterine sarcoma cell line and its DOX resistant counterpart, MES-SA/Dx5, were our cell models. It is known that the mechanism of MES-SA/Dx5 resistance is mainly correlated with the overexpression of p-glycoprotein (PGP),[166, 167] which expels drugs such as DOX from cells, thereby reducing their accumulation.[168] It is reported that by modifying the sugar moiety of daunorubicin, an analog of doxorubicin, PGP-mediated drug resistance can be overcome.[169] Our results confirm not only the putative drug resistance of the MES-SA/Dx5 cell line, but uncovers high transformation rate of LeuDOX into DOX and high DOX intracellular levels in this cell line at equitoxic dose. In addition, we determined that the low-density organelle fraction, containing lysosomes, has a high DOX/LeuDOX ratio. The results point to the usefulness of capillary electrophoretic separations for investigating prodrug transformations while revealing more details on what occurs intracellularly after prodrug administration.

4.2. Material and methods

4.2.1 Chemicals and reagents

Doxorubicin hydrochloride was a generous gift from Meiji Seika Kaisha (Tokyo, Japan). Doxorubicinol was obtained from Qvantas Inc. (Newark, DE). Cetyl trimethyl ammonium bromide (CTAB), tricine, ethylenediaminetetraacetic acid tetrasodium salt dihydrate (EDTA), 3-(4,5-Dimethylthiazol-2-yl)-2,5- diphenyltetrazolium bromide (MTT) and Trypan Blue were from Sigma Aldrich (St. Louis, MO). Sodium borate decahydrate and sodium hydroxide were purchased from Fisher Scientific (Fair Lawn, NJ). 10× phosphate-buffered saline (PBS) was from EMD Chemicals (Gibbstown, NJ). Methanol, isopropanol, sodium dodecyl sulfate (SDS) and hydrochloric acid were from Mallinckrodt (Phillipsburg, NJ). McCoy's 5A medium was from Cellgro (Lawrence, KS). Calf serum, trypsin-EDTA and Rhodamine 123 were from Invitrogen (Carlsbad, CA). MES-SA and MES-SA/Dx5 cell lines were from the American Type Culture Collection (Manassas, VA).

4.2.2 Synthesis of LeuDOX

LeuDOX was synthesized by coupling the *N*-hydroxysuccinimide ester of *N*-trityl leucine with DOX based on the methods described by Stelakatos [170] and Anderson [171]. More details of the synthesis are included in Appendix B. The final yield was 33% and LeuDOX purity was 98.4% (Figure B-1).

4.2.3 Cell culture, IC_{50} value and sample preparation for MEKC analysis

MES-SA and MES-SA/Dx5 cells were incubated at 37°C and 5.2% CO_2 in McCoy's 5A medium supplemented with 10% calf serum. For splitting, once every week cells were detached from the culture flask with 0.5× trypsin - EDTA (0.025% trypsin - 0.27

mM EDTA) and then 90% of the resulting cell suspension was replaced with fresh medium. Between splits, half of the medium was replaced with fresh medium. MES-SA/Dx5 cells were treated with 500 nM DOX for 1 h once every 8 to 10 passages to maintain their DOX resistance.

The IC_{35} (the concentration of a drug that inhibits the growth of 65% of the treated cells as opposed to an untreated culture) and the IC_{50} values of DOX and LeuDOX on MES-SA and MES-SA/Dx5 were determined using the MTT assay [172]. Twenty-four hours after splitting, cells were treated with a medium containing DOX or LeuDOX, ranging in concentration from 10 nM to 100 μM. After 12 h, this medium was removed and the cells were rinsed twice with 1×PBS and incubated in fresh medium for another 60 h. The relative number of surviving cells with respect to an untreated control was determined using the MTT assay. The percent survivals versus drug concentrations were plotted (Figure B-2) and the IC_{35} and IC_{50} values for each compound were calculated from these plots.

The incorporation of LeuDOX and its transformation into DOX was investigated by treating the cells with DOX or LeuDOX for 12 h, 24 h post splitting. Upon completion of these treatments, the cells were pelleted by centrifugation (1000×g, 10 min) and washed with 1×PBS twice. The pellet was lysed with BS-10 buffer (10mM borate, 10mM SDS, pH 9.3) and then analyzed by MEKC. The equivalent cell density in the final lysates was 2×10^6 cells per ml. In order to investigate possible transformations of LeuDOX in the cell culture medium, a LeuDOX control was incubated in cell culture medium alone for 12 h and then analyzed by MEKC.

In order to prepare subcellular fractions, cells were pelleted and washed twice in STEP buffer (200 mM sucrose, 10 mM Tris-HCl, 0.1 mM EDTA, pH = 7.4) and then disrupted by 100 strokes in an ice chilled Dounce homogenizer (0.00025'' clearance, Kontes Glass, Vineland, NJ). The disruption efficiency was checked by Trypan Blue staining to ensure that more than 95% of the cells were disrupted. The nuclear enriched fraction (NF) was obtained as a pellet by centrifugation at 600×g for 20 min. The high density organelle fraction (HDOF), which contains the most mitochondria, was obtained as a pellet by centrifuging the supernatant from the previous fraction at 4000×g for 20 min. The low density organelle fraction (LDOF), which contains the most lysosomes, was obtained as a pellet by centrifuging the supernatant from the previous fraction at 15000×g for 30 min. The remaining supernatant is the cytosolic enriched fraction (CF).[173] All the fractions were diluted in BS-10 buffer so that in each fraction 1 ml of sample contains the organelles from 2×10^6 cells.

All the whole cell lysates and subcellular samples were frozen at -20ºC and analyzed within 10 days of preparation.

4.2.4 CE setup and analysis

MEKC of the whole cell lysates and the subcellular fractions was performed in a previously described home-built instrument.[174] The separation buffer contained 4 mM CTAB and 50 mM tricine, pH=8.5. A 7.1 nL sample was introduced into an uncoated fused-silica capillary (40.5 cm in length, 50 μm inner diameter and 150 μm outer diameter) (Polymicro Technologies, Phoenix, AZ) by hydrodynamic injection at 5.6 kPa

for 3 s and separated using a -400 V/cm electric field. The injection volume was calculated according to the Poiseuille equation

$$V = \frac{\Delta P d^4 \pi t}{128 \eta L} \qquad \text{(Equation 4-1)}$$

where V is the volume of sample injected into the capillary, ΔP is the pressure applied to the capillary when injecting sample (5.6 kPa), d is the inner diameter of the capillary (50 μm), t is the time that the pressure is applied (3 s), L is the total capillary length (40.5 cm), and η is the sample buffer viscosity which is similar to that of water, so that the viscosity of water (8.9×10^{-4} Pa·s) is used in the calculation.

The outlet of the capillary was located in a sheath flow cuvette in which the analytes were excited by a 488 nm argon-ion laser (JDS Uniphase, San Jose, CA) after migrating out from the capillary. The 2 mm polyimide coating at the detection end of the capillary was burned off to reduce background. Fluorescence from the analyte was collected at a 90° angle with respect to the laser beam by a 60× microscope objective (Melles Griot, Rochester, NY). A 505 nm long-pass filter (Omega Optical, Brattleboro, VT) and a pinhole were used to reduce the light scattering. Fluorescence from DOX and LeuDOX was selected by a 635 ± 27.5 nm band-pass filter (XF3015, Omega Optical, Brattleboro, VT) and finally detected by photomultiplier tube (Hamamatsu, Bridgewater, NJ) biased at 1000 V.

Prior to sample analysis, the capillary was conditioned with sequential flushes of 0.1 mM NaOH, water, 0.1 mM HCl, water and separation buffer for 30 min each, using 150 kPa pressure at the inlet. The same conditioning sequence was repeated between the injections of different samples, but for only two minutes per flush. Prior to sample analysis, the instrument was aligned by maximizing the fluorescence response of 1 nM

Rhodamine 123, which was made to continuously flow through the detector by applying a -400 V/cm electric field. The setup was the same as described above, except a 535 ± 17.5 nm band-pass filter (XF3007, Omega Optical, Brattleboro, VT) was used. The calculated limit of detection (LOD) was 15.2 ± 1.6 zmol as determined from the peak height of 7.1 amol Rhodamine 123 and three times the standard deviation of the background. The average peak height of Rhodamine 123 was also used as a reference to correct the variation in the alignment of the instrument on different days.

4.2.5 Data acquisition and analysis

The PMT output was sampled at 10 Hz and collected with a custom-written Labview program (National Instruments, Austin, TX). Data were smoothed using 12 point binomial smoothing in Igor Pro (Wavemetrics, Lake Oswego, OR). The amounts of DOX and LeuDOX in the whole cell lysates and subcellular fractions were estimated by calibration curves which were constructed based on the peak areas of DOX (Equation 4-2) or LeuDOX (Equation 4-3) and the moles of the drugs injected.

These equations are:

$$A_{DOX} = (9.9 \pm 0.1) \times 10^{15}\, m_{DOX} + (0.7 \pm 0.2);\ (r^2 = 0.999) \qquad \text{(Equation 4-2)}$$

$$A_{LeuDOX} = (8.1 \pm 0.3) \times 10^{15}\, m_{LeuDOX} + (1.6 \pm 0.9);\ (r^2 = 0.997) \qquad \text{(Equation 4-3)}$$

where A_{DOX} and A_{LeuDOX} are the peak areas of DOX and LeuDOX; m_{DOX} and m_{LeuDOX} are the moles of DOX and LeuDOX injected. Both curves are linear from 7.1×10^{-17} mol to 7.1×10^{-15} mol.

To compare the drug amounts in different treatments or in different subcellular fractions, statistical significance was tested with the Student's t test using statistic

software “R”. The null hypothesis, “there is no difference in drug amounts between treatments or in subcellular fractions”, was rejected when $P<0.05$.

4.3. Results and Discussion

4.3.1 CTAB based separation system

While MEKC based on SDS-containing buffers had been used previously to separate DOX and its metabolites,[131, 141] these buffer systems are incapable of separating DOX and LeuDOX, which made it necessary to explore the use of other surfactants, such as the cationic surfactant CTAB, for MEKC separations. A buffer containing 4 mM CTAB, 50 mM tricine (pH = 8.5) was adequate for separating DOX and LeuDOX with R_s = 1.98 (Figure 4-2A). Moreover, this separation system was also capable of separating DOX from DOXol (R_s = 1.53) (Figure 4-2B), which cannot be achieved in the borate-SDS buffer system.

In order to explain why DOX and LeuDOX can be separated in 4 mM CTAB, 50 mM tricine (pH 8.5), is it necessary to discuss the factors that contribute to the apparent mobility of the analyte in MEKC separations. They are: its electrophoretic mobility, the electroosmotic flow (EOF), the micelle’s electrophoretic mobility and the analyte’s partitioning into the micelles. The electrophoretic mobilities of DOX and LeuDOX can be easily modulated by changing the pH. According to the pKas of the amine and hydroxyl group of DOX (Figure 4-1), the calculated pIs of DOX and LeuDOX are 8.6 and 9.6, respectively.[8] At pH 8.5, DOX is practically neutral and does not have an electrophoretic mobility, while LeuDOX is positively charged and has an electrophoretic mobility. Because CTAB forms a double layer onto the inner wall of the fused silica

capillary, making this wall positive, the EOF carries analytes from the negative to the positive end of the capillary. In addition, the amino acid, leucine, makes LeuDOX more hydrophobic than DOX, which likely causes LeuDOX to partition into the CTAB micelles to a greater extent than DOX. These factors together make it possible to separate LeuDOX from DOX.

The LODs of DOX and LeuDOX in CTAB-tricine buffer were 4.3 ± 0.5 and 7.1 ± 0.8 amol, respectively, as calculated as the amounts that provide signals that are equal to three times the standard deviations of the background. These LOD's are not as good as those previously reported for MEKC systems using BS-10 buffer; the LOD of DOX was about 70 times lower (i.e. 61 zmol DOX).[141] On the other hand, the LOD of DOX in the CTAB-tricine buffer is 1000 times better than that from a high performance liquid chromatography (HPLC) separation, the most commonly used method in LeuDOX analyses.[161]

Although it is beyond the scope of this report, the reported LOD's may be improved by considering the following factors: (i) peaks are wider in CTAB-tricine buffer than in the BS-10 buffer ($W_{1/2,\ CTAB}$ = 7.13 ± 0.02 versus $W_{1/2,\ BS\text{-}10}$ = 2.05 ± 0.01[131]), (ii) the background noise is higher in the CTAB-tricine buffer than in the BS-10 buffer (i.e. 0.005 versus the 0.001 A.U.[131]), and (iii) fluorescence intensity of DOX is lower in CTAB-tricine buffer than in the BS-10 buffer (Figure B-3).

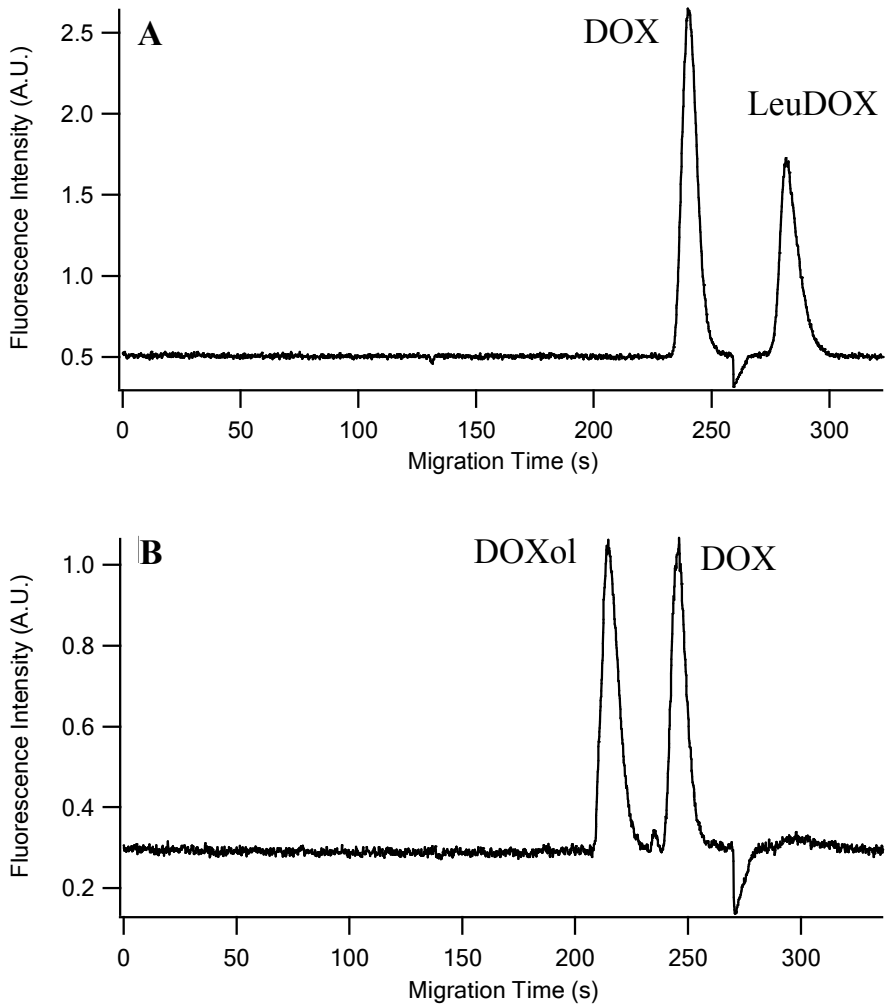

Figure 4-2. MEKC separation of DOX, LeuDOX and DOXol. (A) 3.6×10^{-15} mol DOX and 3.6×10^{-15} mol LeuDOX, (B) 1.4×10^{-15} mol DOX and 1.4×10^{-7} mol DOXol. Separations were performed in 4 mM CTAB, 50 mM tricine buffer (pH = 8.5) in a 40.5 cm long, 50 μm i.d. fused silica capillary at -400 V/cm after 3 s hydrodynamic injection of sample at 5.6 kPa. Analytes were excited by a 488 nm argon-ion laser and the fluorescence was detected with PMT bias at 1000 V after passing through a 635 ± 27.5 nm band-pass filter.

4.3.2 IC_{50} values of DOX and LeuDOX for MES-SA and MES-SA/Dx5 cell lines

The IC_{50} values of DOX for the MES-SA and MES-SA/Dx5 cell lines, as determined by the MTT assay, were approximately 0.7 μM and 7 μM, respectively. It has been reported that MES-SA/Dx5 is about 100-fold more resistant to DOX than is MES-SA when both of the cell lines are treated with DOX for 1 h, with viability the parameter

being measured.[175] However, the IC_{50} value of DOX for MES-SA/Dx5 determined here is only 10-fold higher than for MES-SA. The discrepancy between our values and the reported values is due to the different drug exposure times of our samples and the different parameters that we were measuring. Here, the cells were incubated with DOX for 12 h and cell growth was determined after 72 h of incubation.

The IC_{50} values of LeuDOX for the MES-SA and MES-SA/Dx5 cell lines were 3 and 15 μM, respectively. These IC_{50} values show that LeuDOX has a lower cytotoxicity than DOX in both cell lines, with the cytotoxicity of LeuDOX being 4.3 times lower in the MES-SA cell line and 2.1 times lower in the MES-SA/Dx5 cell line.

4.3.3 Incorporation and transformation of LeuDOX

After treating the MES-SA and MES-SA/Dx5 cells with equimolar or equitoxic concentrations of DOX and LeuDOX, the amounts of DOX and LeuDOX in the whole cell lysates were determined by MEKC-LIF. As a control, LeuDOX was incubated in the same cell culture medium for 12 h without any cells present and was then analyzed by MEKC-LIF: less than 1% of LeuDOX was transformed to DOX (Figure B-4). This demonstrates that there is no significant transformation of LeuDOX into DOX in the medium where no hydrolytic enzymes are present.

Equimolar DOX and LeuDOX treatments

Both MES-SA and MES-SA/Dx5 cells were treated with 10 μM DOX or LeuDOX. This concentration was chosen to keep more than 60% of the cells viable so that the results would be representative. Although this is not a pharmacokinetic study, this LeuDox concentrations used here are comparable to the highest LeuDOX found in the

plasma (21.3 ± 4.2 lM; mean ± SEM; n = 15) in the previous plasma pharmacokinetics of LeuDox in a phase I clinical trial.[160]

As shown in Figures 4-3A and 4-3B, MEKC-LIF was used to determine the amounts of DOX and LeuDOX in the whole cell lysates of the MES-SA and MES-SA/Dx5 cells. The shifts in the migration time of the different traces may be due to the adsorption of cellular components in the sample onto the capillary wall by electrostatic or hydrophobic interaction, which would alter the EOF.[176] The mobility of the small peak around 240 s was calculated and corrected according to the method described by Li, using the DOX peak as a reference [137]. This corrected mobility ($\mu_{corrected}$ = 4.70 ± 0.02 $cm^2 \cdot V^{-1} \cdot s^{-1}$, n=12) indicates that this peak is DOXol ($\mu_{standard}$ = 4.67 ± 0.03 $cm^2 \cdot V^{-1} \cdot s^{-1}$, n=3). Since the peak area of DOXol is less than 2% that of DOX or LeuDOX, any possible cytotoxic effects of DOXol are not considered to be relevant.

The DOX and LeuDOX incorporated into the cells and the percents of LeuDOX transformed into DOX are summarized in Table 4-1. In both LeuDOX treated cell lines, the total amount of LeuDOX plus DOX is similar to the total amount of DOX in the DOX-treated cell lines. These results are surprising because less drug content was expected to be found in the MES-SA/Dx5 cell line. That is, because of PGP expression in the MES-SA/Dx5, DOX was expected to be pumped out from these cells, resulting in lower accumulations of DOX in MES-SA/Dx5 cells than in MES-SA cells under equimolar DOX treatments. The results here suggest that PGP is unable to efflux a sufficient amount of DOX to offset the observed intracellular levels of DOX and LeuDOX.

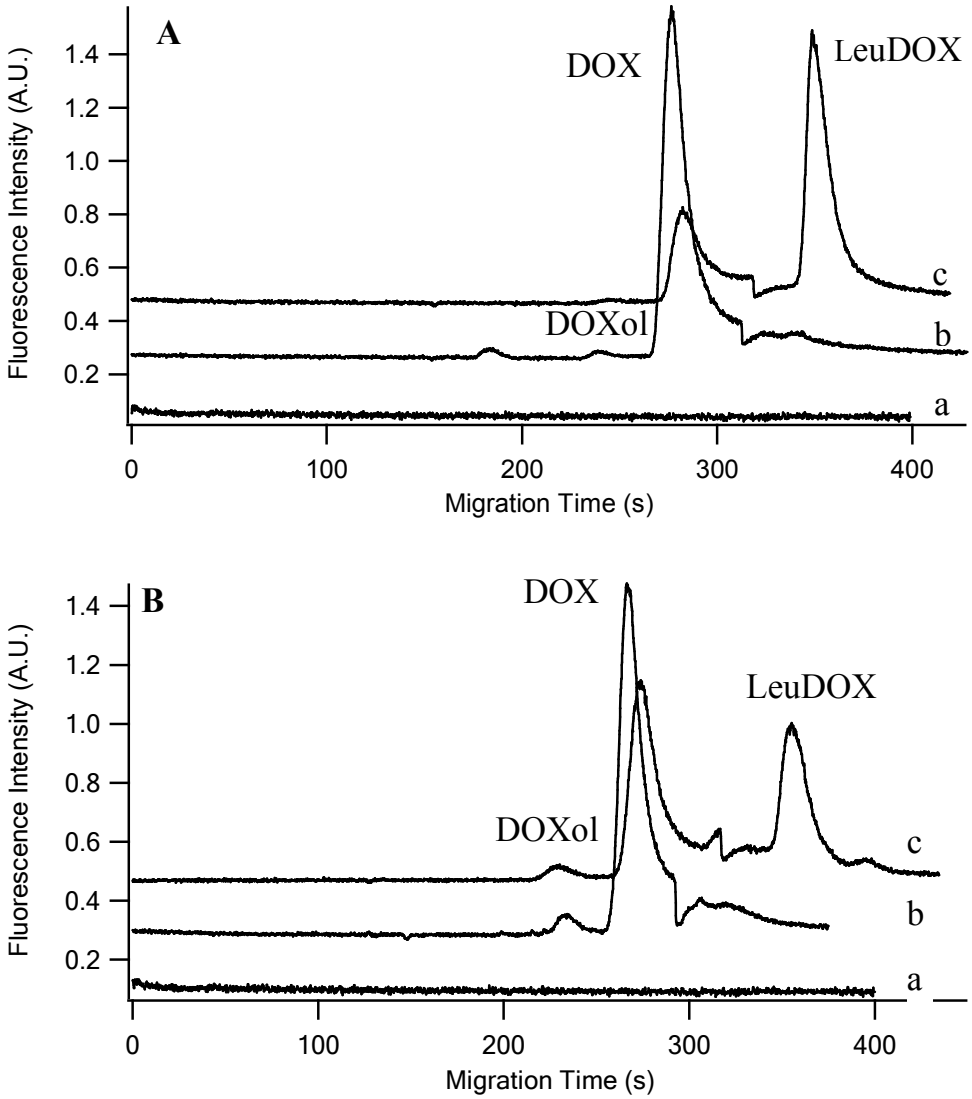

Figure 4-3. MEKC separation of whole cell lysate in DOX or LeuDOX treatments. (A) MES-SA cells, (B) MES-SA/Dx5 cells. In both figures, trace a: untreated cells; trace b: cells treated with 10 μM DOX and trace c: cells treated with 10 μM LeuDOX. Separation and detection conditions were same as in Figure 4-2. Fluorescence intensity of trace b and c were offset by 0.2 A.U. and 0.4 A.U. for clarify. Migration time of trace c was offset to match the DOX peaks with trace b.

The transformation of LeuDOX into DOX was 31.5%, in MES-SA cells, and 68.0% in MES-SA/Dx5 cells. Indeed, higher transformation in the resistant cell line is a sought benefit of any prodrug. Why is the transformation higher in the MES-SA/Dx5 cells? These results suggest that either the activity of hydrolytic enzymes such as capthesins is

higher in MES-SA/Dx5 cells or that more LeuDOX reaches the subcellular sites where the hydrolytic enzymes are found in these cells than in MES-SA cells.

The DOX amounts found in both cell lines after equimolar treatment seem to agree quite well with the IC_{50} values. In MES-SA cells, DOX levels were 3.8 times higher in DOX-treated cells than in LeuDOX-treated cells; the respective IC_{50} values were 4.3 fold lower. In MES-SA/Dx5 cells, DOX levels were 1.5 times higher in DOX-treated cells than in LeuDOX-treated cells; the respective IC_{50} values were 2.1 fold lower. These results confirm that DOX rather than LeuDOX is responsible for the observed cytotoxicity, and that LeuDOX cytotoxicity is determined by the percent of transformation of LeuDOX into DOX.

Table 4-1. Equimolar concentration treatments of DOX and LeuDOX

Cell line (treatment [a])	DOX [b]	LeuDOX [b]	Total [b]	% Transform
MES-SA (DOX)	2.67 ± 0.06 [c]	/	2.67 ± 0.06	/
MES-SA (LeuDOX)	0.71 ± 0.05	1.54 ± 0.07	2.24 ± 0.12	31.5 ± 1.8
MES-SA/Dx5 (DOX)	2.22 ± 0.20	/	2.22 ± 0.20	/
MES-SA/Dx5 (LeuDOX)	1.54 ± 0.20	0.73 ± 0.11	2.26 ± 0.36	68.0 ± 1.3

a. Cells were treated with 10 μM DOX or 10 μM LeuDOX
b. The amount of DOX, LeuDOX and total are in the unit of $\times 10^{-16}$ mole/cell
c. Average ± standard deviation, n=3

A previous report by Bennis indicated that the reduced cytotoxicity of LeuDOX was due to a lower degree of drug incorporation during a 2 h LeuDOX exposure of MCF-7 and K562 cell lines and their resistant counterparts.[62] Contrary to these findings, here we found the transformation of LeuDOX into DOX, rather than the incorporation of LeuDOX, to be the major cytotoxicity factor. However, the differences between this

study and that of Bennis may result from the differences in cell type or treatment time (e.g. 2 h in the Bennis study versus 12 h used here).

Equitoxic DOX and LeuDOX treatments

The incorporation and transformation of LeuDOX after treating both cell lines with the IC_{35} concentrations of DOX and LeuDOX were also investigated. The results of drug incorporation and transformation are listed in Table 4-2. The total amounts of DOX or LeuDOX incorporated into the cells in the four treatments were directly related to the drug amounts used in the treatments. In addition, the DOX levels for a given cell line were of similar magnitude, regardless whether DOX or LeuDOX was administered. These results further confirm that it is the DOX levels in the cells, rather than the DOX plus LeuDOX levels, that are related to the cytotoxicity.

Table 4-2. Equitoxic concentration treatments of DOX and LeuDOX

Cell line (treatment)	Treatment [a] (μM)	DOX [b]	LeuDOX [b]	Total [b]	% Transform
MES-SA (DOX)	2.0	0.53 ± 0.08 [c]	/	0.53 ± 0.08	/
MES-SA (LeuDOX)	8.3	0.36 ± 0.04	1.03 ± 0.09	1.40 ± 0.13	25.8 ± 0.9
MES-SA/Dx5 (DOX)	17.0	2.95 ± 0.59	/	2.95 ± 0.59	/
MES-SA/Dx5 (LeuDOX)	27.5	2.09 ± 0.38	1.88 ± 0.44	3.97 ± 0.82	52.9 ± 1.3

a. Cells were treated with DOX or LeuDOX according to their respective IC_{35} values
b. The amount of DOX, LeuDOX and total are in the unit of $\times 10^{-16}$ mole/cell
c. Average ± standard deviation, n=3

On the other hand a comparison between the two cell lines show that, following DOX and LeuDOX equitoxic treatments, the intracellular amount of DOX in MES-SA/Dx5 cells is about 6-fold higher than that in MES-SA cells. This difference indicates that more intracellular DOX is needed to achieve the same cytotoxicity in the

DOX resistant cell line as in the DOX sensitive cell line. This is surprising because, even in the presence of PGP, the same intracellular concentrations should be required if the origin of cytotoxicity is the same in both cell lines (e.g. via topoisomerase interactions). Thus, other mechanisms of cell resistance reported in other cell lines, such as drug sequestration in intracellular vesicles, increased DNA repair, or altered DOX-topoisomerase interaction may explain the observed differences.[177, 178]

4.3.4 Subcellular distribution of DOX and LeuDOX

The subcellular localization of DOX and LeuDOX provides further clues to the processes involved in the cytotoxicity of these drugs. In these initial studies, we chose the MES-SA/Dx5 cell line because a higher percent of LeuDOX is transformed into DOX by this cell line. Different subcellular fractions of MES-SA/Dx5 cells treated with 10 μM DOX or LeuDOX were prepared by differential centrifugation as described in the Materials and Methods Section. The amounts of LeuDOX and DOX and their ratios in each subcellular fraction are summarized in Table 4-3.

Table 4-3. Subcellular distribution in DOX and LeuDOX treated MES-SA/Dx5 cells.

	LeuDOX treated [a]				DOX treated [a]
	DOX [b]	LeuDOX [b]	Total [b]	Ratio (DOX/LeuDOX)	DOX [b]
CF	0.38 ±0. 04[c]	0.34 ± 0.05	0.72 ± 0.09	1.12 ± 0.05	0.35 ± 0.04
NF	2.4 ± 0.5	0.83 ± 0.06	3.3 ± 0.5	2.9 ± 0.4	3.1 ± 0.3
HDOF	1.4 ± 0.2	0.86 ± 0.06	2.3 ± 0.2	1.7 ± 0.1	0.66 ± 0.05
LDOF	0.23 ± 0.09	0.12 ± 0.04	0.4 ± 0.1	1.9± 0.2	0.19 ± 0.02
Total	4.5 ± 0.7	2.2 ± 0.2	6.7 ± 1.0	2.1 ± 0.4	4.3 ± 0.4

CF: cytosolic enriched fraction, NF: nuclear enriched fraction, HDOF: high density organelle enriched fraction, LDOF: low density organelle enriched fraction.
a. Cells were treated with 10 μM DOX or 10 μM LeuDOX
b. The amount of DOX, LeuDOX and total are in the unit of $\times 10^{-16}$ mole/cell
c. Average ± standard deviation, n=3

Several factors influence the accumulation and subcellular distribution of the DOX and LeuDOX: (i) The organelle volume, (ii) the presence of hydrolytic enzymes in a given organelle, (iii) the pH within the organelle, (iv) and the presence of protein pumps such as PGP. Larger organelles, such as the nucleus, are expected to accumulate more of the drugs. Acidic organelles containing hydrolytic enzymes such as capthesins can more easily transform LeuDOX into DOX. The low pH of acidic organelles may also lead to significant sequestration of DOX and LeuDOX.[177] The expression of active PGP on an organelle membrane leads to a reduction in the levels of any drugs that are PGP substrates.

In our LeuDOX-treated cells, the highest and lowest amounts of DOX were found in the NF and the LDOF, respectively. That NF contains the highest amounts of DOX may be explained by its large nucleus volume and the high affinity of DOX to DNA. That LDOF contains the lowest amounts may be explained by the smaller size and total volume of the organelles found in this fraction (e.g., lysosomes). For LeuDOX-treated cells, the highest amount of LeuDOX was found in both NF and HDOF, and lowest in LDOF. The high amounts of LeuDOX found in HDOF, which contains most mitochondria, may be due to the higher hydrophobicity of LeuDOX, which makes it easier for it to partition into the mitochondria membranes.

It is also worth discussing the DOX/LeuDOX ratio in each subcellular fraction as this parameter tends to normalize differences in organelle size. The lowest DOX/LeuDOX ratio was found in the CF (i.e. 1.12). The highest ratio (i.e. 2.92) was found in the NF, followed by the ratio (i.e. 1.92) in the LDOF that contains lysosomes. That the highest abundance is in the NF may result from DOX having about three times more affinity to

DNA than LeuDOX does.[36] The high DOX/LeuDOX ratio of the LDOF is in agreement with the localization of hydrolytic enzymes, i.e., capthesins, in the lysosomes.

4.4. Conclusions

We report the development of a CTAB-based MEKC-LIF separation of DOX and LeuDOX that made it possible to determine the amounts of LeuDOX and DOX in the whole cell lysates and subcellular fractions of MES-SA and MES-SA/Dx5 cells. The results suggest that only the amount of the parent drug, DOX, within tumor cells is related to the cytotoxicity of LeuDOX. The transformation of LeuDOX into DOX within cells is responsible for the cytotoxicity of the prodrug, as the cellular uptake of DOX and LeuDOX is similar in both cell lines. Our study of the subcellular distribution of LeuDOX-treated cells revealed the amounts and ratios of DOX and LeuDOX in four subcellular fractions. The highest ratio (i.e. 2.92) was found in the NF, followed by the ratio (i.e. 1.92) in the LDOF that contains lysosomes, organelles in which lysosomal hydrolytic enzymes, capthesins, transform LeuDOX to DOX.

Overall, the fast and sensitive MEKC-LIF method reported here has provided some new insights into the intracellular fate of LeuDOX. The method can be further extended to study the fate of other fluorescent prodrugs within cells and elucidate their cytotoxicity mechanisms.

Chapter 5

Micellar Electrokinetic Chromatography Monitors Doxorubicin Metabolism in Subcellular Fractions of Young Adult and Old Fischer 344 Rat Livers

This unpublished work has been submitted to *Journal of Gerontology Series A: Biological Sciences*

HPLC-LIF-MS work was done by Joseph B. Katzenmeyer. The material is included with permission.

We thank Professor L. Thompson and her research group, primarily W. Torgerud, who handled animal protocols and procedures.

The pharmacokinetics and toxicity of doxorubicin (DOX), a widely used anti-cancer drug, is different in young adult and old cancer patients. Since the subcellular distribution and metabolism of DOX are associated with its toxicity, it is critical to develop technologies to establish the effect of aging on DOX metabolism at subcellular level. In this study, we report the use of micellar electrokinetic chromatography with laser-induced fluorescence detection (MEKC-LIF) to monitor the metabolism of DOX over a 2 h period in subcellular fractions isolated from young adult (11 months, 100% survival rate) and old (26 months, ~25% survival rate) Fischer 344 rat livers. The fractions of DOX metabolized in both mitochondria- enriched and post-mitochondria fractions (MF and PMF, respectively) of young adult were larger than the respective fractions of old rat liver. 7-deoxydoxorubicinolone and 7-deoxydoxorubicinone were identified using internal standard addition and structural elucidation by high-performance liquid chromatography with combined LIF and mass spectrometry detection. In addition, two and one unidentified metabolites were observed in young adult rat liver and one of them is only in young PMF. Due to the low sample demands, simplified sample processing procedures, short analysis times and low limit of detections, MEKC-LIF is a promising technique in monitoring drug metabolism at subcellular level and detecting low abundant metabolites in aging studies.

5.1. Introduction

The pharmacokinetics and toxicity of chemotherapy drugs such as doxorubicin (DOX), etoposide, ifosfamide, daunorubicin, mitomycin, cisplatin and methotrexate change with aging.[79] A study of daunorubicin, showed that the area under the time versus

plasma concentration curve of daunorubicinol, one of the major metabolites of daunorubicin, increased by 2-4 times in patients over 60 year old compared to younger patients.[80] As daunorubicinol is associated with cardiotoxicity,[81] this result suggested that the altered metabolism in old patients may compromise the pharmacotherapy of the elderly. In agreement, equal chemotherapy treatments, including treatment with DOX, accelerated toxicity in old than in younger patients.[82] Understanding the altered metabolism of chemotherapy drugs in the elderly would help to administrate proper dose and avoid adverse effects.

The liver is the principal organ for the metabolism of xenobiotics.[179] For example, the metabolism and elimination of DOX is primarily through the hepatobiliary route.[180] Although liver function appears to be well preserved relatively well during aging,[181] the morphological and structural changes suggest the opposite.[182] Liver weight is reduced with aging in both men and women,[183] which is thought to be responsible for the decline in hepatic drug metabolism.[184] However, the studies on the effect of aging on hepatic enzymes reveal conflicting results, i.e., the total enzyme content and/or activity may or may not be affected by aging.[83, 84] Some results showed that no relationship has been found between age and the content and/or activities of various cytochrome P450 enzymes in human liver microsomes,[85] while others showed aging related decline in total cytochrome P450 content and some cytochrome P450 activities (e.g., CYP3A and CYP2E1).[86] To reveal the changing in cytochrome P450 activities at the genetic level, in last ten years, DNA array technology has been applied to study the aging-induced changes in gene expression. A study of 3000 genes in the male rat liver found 47 unique transcripts were affected by aging. Among them, 29 are involved in drug or intermediary

metabolism. [87] For example, the gene expressions of NADPH cytochrome P450 oxidoreductase and CYP2C7 are increased, while the expression of CYP3A2 is reduced.[87] As the results of aging induced changes of enzyme activities are controversial, studying changes of metabolic profile in young adult and old livers is a valuable approach to identify metabolic pathways and enzymes that are affected by aging.

Most studies on aging-related changes in drug metabolism are based on the plasma or tissue pharmacokinetics of the drugs, which may miss important cellular and subcellular information that is associated with cytotoxicity. For example, DOX metabolites accumulating in mitochondria may be involved in cardioctoxicity.[185] Moreover, organelle function may be affected by aging. According to the recognized cellular mechanisms of aging, i.e., oxidative stress and mitochondrial dysfunction,[186] mitochondrion is the organelle that is affected most by aging. Endogenous free radicals are generated within mitochondria and are suspected to cause protein damage and enzyme inactivation.[187] Besides microsomes, mitochondria also contain drug metabolizing enzyme cytochrome P450 such as CYP2B and CYP3A4.[67] These enzymes can be modified and inactivated during aging. For this reason, it is necessary to investigate the subcellular metabolism of anti-cancer drugs, especially in mitochondria in the elderly.

Micellar electrokinetic chromatography with laser induced fluorescence detection (MEKC-LIF) is ideal for the analysis of fluorescent compounds such as DOX and its metabolites. It has low limits of detection (i.e. 10^{-18} to 10^{-20} mole of DOX),[188, 189] making it possible to detect low-abundant metabolites which cannot be otherwise detected. In addition, samples are directly dissolved in the separation buffer containing a surfactant, making sample extraction unnecessary and avoiding analyte losses during the

extraction. Moreover, MEKC only requires nanoliter sample volumes, which is advantageous in the analysis of small volumes, such as those from subcellular fractions. Using MEKC-LIF, 12 metabolites of DOX were detected in subcellular fractions of NS-1 mouse hybridoma cells.[189] On the other hand, MEKC-LIF alone cannot provide unique identification of metabolites. Other techniques such as high performance liquid chromatography with mass spectrometry detection (HPLC-MS) are more suitable to identify metabolites,[190] albeit lacking the attributes of MEKC-LIF mentioned above.

In this study we used MEKC-LIF to monitor liver metabolism of DOX in subcellular fractions (mitochondria-enriched fraction (MF) and post-mitochondria fraction (PMF)) from livers of young adult (11 months, 100% survival rate) and old (26 months, ~25% survival rate) Fischer 344 rats. Aided by spiking of samples with neat standards and complementary analysis of PMF by HPLC-LIF-MS we were able to suggest the identity of two metabolites, 7-deoxydoxorubicinone (7-deoxyDOXone) and 7-deoxydoxorubicinolone (7-deoxyDOXolone), and suggested the absence of doxorubicinol (DOXol) and doxorubicinone (DOXone) in rat liver metabolism. Furthermore, two unidentified metabolites were observed in young adult liver but absent in the old liver; one of these metabolites was also absent in the young adult MF. While the PMF is more metabolically active than the MF in both young adult and old rats, DOX metabolism was clearly reduced in the old relative to the young adult livers. The analytical approach to monitor subcellular metabolism holds promise in studying the effect of aging on drug metabolism in animal models and human tissue biopsies.

5.2. Material and methods

5.2.1 Chemicals and reagents

Doxorubicin hydrochloride was a generous gift from Meiji Seika Kaisha Ltd. (Tokyo, Japan). Doxorubicinol and doxorobicinone were from Qvantas Inc. (Newark, DE). Bradford reagent, protease inhibitor cocktail and β-nicotinamide adenine dinucleotide 2′-phosphate reduced tetrasodium salt hydrate (NADPH) were purchased from Sigma-Aldrich (St. Louis, MO). Sodium dodecyl sulphate (SDS), hydrochloric acid (HCl), magnesium chloride, potassium phosphate monobasic and dibasic were from were from Mallinckrodt (Phillipsburg, NJ). Sodium borate decahydrate and sodium hydroxide (NaOH) were from Fischer Scientific (Fair Lawn, NJ). 10× phosphate-buffer saline (10× PBS containing 1.37 M NaCl, 14.7 mM KH_2PO_4, 78.1 mM Na_2HPO_4, and 26.8 mM KCl) was from EMD Chemicals (Gibbstown, NJ). γ-cyclodextrin (γ-CD) was from TCI America (Portland, OR). Fluorescein was from Invitrogen (Carlsbad, CA).

Potassium phosphate buffer (100 mM, pH = 7.4) with 1% (v/v) protease inhibitor cocktail was used as homogenization and incubation buffer. MEKC separation buffer was made up of 50 mM borate, 50 mM SDS and 20 mM γCD (pH = 9.3) (BS50-γCD20).

5.2.2 Preparation of liver subcellular fractions

Liver samples were obtained from a pair of young adult (11 months old) and old (26 months old) female Fischer 344 rats with a life span of 29 month.[191] The animal protocol was approved by the University of Minnesota Institutional Animal Care and Use Committee. The livers were removed after anesthesia and kept on ice-cold 1×PBS until homogenization (within 30 min of removal). They were cut into small pieces and washed with 1×PBS three times. After washing, they were homogenized (1.5 ml homogenization

buffer was added to 1 g liver sample) by 5 strokes in an ice-chilled Dounce homogenizer (0.00025" clearance, Kontes Glass, Vineland, NJ). The homogenate was centrifuged at 600g for 10 min to remove nuclei, intact cells and liver chunks. The supernatant (post nuclear fraction, PNF) was further centrifuged at 9,000g. The resulting supernatant (post mitochondria fraction, PMF) was saved for further use and the pellet (mitochondria-enriched fraction, MF) was reconstituted in incubation buffer. MF also contains not only mitochondria but some lysosomes and peroxisomes as well; PMF is made up of microsomes and cytosol. The protein amounts in MF and PMF were determined using Bradford assay according to the manufacture's (Sigma-Alrich) protocol. The volume of the two fractions was adjusted with incubation buffer so that the protein concentrations were the same in both fractions (8 mg/ml).

5.2.3 *In vitro* metabolism of DOX

DOX (10 μM) and cofactors (1 mM NADPH and 5 mM $MgCl_2$) were added into MF and PMF for *in vitro* metabolism. The start of the reaction was defined as the addition of DOX. The mixtures were incubated at 37 ºC in a heated mixer (Eppendorf Thermomixer). Samples were taken out at four different time points (15 min, 30 min, 1 h and 2 h) and the reaction was stopped by freezing the sample in dry ice. The samples were kept at -80 ºC until analysis.

5.2.4 MEKC-LIF analysis

The samples were analyzed by micellar electrokinetic chromatography with laser-induced fluorescence detection (MEKC-LIF). Before analysis, MF and PMF were

diluted 25 or 50 times with separation buffer. Samples were introduced into a fused silica capillary (50 μm I.D. and 150 μm O.D., Polymicro Technologies, Phoenix, AZ) by hydrodynamic injection at 12 kPa for 2 s. Then the capillary was brought into a vial with separation buffer and MEKC was performed under a +400 V/cm electric field in a home-built instrument equipped with post-column LIF detection, previously described.[144] Briefly, a sheath flow cuvette encased the detection end of the capillary. The last 2-mm of this end had the polyimide coating burned off to reduce the background fluorescence caused by this material. As fluorescent analytes migrated out from the capillary, they were excited at 488 nm with an argon ion laser (JDS Uniphase, San Jose, CA). Fluorescence was collected at a 90° angle with respect to the laser beam by a 60× microscope objective (Universe Kogaku, Inc., Oyster Bay, NY). A 505 nm long-pass filter (505 AELP, Omega Optical, Brattleboro, VT) and a 1.4 mm pinhole were used to reduce light scattering. A 635 ± 27.5 nm (XF3015, Omega Optical, Brattleboro, VT) was used to select fluorescence from DOX and metabolites. Fluorescence was then detected in a photomultiplier tube (PMT) (Hamamatsu, Bridgewater, NJ) biased at 1000 V. The PMT output was sampled at 10 Hz and processed with a home-written Labview program (National Instruments, Austin, TX).

Prior to MEKC analysis, the capillary was conditioned with sequential flushes of 0.1 mM NaOH, water and separation buffer for 30 min each using 150 kPa pressure at the inlet. The separation buffer was replaced every 2 h with a fresh one to avoid electrolyte depletion and buffer contamination. Prior to sample analysis, the instrument was aligned by maximizing the response of 5×10^{-10} M fluorescein which continuously flowed through the detector while applying a +400 V/cm electric field.

5.2.5 Data analysis

Electropherograms were processed by Igor Pro (Wavemetrics, Lake Oswego, OR) to determine peak intensity and area of DOX and metabolites. The peak area of each metabolite (A_i) was adjusted with its fluorescence quantum yield relative to that of DOX:

$$A_{i,adj} = \frac{A_i}{\Phi_i} \qquad \text{(Equation 5-1)}$$

where $A_{i,adj}$ is the adjusted peak area of each metabolite and Φ_i is its fluorescence quantum yield relative to DOX. The fluorescence quantum yields of DOXol and 7-deoxyDOXone relative to DOX were determined by comparing the fluorescence intensities over the 607 to 663 nm range of equimolar (5 μM) solutions in the MEKC separation buffer (i.e., BS50-γCD20). This wavelength range was chosen according to the transmission range of the 635 ± 27.5 nm bandpass filter used in MEKC-LIF. The fluorescence intensities were measured at 488 nm excitation with a Jasco FP-6200 spectrofluorometer (Jasco, Tokyo, Japan). The relative quantum yield of DOXol to DOX was 1.38, and 7-deoxyDOXone to DOX was 0.76 (Figure C-1). Since the standard of 7-deoxyDOXolone is not available, it relative quantum yield was estimated from that of DOX, DOXol and 7-deoxyDOXone. The relative quantum yield of DOXol to DOX should be equal to that of 7-deoxyDOXolone to 7-deoxyDOXone due to the similarity in the structures of these two pairs. Thus, the relative quantum yield of 7-deoxyDOXolone to DOX was assumed to be 1.05. The quantum yields of the two unidentified metabolites were assumed to be same as that of DOX.

The percent of DOX and metabolites in each reaction mixture was calculated as

$$Percent = \frac{A_{i,adj}}{\sum A_{i,adj}} \times 100 \qquad \text{(Equation 5-2)}$$

The limit of detection (S/N=3) of DOX in BS50-γCD20 buffer was (4.9 ± 0.5) × 10^{-18} mole (n = 3) as determined from the peak intensity resulting from injecting 8.4 × 10^{-16} mole of DOX.

5.3. Results

5.3.1 Identification of metabolites

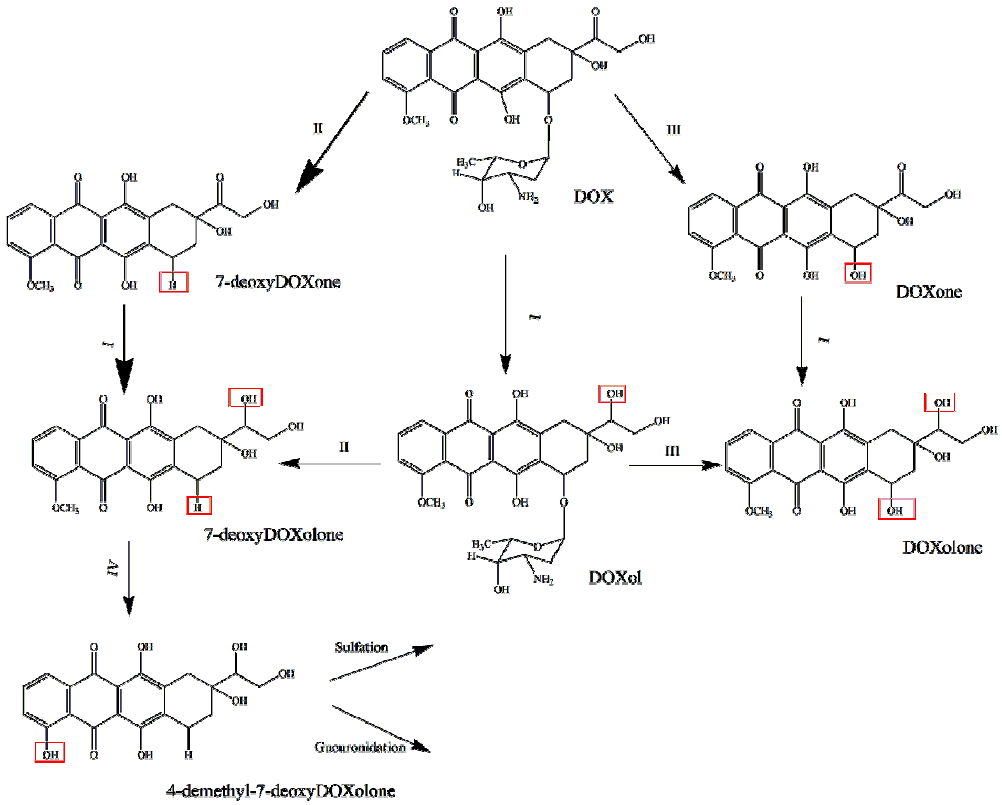

Figure 5-1. Possible metabolic pathways of DOX. Squares indicate the chemical sites of reaction: (I) carbonyl reduction by NADPH-dependent carbonyl reductase, (II) reductase-type deglycosidation by NADPH-cytochrome *c* reductase, (III) hydrolase-type deglycosidation by glycosidase, (IV) demethylation by cytochrome P450. The possible metabolic pathway of DOX in this study is shown in bold arrows

Previous studies showed that DOX is metabolized to different metabolites (e.g., DOXol, DOXone, 7-deoxyDOXone and 7-deoxyDOXolone) in human and animals

through a series of Phase I and phase II reactions include carbonyl reduction, reductive glycosidic cleavage, hydrolytic glycosidic cleavage, demethylation, sulfation and glucuronidation (Figure 5-1).[63, 192, 193]

In our study, three peaks were also observed after incubating DOX with MF of a young adult rat liver for 1h (Figure 5-2, trace a). In MEKC-LIF, the identification of peaks in electropherograms is usually a challenge. Internal standard addition and mobility comparison are the two commonly used methods to identify compounds.

We used the addition of DOXol and DOXone standards to narrow down on the identity of the metabolite peaks (Figure 5-2, trace b). The addition of DOXol resulted in the appearance of two more peaks which were DOXol enantiomers.[144] Neither of the peaks overlapped with the peaks in the sample after 1 h incubation. Thus, DOXol was not detected. DOXone was observed as a shoulder peak in the major metabolite peak (M2). It can be inferred that the major metabolite formed after 1 h incubation has a structure similar to DOXone, but it is not DOXone.

The electrophoretic mobility of each compound in MEKC is also a useful identifier. The procedure of calculating and correcting the mobilities of the metabolites is described in Appendix C. Comparing the corrected mobilities of metabolites with that of the standards confirmed that DOXol was not detected (Table C-1), but it did not exclude the possible detection of DOXone. This is probably due to the similarity in the mobilities of DOXone and M2. In MEKC, the mobility of a compound is affected by many factors such as temperature, sample matrix and inner surface of the capillary wall, which are difficult to control. Therefore, the run-to-run and day-to-day data in mobilities may impede a successful assignments of compounds based on this criterion alone.[194]

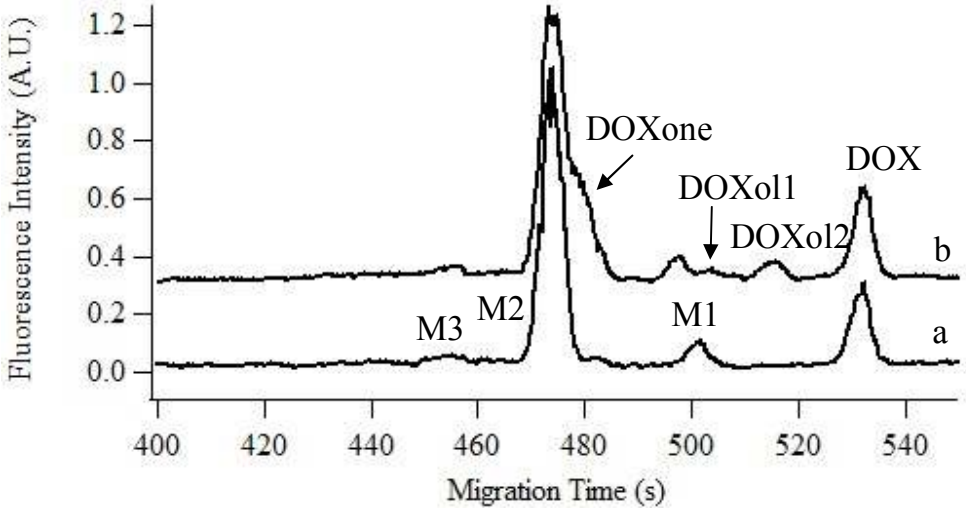

Figure 5-2. Identification metabolites by internal standard addition. Electropherograms of 10 μM DOX incubated in MF for 1 h (trace a) and with internal addition of DOX, DOXol and DOXone (trace b). Trace b is y-axis offset for clarity. M1 is 7-deoxyDOXone and M2 is 7-doxyDOXolone. Separations were performed in a 45.7 cm long, 50 μm i.d. fused silica capillary at 400 V/cm in BS50-γCD20 buffer. Analytes were excited at 488 nm and fluorescence was detected at 635 ± 27.5 nm.

To further indentify the metabolites detected, we used HPLC-LIF-MS to obtain structural information in parallel experiments. The study of DOX metabolism in PMF of a rat liver by HPLC-LIF-MS identified 7-deoxyDOXone and 7-deoxyDOXolone as the only two detectable metabolites. The more abundant of these two was 7-deoxyDOXolone (Figure C-2 and S3). In agreement with MEKC-LIF no DOXol was detected (Figure C-2). Their elution order of 7-deoxyDOXolone, DOXone and 7-deoxyDOXone is in perfect agreement with their hydrophobicity and their molecular structure (Figure 5-1). Since MEKC separations are based on the partition of the analytes into micelles, the separation order follows that of HPLC reverse phase separations. Therefore, M1 is tentatively identified as 7-deoxyDOXone, while M2 or M3 could be 7-deoxyDOXolone. Lastly, based on the relative abundance of 7-deoxyDOXone and 7-deoxyDOXolone in

HPLC-LIF-MS, we established that M2 is 7-deoxyDOXolone and that M1 is 7-deoxyDOXone. These assignments will be used in the rest of this report.

5.3.2 Effect of cofactors NADPH and Mg^{2+} on enzyme metabolic activity

In order to further characterize the metabolites, the metabolic reactions were carried out in the presence or absence of cofactors (i.e., NADPH and Mg^{2+}) (Figure 5-3). Three metabolites were observed after 1 h incubation under both reaction conditions. However, in the buffer with cofactors, about 65% DOX was metabolized, while in the buffer without cofactors, only about 25% DOX was metabolized.

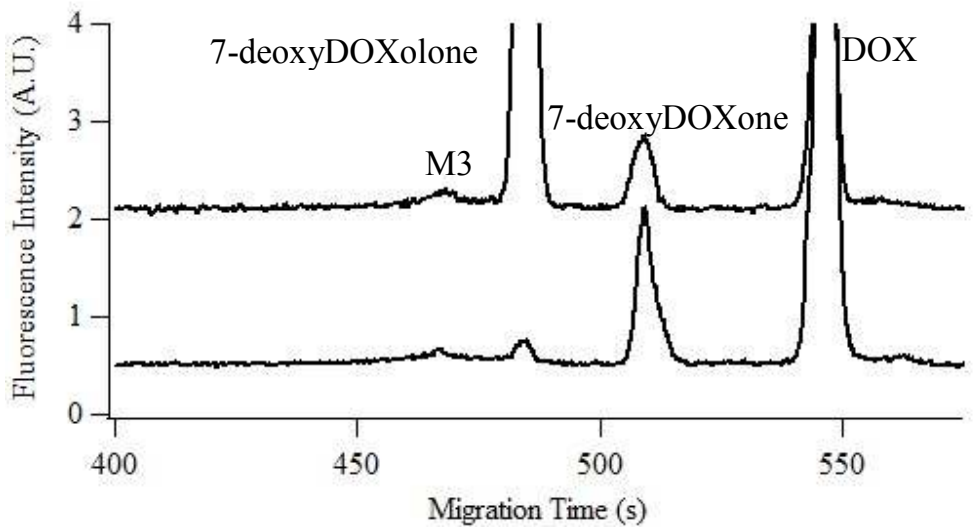

Figure 5-3. Effect of cofactors on the metabolic activity of rat liver. Electropherograms of 10 μM DOX incubated in MF for 1 h without cofactors (trace a) or with 1 mM NADPH and 5 mM Mg^{2+} (trace b); trace b is y-axis offset for clarity. Separations were performed in a 45.3 cm long, 50 μm i.d. fused silica capillary. Other conditions were same as in Figure 5-2.

The percent of each metabolite formed is listed in Table 5-1. The percent of M3 did not significantly change with the addition of cofactors, while the percent of 7-deoxyDOXone and 7-deoxyDOXolone decreased and increased, respectively.

Table 5-1. Percent of DOX and metabolites with and without the addition of cofactors

	7-deoxyDOXone[a]	7-deoxyDOXolone	M3	DOX
with cofactors[b]	8.0 ± 0.2	55.0 ± 0.6	1.5 ± 0.3	35.4 ± 0.7
without cofactors	20 ± 0	1.7 ± 0.1	2.7 ± 0.6	75.6 ± 0.5

a. The results are presented in percent which is calculated according to Equation 2. Variation is represented in standard deviation (n = 3)
b. Cofactors: 1 mM NADPH and 5 mM Mg^{2+}

5.3.3 Metabolism in the MF and PMF of young adult and old rat liver

We determined that the MF and PMF of the young adult are more metabolically active than the respective fractions in the old rat (Figure 5-4). In the PMF of the young adult rat liver, more than 95% DOX was metabolized while only 53% DOX was metabolized in the old rat liver after a two-hour incubation. Regarding the number of detected metabolites, four and two were observed in the PMF of young adult (Figure 5-4A) and the old (Figure 5-4C) rat livers. The trend is similar in the MF of these rat livers, about 27% and 7% DOX was metabolized in the young adult and old, respectively (Figure 5-4B and 5-4D, respectively). Referring to the metabolite identities in the young adult and old livers, 7-deoxyDOXolone was the major metabolite in both PMF and MF; M3 and M4 were only observed in the young adult rat liver, and M4 is unique in young adult PMF.

5.3.4 DOX metabolism in young adult and old as a function of time

The low sample demands and short analysis times of MEKC-LIF relative to HPLC-LIF-MS makes the former an attractive technique when monitoring the changes in abundance of each metabolite. Using MEKC-LIF, we monitored the changes of DOX and the major metabolite, 7-deoxyDOXolone in PMF and MF (Figure 5-5A and B, respectively) and 7-deoxyDOXone, M3 and M4 in PMF and MF (Figure 5-5C and D,

respectively) as a function of time. The numeric values are tabulated in the Supplementary Material (Appendix C), Table C-2.

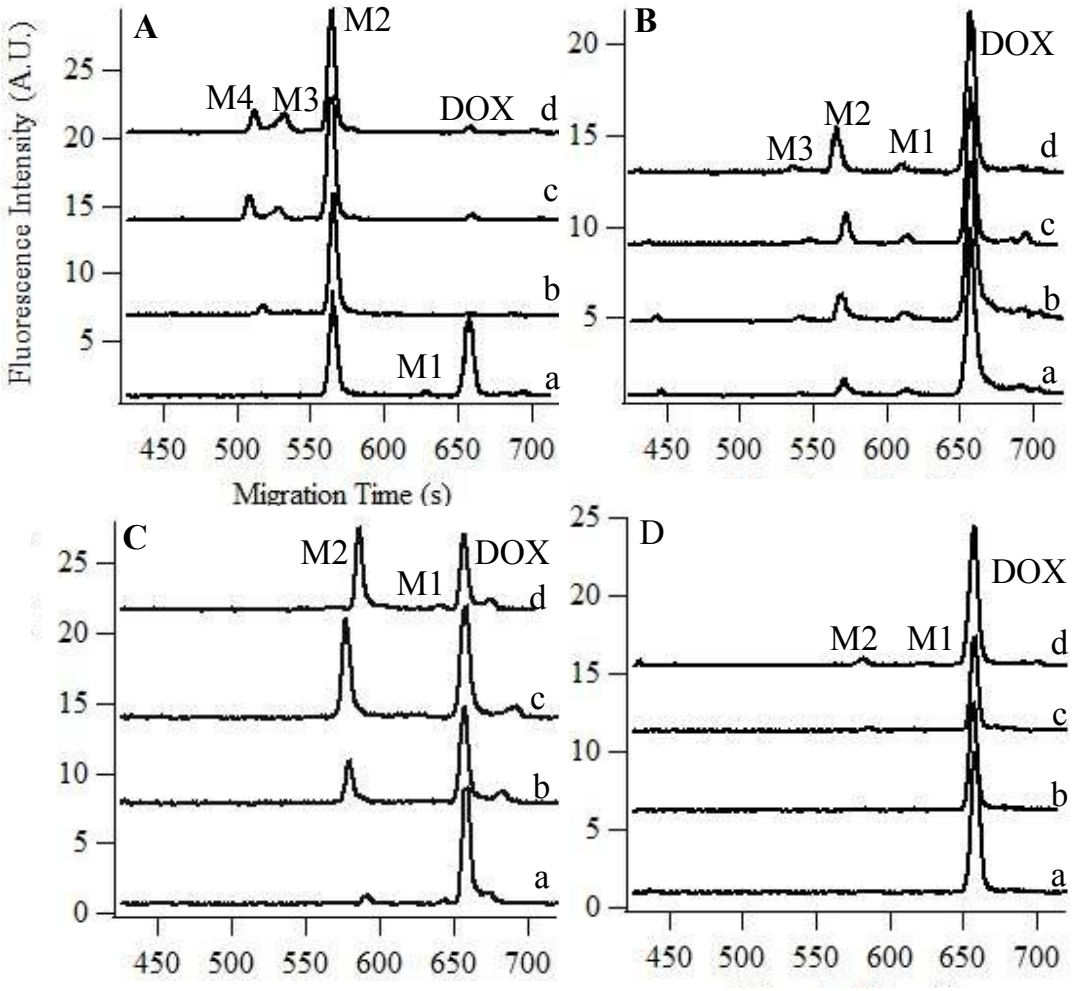

Figure 5-4. In vitro metabolism of DOX in PMF and MF fractions of young and old rat livers. Electropherograms of DOX metabolism in (A) PMF of young rat liver; (B) MF of young rat liver; (C) PMF of old rat liver and (D) MF of old rat liver after 15 min (trace a), 30 min (trace b), 60 min (trace c) and 120 min (trace d). Trace b, c and d are y-axis offset for clarity. M1 is 7-deoxyDOXone and M2 is 7-doxyDOXolone. Separations were performed in a 45 cm (A and B) or 45.8 cm (C and D) long, 50 μm i.d. fused silica capillary. Other conditions were same as in Figure 5-2.

The rate of metabolism was fast during the first 30 min of incubation and then slowed down. The metabolism in PMF of young adult rat liver is different from the rest of the samples. In this sample, 7-deoxyDOXone was only observed in the first 15 min incubation and the percent of 7-deoxyDOXolone increased in the first 30 min and then decreased. These temporal patterns in 7-deoxyDOXolone and 7-deoxyDOXone abundance were also observed in the HPLC-LIF-MS based experiments (Figure C-3), which further confirmed the identification of these two metabolites. In the rest of the samples (i.e., young MF, old PMF and MF), the percent of 7-deoxyDOXone and 7-deoxyDOXolone became steady or increased slightly after 30 min incubation. Two unique metabolites, M3 and M4, were also observed in the young rat liver after 30 min, and M4 was only observed in the PMF.

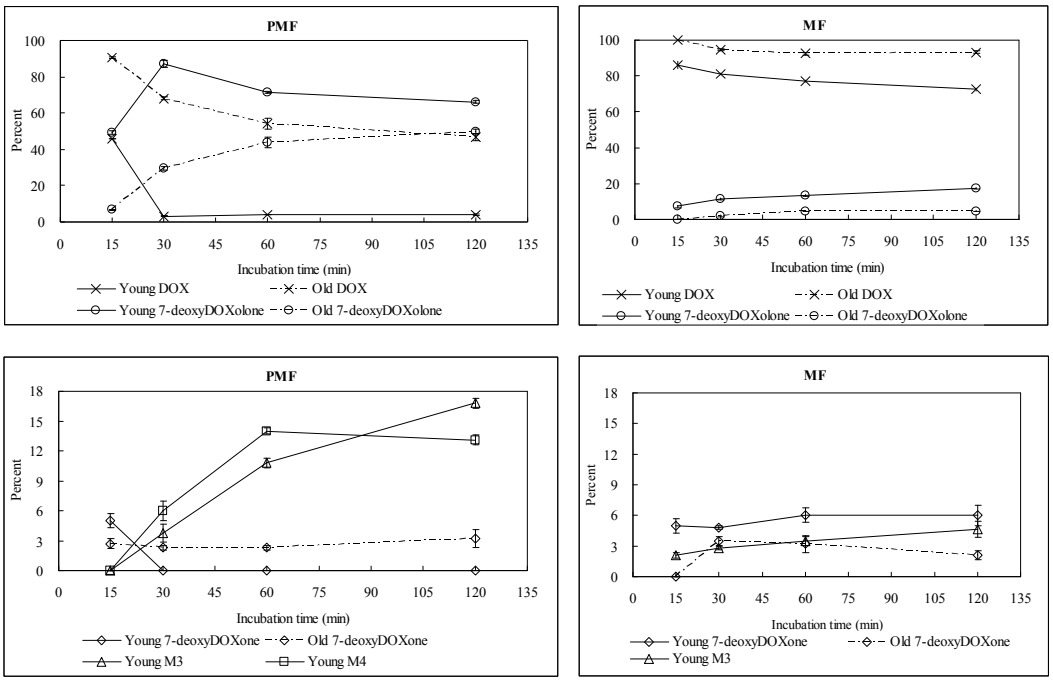

Figure 5-5. Changes in percent of DOX and metabolites over time in PMF and MF. Percentages are calculated using Equation 2. The young and old rat livers are represented in solid and dash lines, respectively. DOX and metabolites are labeled as DOX (×), 7-deoxyDOXone (◊), 7-deoxyDOXolone(○), M3(Δ) and M4 (□).

5.4. Discussion

5.4.1 Identification of DOX metabolites in MEKC-LIF

We demonstrated the use of MEKC-LIF in monitoring metabolism of DOX over time in MF and PMF of young and old rat livers. MEKC-LIF is a separation technique with high separation efficiency, short separation times, low sample volume sample requirements and little sample preparation. Therefore, MEKC-LIF is highly suitable to monitor metabolism of DOX in samples with complex matrices (e.g., tissues) and in small amounts (e.g., subcellular fractions). On the other hand identification of metabolites based on structural information is not a capability of MEKC-LIF. In order to accurately identify metabolites, we combined the information gathered from three methods: internal standard addition, mobility comparisons and cross-validation of metabolite identity with HPLC-LIF-MS results. Internal standard addition is limited by the availability of the standards and the possible comigration of the standard with a metabolite that actually has a different structure. The mobilities of analytes in MEKC are affected by many factors such as the electroosmotic flow, the viscosity of the separation buffer and the temperature,[137] and thus comparing mobilities may not be accurate and precise. Therefore, in this study, besides the two methods mentioned above, we also used the results from parallel HPLC-LIF-MS experiments to cross-validate metabolite identification. Both the relationship of molecular features and the elution sequence as well as the relative abundance of the metabolites observed in both HPLC-LIF-MS and MEKC-LIF helped in narrowing down the identities of 7-deoxyDOXolone and 7-deoxyDOXone.

5.4.2 Effect of cofactors on the metabolism of DOX

Cofactors play an essential role in a large number of biochemical reactions. In addition, they can give clues to the characteristics of the metabolites formed as different types of enzymatic reactions need their specific cofactors.

NAD(P)H is the cofactor required for oxidoreductase reactions that leads to reduction of metabolites and formation of $NAD(P)^+$.[195] Magnesium is another important cofactor that increases the activity of a number of drug metabolizing enzymes such as microsomal NADPH oxidase, NADPH-cytochrome *c* reductase and cytochrome P450 reductase.[196]

In these studies, the addition of NADPH and Mg^{2+} decreased 7-deoxyDOXone and increased 7-deoxyDOXolone formation. These changes are consistent with the enhanced activity of carbonyl reductase in the presence of such cofactors, which facilitate the transformation of 7-deoxyDOXone to 7-deoxyDOXolone. On the other hand, the percent of M3 did not significantly change with the addition of cofactors. This suggested that M3 may not be a metabolite formed by oxidoreductive reactions. In addition, its shorter migration time relative to that of 7-deoxyDOXone and 7-deoxyDOXolone suggests that M3 is more hydrophilic than these compounds (e.g. the sulfation or glucuronidation product of 4-demethyl-7-deoxyDOXolone). Identification of these compounds was outside the scope of this study.

5.4.3 DOX metabolism in young adult and old rat livers

Since 7-deoxyDOXone and 7-deoxyDOXolone were always observed in this study, these metabolites are highly likely part of the major pathway of DOX metabolism in rat

liver (Figure 5-1). DOXol which is reported as one of the major metabolites of DOX was not detected in any samples during the 2 h incubation of DOX. Our observation basically agrees with the previous studies of Gewirtz and Vrignaud using homogenized rat hepatocytes and livers.[193, 197] However Vrignaud indicated that DOX aglycone metabolites were only observed in large amounts in homogenized hepatocytes but not in intact ones.[197] They suggested the homogenization procedure may cause the release of the enzymes (e.g., glycosidases) that catalyzes the formation of aglycones.

In the PMF of young rat liver, 7-deoxyDOXone was only observed in the first 30 min, while in other samples, the percent of this metabolite became steady after 30 min of DOX incubation. This suggested possible higher activity of carbonyl reductase which metabolizes 7-deoxyDOXone to 7-deoxyDOXolone in young rat liver. After 30 min, M3 and M4 started to appear and increase in the PMF of young rat with the slightly decrease of 7-deoxyDOXolone. Based on the metabolic pathways in Figure 5-1 and the discussion of the effect of cofactors (c.f. Section 4.2), M3 and M4 could be the glucuronidation or sulfation products of 4-demethyl-7-deoxyDOXolone. These products are hydrophilic and facilitate the elimination of DOX. M3 and M4 were not detected in old rat liver, indicating possible lower activity of the enzymes (i.e., UDP-glucuronosyltransferases[198] and sulfotransferases[199]) that catalyze the formation of the conjugates of 4-demethyl-7-deoxyDOXolone. Other studies on Phase II drug metabolizing enzymes also showed low activities for these two enzymes in old rat livers.[200, 201] Together, these previous results and our observations may suggest that the absence of M3 and M4 in old rat liver is associated with in the decreased hepatic clearance of DOX in old rats.[78]

5.4.4 Purity of subcellular fractions

The isolated subcellular fractions used here simplify the metabolism system, but are not adequate to provide the identities of organelle-specific metabolites because the subcellular fractions are only enriched, not pure. To further identifying mitochondria-specific metabolites, mitochondria with higher purity are desirable. The purification can be achieved by more selective methods such as immunoisolation. Hornig-Dong and coworkers reported a method to isolate functional pure mitochondria using anti-TOM22 antibody which is specific to a mitochondria surface protein.[95] In the future, these mitochondria may be used for study mitochondria-specific DOX metabolism.

5.5. Conclusions

In this study, we demonstrated the feasibility of utilizing MEKC-LIF to monitor the metabolism of DOX in MF and PMF of young adult and rat livers over 2 h. This method only needs nanoliter sample volumes, does not require a complex sample extraction procedure and has attomole limits of detection. This method relied in internal standard addition, mobility comparisons and cross-validation with HPLC-LIF-MS to identify 7-deoxyDOXolone and 7-deoxyDOXone. The study revealed that young adult rat liver is more metabolic active in both the MF and PMF. Two unidentified metabolites were also observed only in the young adult rat liver. Further identification of these two metabolites may help identify enzymes whose activities are affected dramatically by aging.

Chapter 6

Biotransformation of Doxorubicin in Immunoisolated Peroxisomes

Peroxisomes contribute to several crucial metabolic processes such as β-oxidation of fatty acids and metabolism of reactive oxygen species. However, biotransformation of xenobiotics such as doxorubicin (DOX) in these organelles is largely unknown. Isolating functional peroxisomes with low levels of contaminants would be a useful tool to investigate biotransformations that occur in these organelles.

Here we describe an immunoisolation method to enrich peroxisomes within 1-2 hours. In this method, an antibody targeting a 70 kDa peroxisomal membrane protein was immobilized to silanized iron oxide beads (1-4 μm in diameter) coated with Protein A. The bead-antibody conjugates were then used to isolate peroxisomes from L6 rat myoblast homogenates using a magnet. The retained fraction showed a 2-fold enrichment in peroxisome activity relative to the unretained fraction, while the activities of lysosomes and mitochondria activity were only 3% and undetectable compared to the unretained fraction.

The transformations of DOX and a fatty acid analog, BODIPY 500/510 C1C12, ($B_{12}FA$) in the immunoisolated peroxisomes were investigated by micellar electrokinetic chromatography with laser-induced fluorescence detection (MEKC-LIF). The peroxisomal transformation of DOX produced two different peaks in the MEKC-LIF electropherogram. The peroxisomal transformation of $B_{12}FA$ did not show separation of any newly formed peaks, but the $B_{12}FA$ peak increased with the incubation time probably due to the comigration of the metabolites and $B_{12}FA$ in MEKC-LIF electropherograms.

In summary, the immunoisolation method described here is a rapid method to isolate peroxisomes with high purity. These peroxisomes could be used to study peroxisomal

biotransformation of xenobiotics after further confirmation that their biological function is maintained.

6.1. Introduction

In Chapters 4 and 5, the subcellular fractions prepared by differential centrifugation are of low purity. Immunoisolation using antibodies targeting proteins on the surface of a specific type of organelles is a method that could potentially isolate organelles with high purity in a short time.[96] This chapter describes the use of an antibody that targets a 70 kDa peroxisomal membrane protein (PMP70) to isolate peroxisomes from L6 myoblasts and the possible biotransformations of doxorubicin (DOX) and a fatty acid analog in these peroxisomes.

Peroxisomes are single membrane organelles involved in drug metabolism and physiological detoxification.[202] There are about 50 enzymes identified in peroxisomes which are responsible for these processes.[202] The metabolic functions of peroxisomes include balancing cellular reactive oxygen species (ROS),[74] α- and β- oxidation of fatty acids,[203] and biosynthesis of bile acids, docosahexanenoic acids and ether glycerolipids.[204] The deficiencies of peroxisomes or single peroxisomal enzyme lead to inherited diseases such as Zellweger syndrome.[205] Although the vital role of peroxisome function in cellular systems has been widely accepted, its role in the metabolism of drugs and xenobiotics has not been fully investigated. In fact, peroxisomes involved extensively in metabolism of diverse drugs and xenobiotics such as analgesics, anti-inflammatories, nutritional ingestants, insecticides and plasticisers.[206]

To investigate the peroxisomal-specific biotransformation of drugs and xenobiotics,

highly enriched peroxisomes with low contamination of interfering organelles such as mitochondria and lysosomes are necessary. The purifications of peroxisomes are usually done by differential or density centrifugation or a combination of both.[207] However, the purity of the peroxisomes obtained by differential centrifugation is usually low because the sedimentation characteristics of peroxisomes are close to that of mitochondria and lysosomes. A considerable amount (~23%) of peroxisomes was detected in a light mitochondria fraction obtained by differential centrifugation at 25,300g for 20 min.[208] In density centrifugation, the functionality of peroxisomes is impaired due to the long centrifugation time (from 1 to 16 hours) and density gradient media such as sucrose which exert osmotic pressure at the high density end of the gradient. It is necessary to develop purification methods that can isolate peroxisomes with high selectively and without losing their structural and functional integrity. Luers *et al.* reported the immunoisolation of peroxisomes with an antibody conjugated to magnetic beads.[96] In this report, the antibody that targets a 70 kDa peroxisomal membrane protein, PMP70, was conjugated to tosyl-activated beads by forming a covalent bond between the tosyl group and the primary amine of the antibody. The beads were then used to capture peroxisomes from light mitochondria fraction of rat livers. The ratios of peroxisomal urate oxidase activity to the activities of enzymes markers for microsomes, mitochondria and lysosomes before and after immunoisolation indicated a significant enrichment of the peroxisomes.[96] Kikuchi used this method to isolate peroxisomes for peroxisomal protein profiling.[209] Up to now, there are no reports describing the use of immunoisolated peroxisomes to investigate the biotransformation of drugs and xenobiotics. In this report, we immunoisolate peroxisomes from L6 rat myoblasts and then study the

biotransformation of an anthracycline, DOX (Figure 6-1A) a fluorescent fatty acid analog, BODIPY 500/510 C1C12 ($B_{12}FA$, Figure 6-1B) in these organelles .

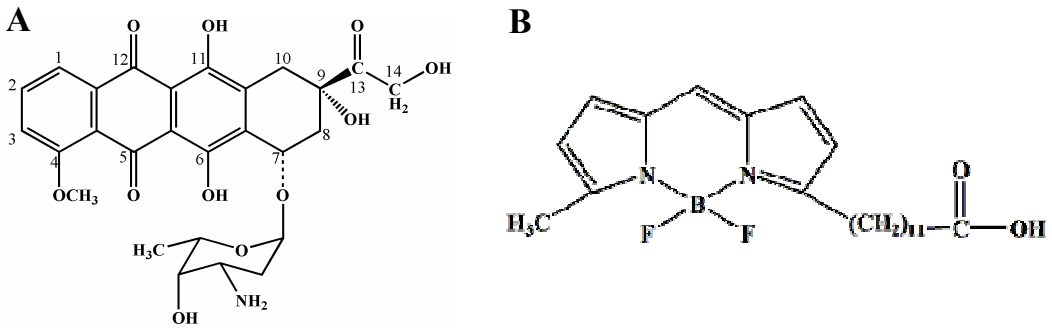

Figure 6-1. Structures of $B_{12}FA$ and DOX

DOX is an anthracycline that is widely used in treating solid tumors and leukemia.[3] Anthracyclines are susceptible to be oxidized and degraded by reactive oxygen species (ROS) such as H_2O_2 in the presence of peroxidase or myoglobin.[75] Such a process may serve as a salvage pathway for diminishing the levels and toxicity of anthracyclines in cardiomyocytes.[76] Besides mitochondrion, peroxisome is another important site of producing ROS.[74] However, the metabolism of DOX in peroxisomes is largely unknown compared to that in other organelles such as microsomes and mitochondria. In this study, we focus the transformation of DOX by ROS in peroxisomes to elucidate its peroxisomal oxidation.

The other important peroxisomal functions is the metabolism of lipid such as fatty acids and cholesterols both endogenous and from external sources. The major process for oxidative breaking down fatty acids is β-oxidation which can occur both in peroxisomes and mitochondria.[210] About 60% of the β-oxidation of 12-(1-pyrene)dodecanoic acid appears to occur in peroxisomes.[211] Here we used a BODIPY fatty acid analog, $B_{12}FA$, to assess the functionality of the peroxisomes after immunoisolation. BODIPY is lipophilic

and partition into the cell membrane easily.[212] Furthermore, the fluorophore on the C1 position of B_{12}FA is far away from the carboxylic acid group which decreases possible perturbations on fatty acid processing by peroxisomes.[213]

Capillary electrophoresis (CE) with laser-induced fluorescence detection (LIF) has been used to analyze both DOX and its metabolites in plasma[214, 215] and cells.[141] It also has been applied to analyze aminofluorescein-fatty acid derivatives.[216] The requirement of small volume (i.e., nanoliters) of samples by CE and the high sensitivity of LIF detection make it possible to analyze extremely small amounts (e.g. zeptomoles) of fluorescent analytes. Therefore, CE-LIF is extremely powerful in analyzing subcellular biotransformations. In this study, we used micellar electrokinetic chromatography (MEKC), a mode of CE, with LIF detection (i.e., MEKC-LIF) to determine whether B_{12}FA and DOX are metabolized by immunoisolated peroxisomes.

The *in vitro* metabolism of DOX showed that the two metabolites observed in the retained peroxisomal fraction are different from those two in the unretained fraction. The biotransformation of B_{12}FA did not produce detectable peaks, but the B_{12}FA peak intensity increased with incubation time in both retained and unretained fractions. This observation is probably due to the comigration of the metabolites and B_{12}FA in MEKC-LIF electropherograms. Further assessment of the bioactivity of the immunoisolated peroxisomes could also be performed to confirm their functionality.

6.2. Material and methods

6.2.1 Chemicals and reagents

MagnaBind Protein A Beads and BCA kit were purchased from Thermo Fisher Scientific (Rockford, IL). Anti-PMP70 antibody (produced in rabbit), Coenzyme A trilithium salt (CoA), β-Nicotinamide adenine dinucleotide (NAD), flavin adenine dinucleotide disodium salt hydrate (FAD), palmitoyl-coenzyme A lithium salt (palmitoyl-CoA), protease inhibitor cocktail, gentamicin, imidazole, Triton X-100, titanium (IV) oxysulfate and p-nitrophenyl-N-acetyl-β-D- glucosamide were purchased from Sigma-Aldrich (St. Louis, MO). BODIPY® 500/510 C1C12 ($B_{12}FA$), BODIPY® FL C3 (B_3FA), BODIPY® FL C5 (B_5FA) and BODIPY® FL C11 ($B_{11}FA$) (Figure 6-3 insertion), 10-*N*-nonyl-Acridine Orange (NAO), fluorescein, Dulbecco's modified Eagle's medium (DMEM), trypsin (5.0 g/L, 10×)-EDTA (2.0 g/L) and bovine serum were purchased from Invitrogen (Carlsbad, CA). Adenosine-5'-triphosphate (ATP) was from Roche Scientific (Indianapolis, IN). Doxorubicin hydrochloride was a generous gift from Meiji Seika Kaisha Ltd. (Tokyo, Japan). Sodium dodecyl sulfate (SDS), sodium citrate, sodium phosphate monobasic and dibasic, sodium carbonate, sodium bicarbonate, sulfuric acid (H_2SO_4), hydrochloric acid (HCl) and hydrogen peroxide (H_2O_2) were purchased from Mallinckrodt Chemicals (Phillipsburg, NJ). Sodium borate decahydrate, sodium hydroxide (NaOH) and sucrose were from Fisher Scientific (Fair Lawn, NJ). γ-cyclodextrin is purchased from TCI America (Portland, OR). 10× phosphate-buffer saline (10× PBS containing 1.37 M NaCl, 14.7 mM KH_2PO_4, 78.1 mM Na_2HPO_4, and 26.8 mM KCl) was purchased from EMD Chemicals (Gibbstown, NJ).

The cell homogenization buffer (pH = 7.4) contained 250 mM sucrose, 3 mM imidazole, 1 mM EDTA and 1% protease inhibitor cocktail. The binding buffer used in immunoisolation contained 100 mM sodium phosphate (pH = 8.0). The MEKC

separation buffers (pH = 9.3) were made of 10 mM borate and 10 mM SDS (BS10) for DOX and metabolites; 30 mM borate, 30 mM SDS and 5 mM γ-cyclodextrin ((BS30-γCD5) for B_{12}FA and metabolites. All the buffers were made using 18 MΩ water purified from a Millipore water purification system (Millipore, Billerica, MA) and the pH was adjusted with 0.1 M HCl or NaOH.

The stock solutions of DOX and BODIPY fatty acid analogs were prepared by dissolving them in methanol to a concentration of 1 mM.

6.2.2 Cell culture and sample preparation

L6 myoblasts (ATCC, Manassas, VA) were cultured in DMEM containing 10% (v/v) bovine serum and 10 μg/ml gentamicin in 75-cm^2 vented culture flasks at 37 °C and 5% CO_2. The cells were split every 3 to 4 days before they reached confluence. For splitting, the cells were rinsed with 1×PBS, lifted with 5 ml 0.25 g/L trypsin and diluted in fresh growth medium to 20 ml.

For sample preparation, L6 cells were pelleted by centrifugation at 1000g for 10 min, washed twice in 1×PBS and reconstituted in the homogenization buffer to a cell density of 2×10^7 cells/ml. The cells were then disrupted by 30 strokes in an ice-chilled Dounce homogenizer (0.00025" clearance, Kontes Glass, Vineland, NJ). Trypsin blue stain was used to insure that more than 95% of the cells were disrupted. The cell homogenate was centrifuged at 600g for 10 min to remove unbroken cells, nuclei and cell debris. The post nuclear fraction (PNF) was used for immunoisolation of peroxisomes.

6.2.3 Immunoisolation of peroxisomes

Protein A beads were first incubated in binding buffer containing 1% BSA for 1 h to block non-specific binding sites. Anti-PMP70 antibody (4×10^{-10} mg IgG/bead) was then bound to the protein A beads at 4 °C for 1 h while the mixture was gently vortexed. After incubation, the antibody-bead conjugates were washed three times with binding buffer to remove any unbound antibody. PNF was added to the conjugates at a ratio of 25 beads per cell and incubated for 1 h at 4 °C. The supernatant (unretained fraction) containing cytosol and unbound organelles was removed and saved for further analysis; the beads with bound peroxisomes (retained fraction) was washed 3 times in binding buffer and reconstituted in homogenization buffer.

6.2.4 Protein quantification and enzyme assays

Protein amounts in the retained and unretained fractions were quantified with a BCA kit according to the manufacture's protocol. The retained fraction was first eluted from the beads with 10% SDS and the eluent was used for protein quantification. Beads with anti-PMP70 antibody only were used as control whose absorbance was subtracted from that of the retained fraction.

Catalase and β-hexosaminidase assays were used to assess the enzyme activities in retained and unretained fractions. Catalase assay, an peroxisomal enzyme activity assay, was carried out according to Storrie's protocol.[99] Briefly, H_2O_2 (11.7 mM) in 2 mM imidazole buffer containing 5% BSA and 0.2% Triton X-100 was incubated with both fractions for 10 min at room temperature. After incubation, titanium (IV) oxysulfate in 0.5 M H_2SO_4 was added to form a yellow complex with the unreacted H_2O_2. The absorbance of the complex was measured at 405 nm with a Synergy 2 plate reader

(Biotek, Winooski, VT). β-hexosamindase assay was used to assess the lysosomal activity in both retained and unretained fractions. The assay was modified from that described by Barret.[101] Both fractions were mixed with p-nitrophenyl-*N*-acetyl-β-D-glucosaminide (7.5 mM) in citrate buffer (0.3 M sodium citrate and 0.3 M NaCl, pH = 4.3) and incubated at 37 ºC for 45 min. After incubation, terminating solution (0.5 M Na_2CO_3 and 0.5 M $NaHCO_3$) was added to the mixture to stop the reaction. The absorbance of the product, *p*-nitrophenol, was measured at 410 nm.

Since the beads used for peroxisome isolation interfere with the absorbance measurements, stop enzyme assays in which beads can be removed after incubation are more suitable to measure the enzyme activities. No appropriate stop assay was found to measure mitochondria activity, so the abundance of mitochondria in both fractions was determined by NAO labeling. NAO is a fluorescent marker labeling cardiolipin in the mitochondria inner membrane.[217] In this assay, cells was labeled with 5 μM NAO on ice for 10 min and washed twice with 1×PBS before homogenization. After immunoisolation, the unretained fraction was centrifuged at 16,000g and the resulting pellet was dissolved in 10% SDS. The retained fraction was eluted from the beads with 10% SDS. The fluorescence intensities of dissolved pellet (unretained fraction) and eluent (retained fraction) were measured with a Synergy 2 plate reader (λ_{ex} = 480 nm and λ_{em} = 528 nm).

In both enzyme assays and NAO labeling, Protein A beads without anti-PMP70 antibody were incubated with PNF and used as a control for non-specific binding. To make the enzyme activity/fluorescence intensity determined by the same assay comparable in different fractions, the enzyme activity/fluorescence intensity was normalized by the amount of protein in the respective fraction and expressed as specific

activity. The null hypothesis "there is no significant difference in the specific activities or the NAO amounts between the retained and unretained fractions was tested using the Student's t-test using statistical software "R". The null hypothesis was rejected when the p-value (p) <0.02 (98% confidence level).

6.2.5 *In vitro* metabolism of B_{12}FA and DOX in isolated peroxisomes

The peroxisomes were isolated as described in section 6.2.3. The retained and unretained fractions were incubated with 5 μM B_{12}FA at 37 °C. Coenzyme A (0.5 mM), NAD (1 mM), FAD (0.5 mM) and ATP (5 mM) which are necessary cofactors in β-oxidation were also added to the reaction mixture.[218] A fraction of the mixture was taken out at 15, 30, 60 and 120 min and frozen at -80 °C until MEKC analysis.

DOX (10 μM) was incubated with retained and unretained fractions at 37 °C. Palmitoyl-CoA (0.5 mM) was added to induce the production of H_2O_2.[219] FAD (0.5 mM) and NAD (1 mM) were added as cofactors for peroxisomal β-oxidation of palmitoyl-CoA.[220] A fraction was sampled from the mixture at 15, 30 60 and 120 min and frozen at -80 °C until MEKC analysis.

6.2.6 MEKC analysis of B_{12}FA or DOX *in vitro* metabolites

The separation system of DOX and metabolites was reported previously,[141] while the separation system of B_{12}FA required development of a new buffer system containing borate, SDS and γ-cyclodextrin.

After incubation with xenobiotics, the unretained fraction was directly diluted with separation buffer for analysis; the retained fraction was diluted in separation buffer,

gently mixed and the beads were removed with a magnet. Samples were introduced into a fused silica capillary (50 μm I.D. and 150 μm O.D., Polymicro Technologies, Phoenix, AZ) by hydrodynamic injection at 10.8 kPa for 1 s. Then the capillary was then brought into a vial containing separation buffer and MEKC was performed under a +400 V/cm electric field in a home-built instrument equipped with post-column LIF detection, previously described.[144] A sheath flow cuvette encased the detector end of the capillary. The last 2-mm of this end had the polyimide coating burned off to reduce the background fluorescence caused by this material. As fluorescent analytes migrated out from the capillary, they were excited at 488 nm with an argon ion laser (JDS Uniphase, San Jose, CA). Fluorescence was collected at a 90° angle with respect to the laser beam by a 60× microscope objective (Universe Kogaku, Inc., Oyster Bay, NY). A 505 nm long-pass filter (505 AELP, Omega Optical, Brattleboro, VT) and a 1.4 mm pinhole were used to reduce light scattering. A 635 ± 27.5 nm (XF3015) or a 520 ± 17.5 nm (XF3007) band-pass filter (Omega Optical, Brattleboro, VT) was used to select fluorescence from DOX and metabolites or B12FA and metabolites, respectively. Fluorescence was then detected in a photomultiplier tube (PMT) (Hamamatsu, Bridgewater, NJ) biased at 1000 V. The PMT output was sampled at 10 Hz and processed with a home-written Labview program (National Instruments, Austin, TX).

Prior to the initial use of MEKC-LIF every day, the capillary was conditioned with sequential flushes of 0.1 mM NaOH, water and separation buffer for 30 min each using 150 kPa pressure at the inlet. The same sequence, but running for 2 min each, was carried out between different samples. The separation buffer was replaced every 2 h with a new vial to avoid buffer contamination and electrolyte depletion which causes migration time

drift.[221] Prior to sample analysis, the instrument was aligned by maximizing the response of 5 $\times 10^{-10}$ M fluorescein which continuously flowed through the detector while applying a +400 V/cm electric field.

6.2.7 MEKC data analysis

Electropherograms were processed using Igor Pro (Wavemetrics, Lake Oswego, OR) to determine peak intensities and areas.

In the study of DOX transformation, corrected mobilities were used to compare peaks in retained and unretained fractions. The correction was done according to the two marker method described by Li *et al*.[137] that uses the expression

$$t_{X,corrected} = \left[\frac{1}{t_{m_1}} - \frac{1}{r}\left(\frac{1}{\hat{t}_{m_1}} - \frac{1}{\hat{t}_x} \right) \right]^{-1} \qquad \text{(Equation 6-1)}$$

$$r = \frac{\frac{1}{\hat{t}_{m_1}} - \frac{1}{\hat{t}_{m_2}}}{\frac{1}{t_{m_1}} - \frac{1}{t_{m_2}}} \qquad \text{(Equation 6-2)}$$

where $t_{X,corrected}$ is the corrected migration time of a peak X in a sample and $\hat{t}_x$ is its observed migration time; $\hat{t}_{m_1}$ and $\hat{t}_{m_2}$ are the migration times of the markers, and t_{m_1} and t_{m_2} are the migration times of the markers in the reference run. The corrected mobility of the peak X was calculated by

$$\mu_{X,corrected} = \frac{L^2}{V \times t_{X,corrected}} \qquad \text{(Equation 6-3)}$$

where L is the length of the capillary, and V is the separation voltage.

The corrected mobilities of the peaks in the retained and unretaind fractions were

compared using Student's t-test. The null hypothesis "there is no significant difference in the mobility of peak X in the retained and unretained fractions" was rejected when the *p*-value <0.02 (98% confidence level).

6.3. Results and discussion

6.3.1 Purity of the immunoisolated peroxisomes

Catalase and β-hexosaminidase are established enzyme markers of peroxisomes[4] and lysosomes, respectively.[222] we used their specific activities to determine the relative abundance of these organelles in the retained and unretained fractions. We used NAO which labels the cadiolipin in the mitochondria inner membrane[217] to determine the relative amounts of mitochondria in these fractions because the purification beads interfere with existing mitochondria enzyme assay. Table 6-1 shows the results of enzyme assays and NAO labeling of retained and unretained fractions. The peroxisome activity in retained fraction was twice compared with the unretained fraction. The peroxisome activity observed in unretained fraction is because that the bead-antibody conjugates are not enough to capture all peroxisomes in the cell homogenate. This is not critical as this study focuses on the immunoisolated peroxisomes. The lysosomal activity in the retained fraction is 3% of that of unretained fraction and no detectable level of mitochondria was observed in the retained fraction. Based on these results, the immunoisolated peroxisomes have enough purity to study peroxisomal biotransformations.

Western blot is another useful method in assessing the purity of subcellular fraction, but it is not applicable to the retained fraction from immunoisolation (results not shown).

The anti-PMP antibody used in the immunoisolation appeared as a dark broad band in western blot, interfering with the detection of protein of interest.

Table 6-1. Catalase, β-hexosaminidase activities and NAO accumulation in retained and unretained fractions

	catalase activity (μmol/μg protein/min)	β-hexosaminidase activity (μmol/μg protein/min)	NAO (μmol/μg protein)
Retained	1.27 ± 0.06	0.003 ± 0.001	ND
Unretained	0.61 ± 0.02	0.111 ± 0.004	0.37 ± 0.04

Results are the average ± standard deviation (n=3)

6.3.2 MEKC of BODIPY fatty acid analogs of different chain length

The expected metabolism of $B_{12}FA$ in peroxisomes is β-oxidation, which shortens the chain by two carbons each cycle. Figure 6-2 illustrates the first cycle of β-oxidation of $B_{12}FA$. The resulting products are usually analyzed by HPLC or GC.[211, 212] Both methods require extensive extraction procedures prior to the analysis. Here we developed a MEKC separation that is in principle suitable to analyze the β-oxidation products of $B_{12}FA$. The limit of detection of $B_{12}FA$ is $(1.7 \pm 0.2) \times 10^{-20}$ mole (average ± standard deviation, n = 3) as determined from the peak intensity resulting from injecting 9.5×10^{-19} mole of $B_{12}FA$.

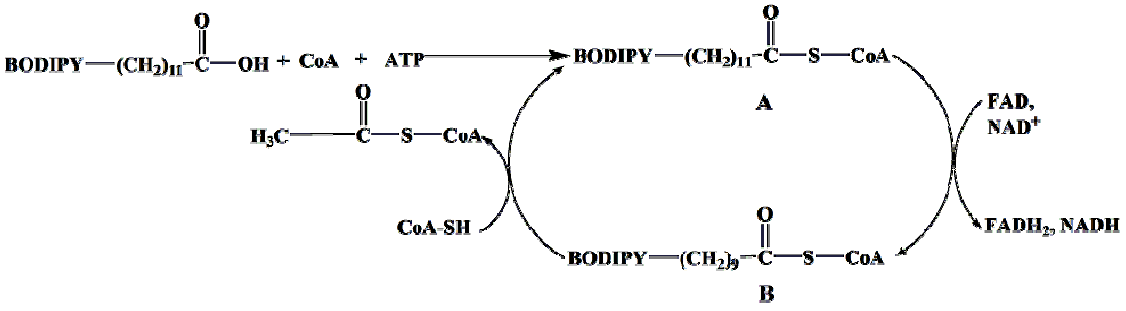

Figure 6-2. Reaction scheme of β-oxidation of $B_{12}FA$ (first cycle). $B_{12}FA$ is first activated to the acyl-CoA ester (compound A) by ATP and CoA. The acyl-CoA ester then undergoes β-oxidation that shortens the fatty acid chain by two carbons (compound B).

To ensure the MEKC system can separate $B_{12}FA$ from potential β-oxidation products we optimized the MEKC-LIF separation using commercially available BODIPY fatty acid analogs that include B_3FA, B_5FA and $B_{11}FA$ (Figure 6-3 insert). At low concentration of borate and SDS (10 mM each), B_3FA and B_5FA could not be separated, while at high concentration of borate and SDS (30 mM), $B_{11}FA$ and $B_{12}FA$ comigrated. We therefore investigated the use of a CE buffer modified, γCD commonly used in separations of lipids that increase their solubility and selectivity.[223, 224] The addition of 5 mM γ-cyclodextrin (γCD) to 30 mM borate, 30 mM SDS buffer (BS30) facilitated the separation of $B_{11}FA$ and $B_{12}FA$ (R_s = 1.6).

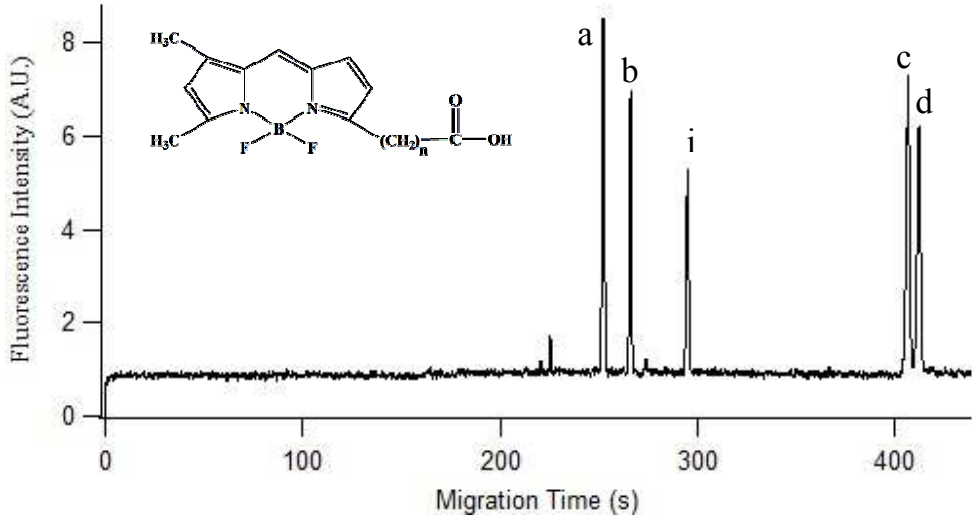

Figure 6-3. Separation and detection of BODIPY fatty acid analogs using MEKC-LIF. The MEKC was performed in a 43.3 cm fused silica capillary under a 400 V/cm electric field in a buffer containing 30 mM borate, 30 mM SDS and 5 mM γ-cyclodextrin (pH = 9.3). A standards mixture containing 2.5×10^{-10} M of (a) B_3FA, (b) B_5FA, (c) $B_{12}FA$, (d) $B_{11}FA$ and (i) 1×10^{-10} M fluorescein (internal standard) each was injected at 10.8 kPa for 1 s. The fluorescence was selected by a 520 ± 17.5 nm bandpass filter and detected by a photomultiplier tube biased at 1000V. Insert: structures of B_3FA (n=2), B_5FA (n=4) and $B_{11}FA$ (n=10)

It should be noted that these two compounds are actually structural isomers (Figure 6-1B and Figure 6-3 insert). The BS30-γCD5 system is capable of separating not only BODIPY standards with chain length different in two carbons (B_3FA and B_5FA) as well as structural isomers ($B_{11}FA$ and $B_{12}FA$). Therefore, we used this separation system to investigate the presence of β-oxidation of $B_{12}FA$ in immunoisolated peroxisomes.

6.3.3 *In-vitro* metabolism of $B_{12}FA$

We attempted to monitor β-oxidation of $B_{12}FA$ in immunoisolated peroxisomes. Figure 6-4 shows the electropherograms after 2 h incubation of $B_{12}FA$ in the unretained (trace b) or retained peroxisomal fraction (trace c). Compared with control (trace a) which only contains $B_{12}FA$ and cofactors, only one extra peak (peak 3) was observed in both retained peroxisomal and unretained fractions. Interestingly, the $B_{12}FA$ peak (peak 1) increases with incubation time in both fractions (Table 6-2). The extra peak and increase in $B_{12}FA$ indicating possible metabolism of $B_{12}FA$. The changes observed in the unretained fraction are probably due to (1) there are still peroxisomes existing in this fractions (c.f. Table 6-1) and/or (2) mitochondrial β-oxidation of $B_{12}FA$.

Table 6-2. Peak area of $B_{12}FA$ and possible metabolites in retained peroxisomal and unretained fractions

	peak 1		peak 2		peak 3	
	30 min	2 h	30 min	2 h	30 min	2 h
control	9.7±0.3		0.33±0.03		-	
retained	10.0±0.1	14.2±0.2	0.34±0.02	0.4±0.1	0.26±0.04	0.27±0.01
unretained	10.9±0	17.6±0.7	0.36±0.08	0.54±0.02	0.6±0.1	0.78±0.03

Results are represented in average ± standard deviation (n=3). For peak assignment see Figure 6-4

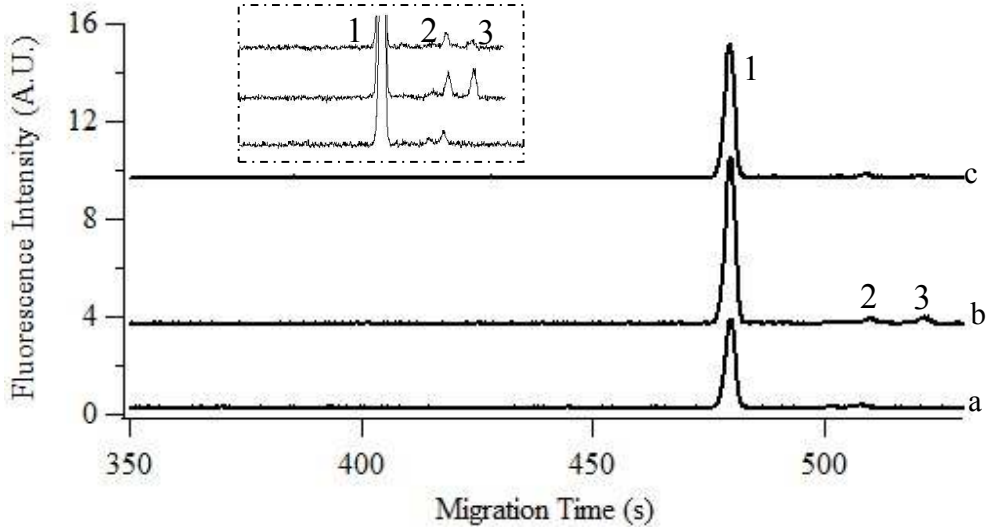

Figure 6-4. *In vitro* metabolism of $B_{12}FA$ in a retained peroxisomal and unretained fraction. The MEKC was performed in a 43.5 cm fused silica capillary. $B_{12}FA$ (5 μM) was incubated with buffer (trace a), unretained fraction (trace b) or retained fraction (trace c) as well as CoA (0.5 mM), FAD (0.5 mM), NAD (1 mM) and ATP (5 mM) for 2 h at 37 ºC. Trace b and c were y-axis offset for clarity. Other conditions were the same as those described in Figure 6-3. Insertion is the enlargement of the range from 400 to 550 s.

Peak 3 has lower mobility compared with $B_{12}FA$ which suggests that it has higher hydrophobicity than $B_{12}FA$. It could be the triacylglycerol of $B_{12}FA$ formed. Similar peaks whose mobility is lower than that of $B_{12}FA$ are also observed in L6 myoblasts cultured in medium with $B_{12}FA$ (Appendix D, Figure D-1). L6 myoblasts are shown to accumulate large amounts of triacylglycerol when cultured in fatty acid-supplemented growth medium.[225]

The increase of $B_{12}FA$ peak may indicate that $B_{12}FA$ and the β-oxidation products, such as the acyl-CoA esters with a shorter carbon chain (Figure 6-2), comigrate. To explore this possibility, we attempted to hydrolyze the samples via alkaline hydrolysis to their corresponding fatty acids.[212] If successful, this procedure would result in electropherograms resembling those of the standards (c.f. Figure 6-3). However, $B_{12}FA$ did not withstand the hydrolysis and became undetectable (results not shown). Another

alternative to identify the possible products comigrating with the B_{12}FA peak would be to analyze the reaction products by HPLC-MS. Although there are no reports on monitoring β-oxidation of a saturated fatty acid by HPLC-MS, there are reports on the use of this technique to detect free fatty acids[226] and fatty acyl-CoAs[227, 228] in cell and tissue extracts.

Low β-oxidation activity in the immunoisolated peroxisomes is another possible explanation for the lack of metabolites in the retained peroxisomal fraction. In the future, we plan to use the fluorogenic reagent Amplex Red[229] to assess the bioactivity of the peroxisomes. This reagent is suitable to detect H_2O_2 produced during the β-oxidation of a fatty acid (e.g., palmitoyl-CoA).[219]

6.3.4 *In-vitro* metabolism of DOX

The hydroquinone moiety in the structure of DOX is susceptible to oxidation by H_2O_2-activated peroxidases or myoglobin.[76] Taatjes *et al.* found that DOX incubated with concentrated H_2O_2 (16 mM) for 6 days can be oxidized via Baeyer-Villiger type oxidations at the C14 to yield aglycones and a carboxylic acid at C9 without the presence of any catalyst.[230] We also observed evidence for the reaction of DOX with H_2O_2 in an *in vitro* system. After incubating DOX with 1 mM H_2O_2 for 3 h, several products that account for 20% of the total peak area were detected by MEKC-LIF electropherograms (Figure 6-5). Indeed, we cannot exclude the possibility of formation of non-fluorescent products such as 3-methoxyphthalic acid or simple phthalates[231] that are undetectable by the LIF detector used in these studies.

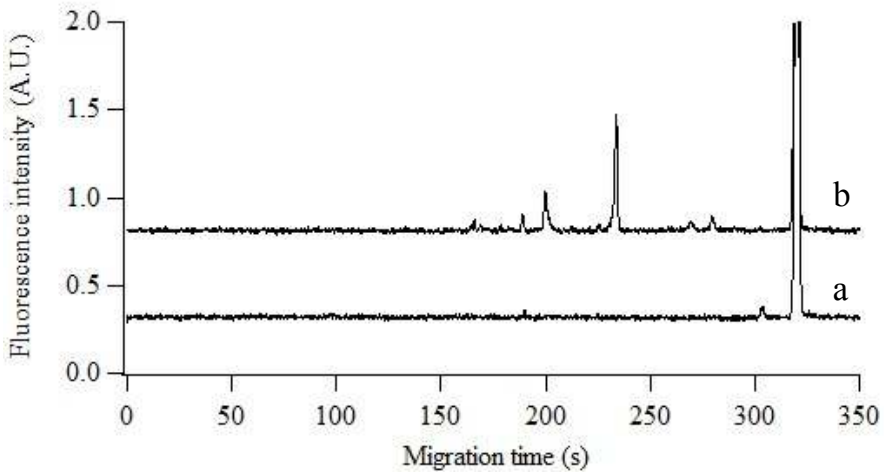

Figure 6-5. DOX and products after reacting with H_2O_2 *in vitro*. The MEKC was performed in a 42.5 cm fused silica capillary under a 400 V/cm electric field in a buffer containing 10 mM borate and 10 mM SDS (pH = 9.3). Trace a is 10 μM DOX alone at 37 ºC for 3 h and trace b is 10 μM DOX incubated with 1 mM H_2O_2 for 3 h at 37 ºC. Trace b was y-axis offset for clarity. Other conditions were same as that described in Figure 6-3 except a 635±27.5 band pass filter was used.

H_2O_2 is the major byproduct of reactions using oxidase in peroxisomes such as the oxidation of urate, glycolate and activated fatty acids.[219] The H_2O_2 can oxidize DOX accumulating in peroxisomes. Thus, immunoisolated peroxisomes mixed with palmitoyl-CoA, NAD and FAD are expected to produce H_2O_2. When adding DOX to such peroxisomal system, new peaks appeared (Figure 6-6). Since the electropherograms of the control (i.e. without peroxisomes) show multiple peaks, possibly corresponding to palmitoyl-CoA, FAD, NAD and other impurities that may overlap with DOX oxidation products, the identification of these products may be compromised. Nevertheless, comparing the electropherograms of the retained peroxisomal and unretained fractions, different peaks were observed (indicated by arrows in Figure 6-6).

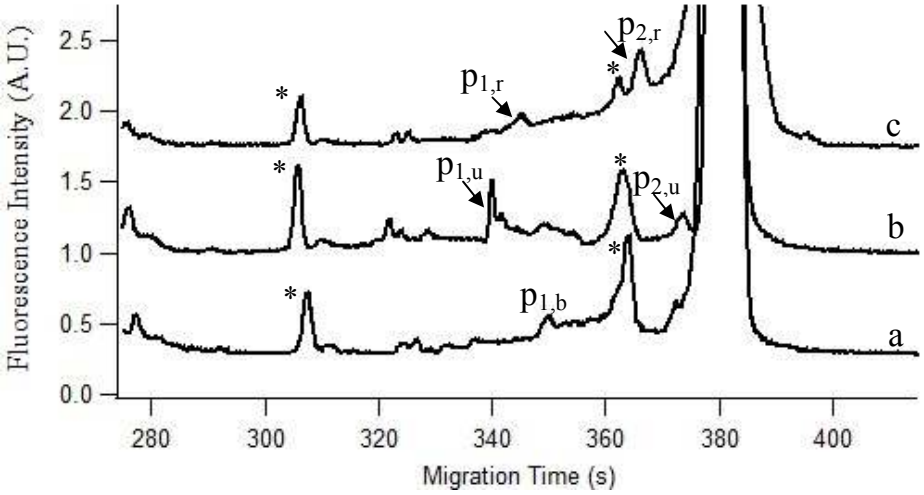

Figure 6-6. *In vitro* metabolism of DOX in retained peroxisomal and unretained fractions. The MEKC was performed in a 43.5 cm fused silica capillary under a 400 V/cm electric field in a buffer containing 10 mM borate and 10 mM SDS (pH = 9.3). The reaction mixture contained DOX (10 μM) palmitoyl CoA (0.5 mM), FAD (0.5 mM) and NAD (1 mM) and was incubated with only buffer (trace a), the unretained fraction (trace b) or retained fraction (trace c) for 2 h at 37 ºC Trace b and c were y-axis offset for clarity. Possible different metabolites in retained and unretained fractions are indicated by arrows. Other conditions were same as that described in Figure 6-5.

To further confirm that the peaks marked with arrows are unique to a given sample, we calculated their corrected mobilities using Equations 6-1 to 6-3, according to the peaks labeled with stars in Figure 6.6, and compared with Student's t-tests. Peaks 1 are different in the retained peroxisomal and unretained fractions (p-value = 3.3×10^{-4}) and are different from the peak observed in the buffer (p-value = 0.018 and 1.8×10^{-4} for the retained and unretained fraction, respectively). Peaks 2 are also different in the retained peroxisomal and unretained fraction (p-value = 1.1×10^{-3}). As seen in Figure 6-6, these peaks are small in respect to the DOX peak. These results are not surprising because low H_2O_2 concentrations are expected to be found in peroxisomes where H_2O_2 is degraded by catalase. It would be possible that intra-peroxisomal H_2O_2 concentrations are similar to its physiological levels (~micromolar and submicromolar),[232] which are much lower than

those used in the in vitro study (i.e. 1 mM) reported in Figure 6-5. In agreement, no DOX transformation was observed after 2 h incubation with 1 μM H_2O_2 at 37 ºC (results not shown).

Table 6-3. Corrected mobilities of possible different metabolites in retained peroxisomal and unretained fractions

	buffer	unretained	retained
p_1	3.098 ± 0.007	3.175 ± 0.006	3.119 ± 0.005
p_2	-	2.886 ± 0.005	2.936 ± 0.002

Values are the average ± standard deviation (n=3) and are given as $\times 10^{-4}$ $cm^2/(V \cdot s)$

6.4. Conclusions

We immunoisolated peroxisomes with high purity in less than 2 h. We could not identify the various -oxidation products of a fluorescently labeled fatty acid, $B_{12}FA$, even when the MEKC-LIF separation conditions were optimized using fluorescently labeled short-chain fatty acid analogs. Possible explanations are: comigration of the -oxidation products with $B_{12}FA$ or low bioactivity of the immunoisolated peroxisomes. In the future, we will explore the first possibility using HPLC-MS to indentify the fluorescent products in the reaction mixture. The second possibility will be explored by testing for the production of H_2O_2 resulting from β-oxidation of palmitoyl-CoA. Monitoring of the *in vitro* metabolism of DOX in the retained peroxisomal and unretained fractions by MEKC-LIF suggests that some low abundance oxidation products of DOX are being formed. Use of a catalase inhibitor (e.g., NaN_3) would increase the concentration of H_2O_2 in peroxisomes,[219] which could increase the transformation of DOX by H_2O_2.

Chapter 7

Conclusions and Future Work

7.1 Conclusions

This thesis demonstrates the development and application of capillary electrophoretic (CE)-based separation techniques and methodologies to analyze doxorubicin (DOX), its prodrug and metabolites in different biological samples.

The direct tissue analysis technique described in Chapter 3 has high spatial resolution (100 μm) and reproducibility. It can sample picoliter volumes of tissues samples into a capillary that is analyzed by micellar electrokinetic chromatography with laser-induced fluorescence detection (MEKC-LIF). The analysis of samples from the tumor and non-tumor regions of a hepatocellular carcinoma (HCC) liver after transarterial catheter chemoembolizaiton (TACE) revealed that the concentrations of DOX in these regions vary from 0.4 to 1.3 μM and from 0.3 to 0.5 μM, respectively. No significant difference in DOX concentrations in these two regions were observed probably due to the small number of samples analyzed. Power analysis shows that at least 82 samples need to be analyzed in both regions combined to reach a statistical significant conclusion. After improving the throughput, this technique is promising in determining the distribution and metabolism of drugs in tissue cross-sections. Due to the small size of a capillary (150 μm O.D.), direct sampling using a capillary can be a non-invasive method to sample tissue or body fluids.

Chapter 4 demonstrated that a CTAB-based MEKC separation system can separate *N*-L-leucyl-doxorubicin (LeuDOX) from DOX and its major metabolite, doxorubicinol (DOXol). To our knowledge, this is the first CE-based system for analyzing DOX prodrugs. The MEKC-LIF analysis of LeuDOX treated DOX MES-SA and MES-SA/Dx5 uterine sarcoma cells showed that twice more LeuDOX was transformed

into DOX in MES-SA/Dx5 cells than in MES-SA cells. We hypothesize that higher expression level of hydrolytic enzymes such as cathepsins is responsible for the more active prodrug transformation in the MES-SA/Dx5 cell line which is DOX reistant. If elevated expression level of hydrolytic enzymes is common to drug resistant cell lines, this property could be utilized to design hydrolytic enzyme-activated prodrugs that overcome drug resistance. Low density organelle fraction which contains most lysosomes showed high DOX to LeuDOX ratio, which indicates the possibility of LeuDOX activation in this organelle. One of the limitations of this study is that cells were treated with LeuDOX first and then subcellular fractions were isolated for analysis. During the treatment, LeuDOX and metabolites could redistribute among different subcellular compartments and make it difficult to determine the original place where the transformation of LeuDOX to DOX occurs. In the future, isolated pure subcellular fractions may be used to investigate the activation of LeuDOX as well as other prodrugs in various types of subcellular compartments.

Studying drug metabolism and transformation in isolated subcellular fractions reduces complexity of the matrices, avoids redistribution of drugs and metabolites during drug treatment, and minimizes losses of drugs and metabolites during sample processing. Chapter 5 described the use of isolation subcellular fractions (mitochondria-enriched and post-mitochondria fractions (MF and PMF)) to compare the metabolism of DOX of young and old rat livers. The results showed that aging affects the metabolic activity of both MF and PMF. The young rat liver is more metabolically active than the old one as it metabolizes higher percent of DOX and produces more metabolites. Based on the results of parallel HPLC-LIF-MS experiments, we determined that

7-deoxy-doxorubicinolone and 7-deoxydoxorubicinone present in all the samples analyzed. Two unidentified metabolites are only formed in young rat liver and one of them is only formed in young PMF.

Organelle impurities found in subcellular fractions may compromise the interpretation of the results of MEKC-LIF analysis of DOX metabolism. Chapter 6 introduced an immunoisolation method that uses an antibody targeting a 70 kDa peroxisomal membrane protein to isolate peroxisomes from L6 rat myoblasts. The retained fraction showed a two-fold enrichment of peroxisomes compared with the unretained fraction, while the lysosomes and mitochondria contamination is low (5% and undetectable, respectively). Two different DOX metabolites are observed in the retained and unretained fractions even though their abundance is low. No obvious metabolite of a fatty acid analog, BODIPY C1C12 500/510 ($B_{12}FA$) was detected probably due to the comigration of the metabolites and the fatty acid analog or the low β-oxidation activity of the immunoisolated peroxisomes

The CE-based methodologies and techniques developed in this thesis work have the following characteristics: they are sensitive and versatile in sampling; they also require small amount of sample and minimum sample preparation. These attributes are valuable in studying the distribution and metabolism of DOX in tissues, cells and subcellular fractions. Although this thesis describes proof-of-principle techniques and methodologies, the future developments could make possible to explore their potential in preclinical and clinical studies of DOX distribution and metabolism that are ultimately related to the efficacy and toxicity of DOX.

7.2 Future work

While the techniques and methodologies described in this thesis are promising for cellular and subcellular drug analysis, there are areas that require further development. They include improving the efficiency and throughput of the direct tissue analysis technique (Chapter 3), increasing the purity of subcellular fractions (Chapters 4 and 5), identifying metabolites detected by MEKC-LIF and extending the techniques to monitor the accumulation and metabolism of non-fluorescent drugs (all chapters).

7.2.1 Direct tissue sampling

High throughput direct sampling-analysis system

The low throughput of the direct tissue analysis technique prevents applying it to sample multiple spots in a tissue cross-section that are required to establish spatial distribution maps of DOX and its metabolites (c.f. Chapter 3). According to the discussion in Chapter 3, 82 samples in both tumor and non-tumor regions combined need to be analyzed to reach a statistic significant conclusion on the distribution of DOX in a tissue cross-section. With the present system, the analysis would take about 40 h. In order to improve the throughput, a multi-capillary system may be developed which can sample and analyze multiple tissue spots at the same time. Dovich's group introduced a multi-capillary array for simultaneous sampling of single cells.[233] A similar system that can simultaneously sample multiple spots in both tumor and non-tumor regions on a tissue cross-section could be developed. A 10×10 array could cover the entire are of a 1 cm × 1 cm tissue cross-section if the spot is 100 μm in diameter. After sampling, the analytes in the sampled tissue spots could then be separated using the conditions

described in this thesis and detected simultaneously. The commercially available 96 capillary (8×12 format) arrays (e.g., cePRO 9600^{TM} from Advanced Analytical) could be used in this study. The biggest challenge anticipated is the precise control of the position of the capillary in the tissue which determines the reproducibility of the sampling. The system could be first tested by a tissue mimic with homogenous DOX distribution using the method described in Chapter 3. If a big variation in the sampling amount is observed in one or several spots, the specific capillary could be adjusted accordingly.

Spatial distribution of doxorubicin

In TACE treatment, DOX is delivered via the hepatic artery and goes directly to the tumor. Therefore the concentration of DOX should be highest at the tumor and decrease gradually from the release point. To test this hypothesis, the high throughput multi-capillary system can be used to establish the spatial distribution map of DOX in a tissue cross-section. However, it is difficult to find the point where DOX releases in the tissue samples used in Chapter 3. In a newer TACE method which uses drug-eluting beads,[234] the center of drug administration is easier to define in a tissue cross-section (Figure 7-1). These tissues can be used to determine the relationship between tissue DOX concentration and its distance from the point of delivery, i.e., the beads. These measurements would be extremely beneficial in evaluating the efficiency of the treatments that use drug-eluting beads.

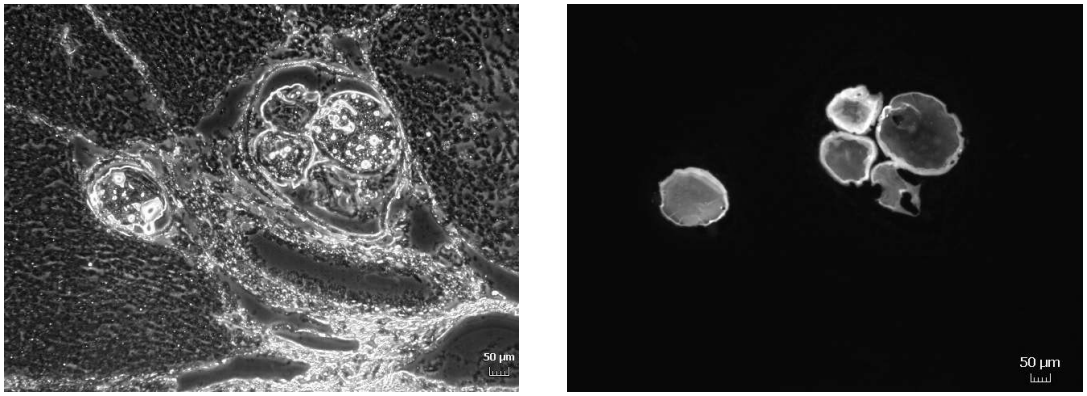

Figure 7-1. Images of a swine liver cross-section after treatment with TACE using doxorubicin-eluting beads. The beads (100-300 µm in diameter) can be easily observed in both (A) bright field and (B) epi-fluorescence images.

In vitro metabolism of doxorubicin in tissue cross-sections

Formation and progression of tumors appear to affect the activities of drug-metabolizing enzymes. In hepatocellular carcinoma tissues, the activity of glucose-6-phosphatase was lost in 6 out of 9 hepatocellular carcinoma (HCC) cases.[235] Another study showed that compared with normal prostate epithelia, human prostate cancers loose expression of carbonyl reductase, an important enzyme in metabolizing DOX to secondary alcohol metabolites, such as DOXol.[236] We hypothesize that the metabolic activity throughout an HCC liver is different, which results in heterogeneous types and concentrations of DOX metabolites in different regions of the liver. Since different metabolites have different efficacy and toxicity, revealing this heterogeneity will help to understand the efficacy and toxicity of DOX treatments. Treatment of tissue homogenates from the tumor and non-tumor regions of an HCC liver with DOX revealed different metabolic activities in these two regions (Figure 7-2). This is in agreement with our hypothesis that tumor and non-tumor regions have different metabolic activity. It is worth to mention that the tissue has been stored in Optimal Cutting Temperature

compound at -80˚C for 1 year and still have metabolic activity. This is in agreement with the findings that drug metabolizing enzymes such as cytochrome P450 activity and NADPH-cytochrome c reductase activities in human liver microsomes are largely preserved after long term storage at -80˚C.[237]

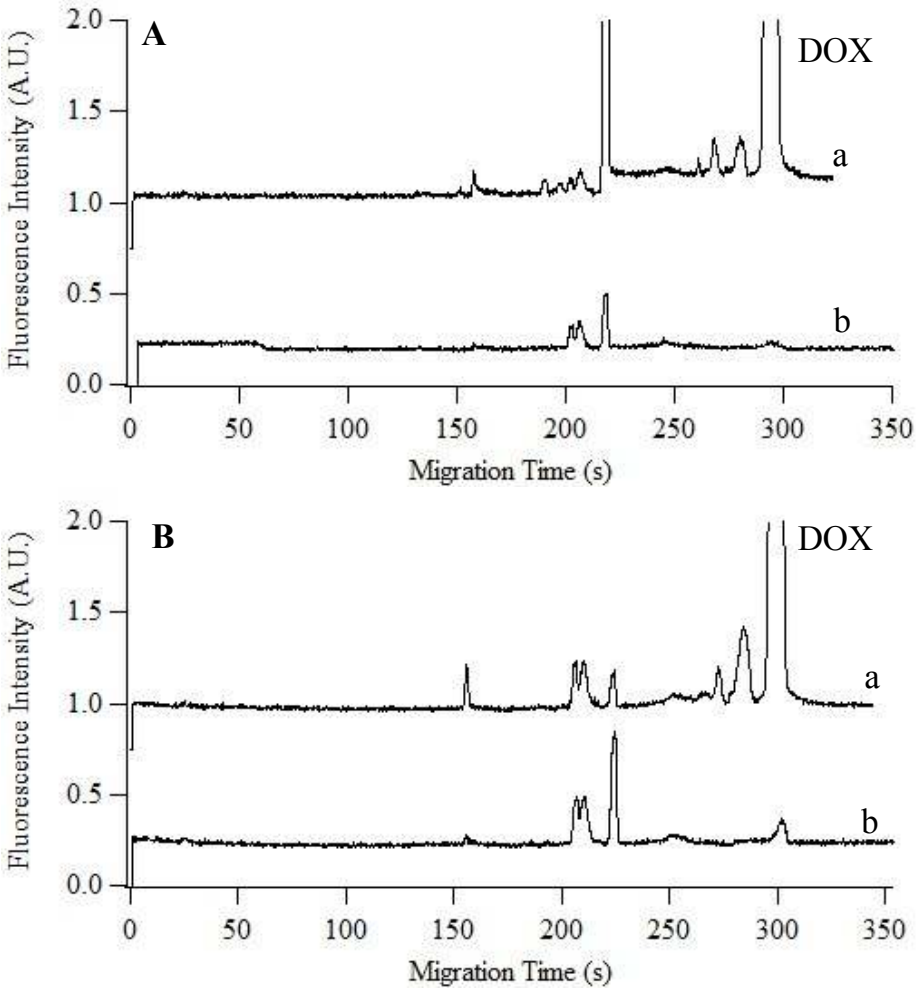

Figure 7-2. *In vitro* metabolism of doxorubicin in liver sample after being frozen for one year at -80ºC. A small piece of tissue was cut from the tumor (A) or non tumor (B) regions of an HCC liver and homogenized. The post-nuclear fractions (PNF) were incubated with 10 μM DOX, 1 mM NADPH and 5 mM $MgCl_2$ for 2 h at 37ºC (trace a). PNF without DOX addition was used as control (trace b). The MEKC was performed in a 43.5 cm fused silica capillary under a 400 V/cm electric field in a buffer containing 10 mM borate and 10 mM SDS (pH = 9.3). The fluorescence was selected by a 635 ± 27.5 nm bandpass filter and detected by a photomultiplier tube biased at 1000V. Upper traces are offset offset along the y-axis for clarity.

Although bulk studies reveal different metabolic activities in the tumor and non-tumor regions of an HCC liver, it cannot reveal the heterogeneity within the same region. To solve this problem, the direct tissue sampling technique (c.f. Chapter 3) could be used to investigate the in vitro metabolites of DOX in different spots within the same region Briefly, DOX could be homogeneously delivered to a tissue cross-section with a gelatin slice (5 μM) overlaid on the top of the tissue cross-section. After incubation at 37˚C after a period of time (e.g., 2 h), tissues at different spots in tumor and non-tumor regions can be sampled by direct tissue sampling and the metabolites can be analyzed by MEKC-LIF.

After these further developments, this direct tissue analysis technique has potential applicability for analyzing other highly heterogenous tissues such as brain tissue to determine the tissue distribution of fluorescence biomolecules or xenobiotics.

7.2.2 Subcellular metabolism

Organelle Purification

In Chapters 4 and 5, the subcellular fractions used to investigate metabolism were prepared by differential centrifugation. The purity of the fractions obtained by this method is usually low, which is a major limitation in characterizing the subcellular metabolism of DOX. Highly enriched subcellular fractions could be prepared using immunoisolation (c.f. Chapte 6). This method used antibodies specific to protein targets on the organelle surface to capture the organelles of interest. Table 7-1 lists the antibodies that have been used in enriching mitochondria, lysosomes and peroxisomes.

Aptamers which are single stranded DNA or RNA binding to molecular targets with high affinity and specificity might be another affinity reagent useful in the enrichment of organelles. There are reports on using aptamers to select small-cell lung cancer cells and acute myeloid leukemia cells,[1, 238] but none of them target subcellular organelles. Aptmers specific to a type of organelles could be developed using SELEX (systematic evolution of ligands through exponential enrichment) and replace antibodies.

Table 7-1. Antibodies for immunoisolation of organelles

Organelle	Antibody*
Mitochondria	Anti-TOM22[95]
Peroxisomes	Anti-PMP70[96]
Early endosomes	Anti-EEA1[239]
Late endosomes/lysosomes	Anti-LAMP-1[239]

*TOM22: ***Translocase*** of outer membrane ***22 kDa*** subunit, PMP70: 70 kDa peroxisomal membrane protein, EEA1: Early Endosome Antigen 1, LAMP-1: lysosomal -associated membrane protein 1

Microfluidic bioreactors

Determination of biotransformation kinetics of DOX or other drugs in subcellular fractions requires monitoring different concentrations of substrate and different reaction times. As multiple conditions need to be tested, a high-throughput device could be designed to carry out and monitor many reactions in parallel. A microfluidic device with multiple channels and a bottom covered with paramagnetic elements could be useful for these studies (Figure 7-3A). Organelles isolated via antibody-bound supermagnetic beads could be trapped in the wells by applying a magnetic field to the device. DOX with different concentrations and cofactors could then be delivered. After a short time upon delivery, DOX and cofactors outside the organelles could be washed off. After incubation for a given period of time, the organelles would be exposed to a lysing buffer. DOX and

metabolites could then be separated in the following separation channels and detected with LIF at 90ºin respect to the excitation laser (Figure 7-3C).[240] The device could be reused by removing the magnetic field and washing off the supermagnetic beads.

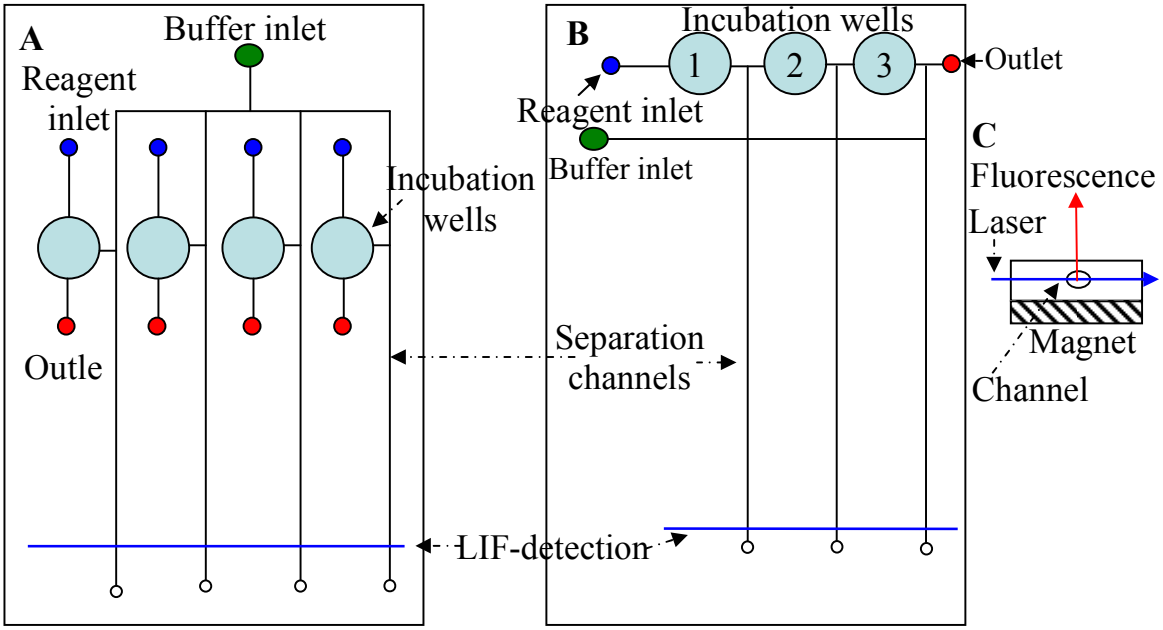

Figure 7-3. Proposed microfluidic device designed for subcellular metabolism analysis. (A) Device for kinetic studies. Substrate in different concentrations could be incubated with organelles bounded to supermagnetic beads in the incubation wells. The resulting metabolites could be separated in the separation channels. (B) Device for sequential metabolism which could be performed in well 1 to 3 where different types of organelles are immobilized. The metabolites from each step could be separated in the separation channel. (C) Side-view of the microfluidic device. The magnet is placed at the bottom of the device. The emitted fluorescence of the analytes is collected at 90º in respect to the excitation laser.

A slightly modified microfluidic device could be used to study the sequential metabolism of DOX in multiple subcellular compartments. In these studies, the metabolites formed in a type of organelle might be the substrate of another type of organelle (Figure 7-2B). As the organelles are immobilized on supermagnetic beads and trapped in the devices with a magnet, this sequence of organelles could be changed easily,

which may result in the formation of different metabolites.. These studies would help to elucidate the metabolic pathways and reveal the organelles that are indispensable in the formation of a specific metabolite.

7.2.3 Capillary electrophoresis coupled to mass spectrometry (CE-MS)

Identification of DOX metabolites

Although MEKC-LIF is powerful in separating and detecting metabolites of DOX, their identification is difficult. In Chapter 5, DOX metabolites formed in rat liver subcellular fractions were identified with internal standard addition, mobility comparison with standards and comparing with HPLC-MS results. Since these methods are indirect, the identification of metabolites may not be accurate. In order to identify metabolites directly, understand their roles in the efficacy and toxicity of DOX treatments and elucidate metabolic pathways, development of MEKC-LIF-MS would be a major advance. In this setup, LIF is be used for quantification and MS is used for metabolite identification. The major challenge of coupling MEKC to MS is the buffer used in MEKC is not compatible with MS. The separation buffer used in the projects described in this thesis contained anionic surfactant SDS and high concentration of salts (e.g., 10 or 50 mM borate) which will cause loss of analyte sensitivity and contamination in ion source.[133] Different approaches that may solve this problem include using electrospray-chemical ionization (ES-CI), high-molecular-mass surfactant and a buffer renewal system.[133] ES-CI can tolerate higher concentrations of nonvolatile salts and surfactants than electrospray ionization.[241] The use of high-molecular-mass surfactant allows the formation of micelles at very low surfactant concentration and the reduction of

low-molecular-mass background ions. A buffer renewal system uses a secondary capillary to separate analytes of interest from micelles and buffer additives before the analytes enter the MS.[242]

The sensitivity of MS is another bottleneck of MEKC-MS in subcellular analysis. MEKC is performed in a narrow capillary under a high electric field. The flow rate is low (several hundred nL per min)[243] and the amount of analytes is usually small (less than 10^{-15} mole), which requires high sensitivity. Approaches to improve the sensitivity of MEKC-MS include on-line preconcentration by capillary isotachophoresis or using a pre-column to concentrate samples before CE separation.[134] Another solution for improving the sensitivity of MEKC-MS is the use of mass spectrometers with mass analyzers that have greater sensitivity, such as ion trap, Fourier transform ion cyclotron resonance, time-of-flight (TOF) and orbitrap.[134]

The developed MEKC-LIF-MS system could also be applied to study the transformation of more complicated DOX prodrugs and other fluorescent prodrugs in biological systems. Identifying the products during prodrog activation would help to elucidate the prodrug activation mechanism and understand their efficacy and toxicity.

Other Applications

DOX is usually coadministered as cocktail therapy with other chemotherapy drugs such as mitomycin C and cis-platin in treating cancers such as HCC and non-small cell lung cancers.[244, 245] These non-fluorescent drugs can not be analyzed by MEKC-LIF. If MEKC coupled with MS was developed, it could be used to study fluorescence and non-fluorescent chemotherapy drugs and metabolites in cocktail therapies. This would

provide a better understanding of the treatment than studying DOX and its metabolites alone.

With these improvements, the CE-based methodologies and techniques described in this thesis would add new versatile methods to study the distribution and metabolism of drugs in different biological samples, which is needed to understand the efficacy and toxicity of the treatments in preclinical and clinical studies.

Bibliography

1. Sefah, K.; Tang, Z. W.; Shangguan, D. H.; Chen, H.; Lopez-Colon, D.; Li, Y.; Parekh, P.; Martin, J.; Meng, L.; Phillips, J. A.; Kim, Y. M.; Tan, W. H., Molecular recognition of acute myeloid leukemia using aptamers. *Leukemia* **2009,** 23, (2), 235-44.
2. Arcamone, F.; Cassinelli, G.; Fantini, G.; Grein, A.; Orezzi, P.; Pol, C.; Spalla, C., Adriamycin, 14-hydroxydaunomycin, a new antitumor antibiotic from S. peucetius var. caesius. *Biotechnol Bioeng* **1969,** 11, (6), 1101-10.
3. Blum, R. H.; Carter, S. K., Adriamycin. A new anticancer drug with significant clinical activity. *Ann Intern Med* **1974,** 80, (2), 249-59.
4. Kanjeekal, S.; Chambers, A.; Fung, M. F.; Verma, S., Systemic therapy for advanced uterine sarcoma: a systematic review of the literature. *Gynecol Oncol* **2005,** 97, (2), 624-37.
5. Marelli, L.; Stigliano, R.; Triantos, C.; Senzolo, M.; Cholongitas, E.; Davies, N.; Tibballs, J.; Meyer, T.; Patch, D. W.; Burroughs, A. K., Transarterial therapy for hepatocellular carcinoma: which technique is more effective? A systematic review of cohort and randomized studies. *Cardiovasc Intervent Radiol* **2007,** 30, (1), 6-25.
6. Karukstis, K. K.; Thompson, E. H.; Whiles, J. A.; Rosenfeld, R. J., Deciphering the fluorescence signature of daunomycin and doxorubicin. *Biophys Chem* **1998,** 73, (3), 249-63.
7. Barabas, K.; Sizensky, J. A.; Faulk, W. P., Transferrin conjugates of adriamycin are cytotoxic without intercalating nuclear DNA. *J Biol Chem* **1992,** 267, (13), 9437-42.
8. Dalmark, M.; Storm, H. H., A Fickian diffusion transport process with features of transport catalysis. Doxorubicin transport in human red blood cells. *J. Gen. Physiol.* **1981,** 78, (4), 349-64.
9. Malisza, K. L.; McIntosh, A. R.; Sveinson, S. E.; Hasinoff, B. B., Semiquinone free radical formation by daunorubicin aglycone incorporated into the cellular membranes of intact Chinese hamster ovary cells. *Free Radic Res* **1996,** 24, (1), 9-18.
10. Matheny, C. J.; Lamb, M. W.; Brouwer, K. R.; Pollack, G. M., Pharmacokinetic and pharmacodynamic implications of P-glycoprotein modulation. *Pharmacotherapy* **2001,** 21, (7), 778-96.
11. Singal, P. K.; Li, T.; Kumar, D.; Danelisen, I.; Iliskovic, N., Adriamycin-induced heart failure: mechanism and modulation. *Mol Cell Biochem* **2000,** 207, (1-2), 77-86.
12. Vora, J.; Boroujerdi, M., Pharmacokinetic-toxicodynamic relationships of adriamycin in rat: prediction of butylated hydroxyanisole-mediated reduction in anthracycline cardiotoxicity. *J Pharm Pharmacol* **1996,** 48, (12), 1264-9.
13. Gottesman, M. M.; Fojo, T.; Bates, S. E., Multidrug resistance in cancer: role of ATP-dependent transporters. *Nat Rev Cancer* **2002,** 2, (1), 48-58.
14. Cusack, B. J.; Young, S. P.; Driskell, J.; Olson, R. D., Doxorubicin and doxorubicinol pharmacokinetics and tissue concentrations following bolus injection and continuous infusion of doxorubicin in the rabbit. *Cancer Chemother Pharmacol* **1993,** 32, (1), 53-8.
15. Peters, J. H.; Gordon, G. R.; Kashiwase, D.; Acton, E. M., Tissue distribution of doxorubicin and doxorubicinol in rats receiving multiple doses of doxorubicin. *Cancer Chemother Pharmacol* **1981,** 7, (1), 65-9.
16. Muller, C.; Chatelut, E.; Gualano, V.; De Forni, M.; Huguet, F.; Attal, M.; Canal, P.; Laurent, G., Cellular pharmacokinetics of doxorubicin in patients with chronic

lymphocytic leukemia: comparison of bolus administration and continuous infusion. *Cancer Chemother Pharmacol* **1993,** 32, (5), 379-84.
17. Yamada, R.; Sato, M.; Kawabata, M.; Nakatsuka, H.; Nakamura, K.; Takashima, S., Hepatic artery embolization in 120 patients with unresectable hepatoma. *Radiology* **1983,** 148, (2), 397-401.
18. Storm, G.; van Hoesel, Q. G.; de Groot, G.; Kop, W.; Steerenberg, P. A.; Hillen, F. C., A comparative study on the antitumor effect, cardiotoxicity and nephrotoxicity of doxorubicin given as a bolus, continuous infusion or entrapped in liposomes in the Lou/M Wsl rat. *Cancer Chemother Pharmacol* **1989,** 24, (6), 341-8.
19. Florent, J. C.; Monneret, C., Doxorubicin conjugates for selective delivery to tumors. *Anthracycline Chemistry and Biology Ii: Mode of Action, Clinical Aspects and New Drugs* **2008,** 283, 99-140.
20. Aroui, S.; Brahim, S.; Waard, M. D.; Kenani, A., Cytotoxicity, intracellular distribution and uptake of doxorubicin and doxorubicin coupled to cell-penetrating peptides in different cell lines: a comparative study. *Biochem Biophys Res Commun* 391, (1), 419-25.
21. Gabizon, A.; Shmeeda, H.; Barenholz, Y., Pharmacokinetics of pegylated liposomal Doxorubicin: review of animal and human studies. *Clin Pharmacokinet* **2003,** 42, (5), 419-36.
22. Venook, A. P.; Stagg, R. J.; Lewis, B. J.; Chase, J. L.; Ring, E. J.; Maroney, T. P.; Hohn, D. C., Chemoembolization for hepatocellular carcinoma. *J. Clin. Oncol.* **1990,** 8, (6), 1108-14.
23. Rooseboom, M.; Commandeur, J. N. M.; Vermeulen, N. P. E., Enzyme-catalyzed activation of anticancer prodrugs. *Pharmacological Reviews* **2004,** 56, (1), 53-102.
24. Connors, T. A., Prodrugs in cancer chemotherapy. *Xenobiotica* **1986,** 16, (10-11), 975-88.
25. de Groot, F. M. H.; Damen, E. W. P.; Scheeren, H. W., Anticancer prodrugs for application in monotherapy: Targeting hypoxia, tumor-associated enzymes, and receptors. *Current Medicinal Chemistry* **2001,** 8, (9), 1093-1122.
26. Bagshawe, K. D., Antibody-directed enzyme prodrug therapy for cancer: its theoretical basis and application. *Mol Med Today* **1995,** 1, (9), 424-31.
27. Andreasen, P. A.; Egelund, R.; Petersen, H. H., The plasminogen activation system in tumor growth, invasion, and metastasis. *Cell Mol Life Sci* **2000,** 57, (1), 25-40.
28. Bagshawe, K. D.; Springer, C. J.; Searle, F.; Antoniw, P.; Sharma, S. K.; Melton, R. G.; Sherwood, R. F., A cytotoxic agent can be generated selectively at cancer sites. *Br J Cancer* **1988,** 58, (6), 700-3.
29. Dubowchik, G. M.; Firestone, R. A.; Padilla, L.; Willner, D.; Hofstead, S. J.; Mosure, K.; Knipe, J. O.; Lasch, S. J.; Trail, P. A., Cathepsin B-labile dipeptide linkers for lysosomal release of doxorubicin from internalizing immunoconjugates: model studies of enzymatic drug release and antigen-specific in vitro anticancer activity. *Bioconjug Chem* **2002,** 13, (4), 855-69.
30. DeFeo-Jones, D.; Garsky, V. M.; Wong, B. K.; Feng, D. M.; Bolyar, T.; Haskell, K.; Kiefer, D. M.; Leander, K.; McAvoy, E.; Lumma, P.; Wai, J.; Senderak, E. T.; Motzel, S. L.; Keenan, K.; Van Zwieten, M.; Lin, J. H.; Freidinger, R.; Huff, J.; Oliff, A.; Jones, R. E., A peptide-doxorubicin 'prodrug' activated by prostate-specific antigen selectively kills

prostate tumor cells positive for prostate-specific antigen in vivo. *Nat Med* **2000,** 6, (11), 1248-52.
31. Lee, G. Y.; Song, J. H.; Kim, S. Y.; Park, K.; Byun, Y., Peptide-doxorubicin conjugates specifically degraded by matrix metalloproteinases expressed from tumor. *Drug Development Research* **2006,** 67, (5), 438-447.
32. Wu, W.; Luo, Y.; Sun, C.; Liu, Y.; Kuo, P.; Varga, J.; Xiang, R.; Reisfeld, R.; Janda, K. D.; Edgington, T. S.; Liu, C., Targeting cell-impermeable prodrug activation to tumor microenvironment eradicates multiple drug-resistant neoplasms. *Cancer Res* **2006,** 66, (2), 970-80.
33. de Groot, F. M.; Broxterman, H. J.; Adams, H. P.; van Vliet, A.; Tesser, G. I.; Elderkamp, Y. W.; Schraa, A. J.; Kok, R. J.; Molema, G.; Pinedo, H. M.; Scheeren, H. W., Design, synthesis, and biological evaluation of a dual tumor-specific motive containing integrin-targeted plasmin-cleavable doxorubicin prodrug. *Mol Cancer Ther* **2002,** 1, (11), 901-11.
34. Pechar, M.; Ulbrich, K.; Jelinkova, M.; Rihova, B., Conjugates of antibody-targeted PEG multiblock polymers with doxorubicin in cancer therapy. *Macromolecular Bioscience* **2003,** 3, (7), 364-372.
35. Trouet, A. D.-D. C., D.; Baurain, R.; Masquelier, M, N-L-Leucyl derivatives of daunorubicin and doxorubicin as new prodrugs of anthracyclines. *Anthracyclines, [Proc. Int. Symp. Tumor Pharmacother.]* **1983 Meeting Date 1981**, 179-81.
36. Masquelier, M.; Baurain, R.; Trouet, A., Amino acid and dipeptide derivatives of daunorubicin. 1. Synthesis, physicochemical properties, and lysosomal digestion. *J Med Chem* **1980,** 23, (11), 1166-70.
37. Baurain, R.; Masquelier, M.; Deprez-De Campeneere, D.; Trouet, A., Amino acid and dipeptide derivatives of daunorubicin. 2. Cellular pharmacology and antitumor activity on L1210 leukemic cells in vitro and in vivo. *J Med Chem* **1980,** 23, (11), 1171-4.
38. Hess, R., Localization of a cathepsin-like and aminopeptidase activity in various solid tumor transplants. *Cancer Res* **1960,** 20, 940-3.
39. Breistol, K.; Hendriks, H. R.; Berger, D. P.; Langdon, S. P.; Fiebig, H. H.; Fodstad, O., The antitumour activity of the prodrug N-L-leucyl-doxorubicin and its parent compound doxorubicin in human tumour xenografts. *Eur J Cancer* **1998,** 34, (10), 1602-6.
40. Breistol, K.; Hendriks, H. R.; Fodstad, O., Superior therapeutic efficacy of N-L-leucyl-doxorubicin versus doxorubicin in human melanoma xenografts correlates with higher tumour concentrations of free drug. *Eur J Cancer* **1999,** 35, (7), 1143-9.
41. de Jong, J.; Klein, I.; Bast, A.; van der Vijgh, W. J., Analysis and pharmacokinetics of N-l-leucyldoxorubucin and metabolites in tissues of tumor-bearing BALB/c mice. *Cancer Chemother Pharmacol* **1992,** 31, (2), 156-60.
42. Burden, D. A.; Osheroff, N., Mechanism of action of eukaryotic topoisomerase II and drugs targeted to the enzyme. *Biochimica Et Biophysica Acta-Gene Structure and Expression* **1998,** 1400, (1-3), 139-154.
43. Kellner, U.; Sehested, M.; Jensen, P. B.; Gieseler, F.; Rudolph, P., Culprit and victim -- DNA topoisomerase II. *Lancet Oncol* **2002,** 3, (4), 235-43.
44. Wilstermann, A. M.; Osheroff, N., Stabilization of eukaryotic topoisomerase II-DNA cleavage complexes. *Curr Top Med Chem* **2003,** 3, (3), 321-38.
45. Cutts, S. M.; Nudelman, A.; Rephaeli, A.; Phillips, D. R., The power and potential of doxorubicin-DNA adducts. *IUBMB Life* **2005,** 57, (2), 73-81.

46. Gewirtz, D. A., A critical evaluation of the mechanisms of action proposed for the antitumor effects of the anthracycline antibiotics adriamycin and daunorubicin. *Biochem Pharmacol* **1999,** 57, (7), 727-41.
47. Vergely, C.; Delemasure, S.; Cottin, Y.; Rochette, L., Preventing the cardiotoxic effects of anthracyclines: from basic concepts to clinical data. *Heart Metab* **2007,** 35, 1-7.
48. Kalyanaraman, B.; Joseph, J.; Kalivendi, S.; Wang, S.; Konorev, E.; Kotamraju, S., Doxorubicin-induced apoptosis: implications in cardiotoxicity. *Mol Cell Biochem* **2002,** 234-235, (1-2), 119-24.
49. Zijlstra, J. G.; de Vries, E. G.; Mulder, N. H., Multifactorial drug resistance in an adriamycin-resistant human small cell lung carcinoma cell line. *Cancer Res* **1987,** 47, (7), 1780-4.
50. Ambudkar, S. V.; Dey, S.; Hrycyna, C. A.; Ramachandra, M.; Pastan, I.; Gottesman, M. M., Biochemical, cellular, and pharmacological aspects of the multidrug transporter. *Annu Rev Pharmacol Toxicol* **1999,** 39, 361-98.
51. Maraldi, N. M.; Zini, N.; Santi, S.; Scotlandi, K.; Serra, M.; Baldini, N., P-glycoprotein subcellular localization and cell morphotype in MDR1 gene-transfected human osteosarcoma cells. *Biol Cell* **1999,** 91, (1), 17-28.
52. Solazzo, M.; Fantappie, O.; Lasagna, N.; Sassoli, C.; Nosi, D.; Mazzanti, R., P-gp localization in mitochondria and its functional characterization in multiple drug-resistant cell lines. *Exp Cell Res* **2006,** 312, (20), 4070-8.
53. Chen, G.; Duran, G. E.; Steger, K. A.; Lacayo, N. J.; Jaffrezou, J. P.; Dumontet, C.; Sikic, B. I., Multidrug-resistant human sarcoma cells with a mutant P-glycoprotein, altered phenotype, and resistance to cyclosporins. *J Biol Chem* **1997,** 272, (9), 5974-82.
54. Greer, D. A.; Ivey, S., Distinct N-glycan glycosylation of P-glycoprotein isolated from the human uterine sarcoma cell line MES-SA/Dx5. *Biochim Biophys Acta* **2007,** 1770, (9), 1275-82.
55. Harker, W. G.; Sikic, B. I., Multidrug (pleiotropic) resistance in doxorubicin-selected variants of the human sarcoma cell line MES-SA. *Cancer Res* **1985,** 45, (9), 4091-6.
56. Simon, S.; Roy, D.; Schindler, M., Intracellular pH and the control of multidrug resistance. *Proc Natl Acad Sci U S A* **1994,** 91, (3), 1128-32.
57. Wang, E.; Lee, M. D.; Dunn, K. W., Lysosomal accumulation of drugs in drug-sensitive MES-SA but not multidrug-resistant MES-SA/Dx5 uterine sarcoma cells. *J Cell Physiol* **2000,** 184, (2), 263-74.
58. Heck, M. M.; Hittelman, W. N.; Earnshaw, W. C., Differential expression of DNA topoisomerases I and II during the eukaryotic cell cycle. *Proc Natl Acad Sci U S A* **1988,** 85, (4), 1086-90.
59. de Jong, S.; Zijlstra, J. G.; de Vries, E. G.; Mulder, N. H., Reduced DNA topoisomerase II activity and drug-induced DNA cleavage activity in an adriamycin-resistant human small cell lung carcinoma cell line. *Cancer Res* **1990,** 50, (2), 304-9.
60. Guillemard, V.; Saragovi, H. U., Prodrug chemotherapeutics bypass p-glycoprotein resistance and kill tumors in vivo with high efficacy and target-dependent selectivity. *Oncogene* **2004,** 23, (20), 3613-3621.
61. Liang, J. F.; Yang, V. C., Synthesis of doxorubicin-peptide conjugate with multidrug resistant tumor cell killing activity. *Bioorg Med Chem Lett* **2005,** 15, (22), 5071-5.

62. Bennis, S.; Garcia, C.; Robert, J., Aspects of the cellular pharmacology of N-l-leucyldoxorubicin in human tumor cell lines. *Biochem. Pharmacol.* **1993,** 45, (9), 1929-31.
63. Licata, S.; Saponiero, A.; Mordente, A.; Minotti, G., Doxorubicin metabolism and toxicity in human myocardium: role of cytoplasmic deglycosidation and carbonyl reduction. *Chem Res Toxicol* **2000,** 13, (5), 414-20.
64. Donelli, M. G.; Zucchetti, M.; Munzone, E.; D'Incalci, M.; Crosignani, A., Pharmacokinetics of anticancer agents in patients with impaired liver function. *Eur J Cancer* **1998,** 34, (1), 33-46.
65. Mohutsky, M. A.; Wrighton, S. A.; Ring, B. J., *In vitro metabolism: subcellular fractions. In Handbook of drug metabolism*. 2nd ed.; Informa Healthcare USA, Inc.: New York, 2008; Vol. 186, p 694.
66. Kivisto, K. T.; Kroemer, H. K.; Eichelbaum, M., The role of human cytochrome P450 enzymes in the metabolism of anticancer agents: implications for drug interactions. *Br J Clin Pharmacol* **1995,** 40, (6), 523-30.
67. Neve, E. P.; Ingelman-Sundberg, M., Intracellular transport and localization of microsomal cytochrome P450. *Anal Bioanal Chem* **2008,** 392, (6), 1075-84.
68. Pastan, I.; Gottesman, M. M., Multidrug resistance. *Annu Rev Med* **1991,** 42, 277-86.
69. Serrano, J.; Palmeira, C. M.; Kuehl, D. W.; Wallace, K. B., Cardioselective and cumulative oxidation of mitochondrial DNA following subchronic doxorubicin administration. *Biochimica Et Biophysica Acta-Bioenergetics* **1999,** 1411, (1), 201-205.
70. Altan, N.; Chen, Y.; Schindler, M.; Simon, S. M., Defective acidification in human breast tumor cells and implications for chemotherapy. *Journal of Experimental Medicine* **1998,** 187, (10), 1583-1598.
71. Lazarow, P. B.; De Duve, C., A fatty acyl-CoA oxidizing system in rat liver peroxisomes; enhancement by clofibrate, a hypolipidemic drug. *Proc Natl Acad Sci U S A* **1976,** 73, (6), 2043-6.
72. Wanders, R. J., Peroxisomes, lipid metabolism, and human disease. *Cell Biochem Biophys* **2000,** 32 Spring, 89-106.
73. De Duve, C.; Baudhuin, P., Peroxisomes (microbodies and related particles). *Physiol Rev* **1966,** 46, (2), 323-57.
74. Schrader, M.; Fahimi, H. D., Mammalian peroxisomes and reactive oxygen species. *Histochem Cell Biol* **2004,** 122, (4), 383-93.
75. Reszka, K. J.; McCormick, M. L.; Britigan, B. E., Oxidation of anthracycline anticancer agents by the peroxidase mimic microperoxidase 11 and hydrogen peroxide. *Free Radic Biol Med* **2003,** 35, (1), 78-93.
76. Menna, P.; Salvatorelli, E.; Minotti, G., Anthracycline degradation in cardiomyocytes: a journey to oxidative survival. *Chem Res Toxicol* **2010,** 23, (1), 6-10.
77. Wauthier, V.; Verbeeck, R. K.; Calderon, P. B., The effect of ageing on cytochrome p450 enzymes: consequences for drug biotransformation in the elderly. *Curr Med Chem* **2007,** 14, (7), 745-57.
78. Colombo, T.; Donelli, M. G.; Urso, R.; Dallarda, S.; Bartosek, I.; Guaitani, A., Doxorubicin toxicity and pharmacokinetics in old and young rats. *Exp Gerontol* **1989,** 24, (2), 159-71.
79. Sekine, I.; Fukuda, H.; Kunitoh, H.; Saijo, N., Cancer chemotherapy in the elderly. *Jpn J Clin Oncol* **1998,** 28, (8), 463-73.

80. Egorin, M.; Zuhowski, E.; Thompson, B.; Reich, L.; Lee, E.; Reck, K.; Schiffer, C., Age related alterations in daunorubicin pharmacokinetics. *Proc. Am. Soc. Clin. Oncol.* **1987,** 6, 38.
81. Cusack, B. J.; Mushlin, P. S.; Voulelis, L. D.; Li, X.; Boucek, R. J., Jr.; Olson, R. D., Daunorubicin-induced cardiac injury in the rabbit: a role for daunorubicinol? *Toxicol Appl Pharmacol* **1993,** 118, (2), 177-85.
82. Von Hoff, D. D.; Layard, M. W.; Basa, P.; Davis, H. L., Jr.; Von Hoff, A. L.; Rozencweig, M.; Muggia, F. M., Risk factors for doxorubicin-induced congestive heart failure. *Ann Intern Med* **1979,** 91, (5), 710-7.
83. Schmucker, D. L.; Woodhouse, K. W.; Wang, R. K.; Wynne, H.; James, O. F.; McManus, M.; Kremers, P., Effects of age and gender on in vitro properties of human liver microsomal monooxygenases. *Clin Pharmacol Ther* **1990,** 48, (4), 365-74.
84. Sotaniemi, E. A.; Arranto, A. J.; Pelkonen, O.; Pasanen, M., Age and cytochrome P450-linked drug metabolism in humans: an analysis of 226 subjects with equal histopathologic conditions. *Clin Pharmacol Ther* **1997,** 61, (3), 331-9.
85. Shimada, T.; Yamazaki, H.; Mimura, M.; Inui, Y.; Guengerich, F. P., Interindividual variations in human liver cytochrome P-450 enzymes involved in the oxidation of drugs, carcinogens and toxic chemicals: studies with liver microsomes of 30 Japanese and 30 Caucasians. *J Pharmacol Exp Ther* **1994,** 270, (1), 414-23.
86. George, J.; Byth, K.; Farrell, G. C., Age but not gender selectively affects expression of individual cytochrome P450 proteins in human liver. *Biochem Pharmacol* **1995,** 50, (5), 727-30.
87. Tollet-Egnell, P.; Flores-Morales, A.; Stahlberg, N.; Malek, R. L.; Lee, N.; Norstedt, G., Gene expression profile of the aging process in rat liver: normalizing effects of growth hormone replacement. *Mol Endocrinol* **2001,** 15, (2), 308-18.
88. Lipscomb, J. C.; Poet, T. S., In vitro measurements of metabolism for application in pharmacokinetic modeling. *Pharmacol Ther* **2008,** 118, (1), 82-103.
89. Ekins, S.; Ring, B. J.; Grace, J.; McRobie-Belle, D. J.; Wrighton, S. A., Present and future in vitro approaches for drug metabolism. *J Pharmacol Toxicol Methods* **2000,** 44, (1), 313-24.
90. Graham, J. M.; Rickwood, D., *Subcellular fractionaton: a practical approach*. First ed.; IRL Press at Oxford University Press: Oxford, 1997; p 339 p.
91. Leighton, F.; Poole, B.; Beaufay, H.; Baudhuin, P.; Coffey, J. W.; Fowler, S.; De Duve, C., The large-scale separation of peroxisomes, mitochondria, and lysosomes from the livers of rats injected with triton WR-1339. Improved isolation procedures, automated analysis, biochemical and morphological properties of fractions. *J Cell Biol* **1968,** 37, (2), 482-513.
92. Zischka, H.; Weber, G.; Weber, P. J.; Posch, A.; Braun, R. J.; Buhringer, D.; Schneider, U.; Nissum, M.; Meitinger, T.; Ueffing, M.; Eckerskorn, C., Improved proteome analysis of Saccharomyces cerevisiae mitochondria by free-flow electrophoresis. *Proteomics* **2003,** 3, (6), 906-16.
93. Harms, E.; Kern, H.; Schneider, J. A., Human lysosomes can be purified from diploid skin fibroblasts by free-flow electrophoresis. *Proc Natl Acad Sci U S A* **1980,** 77, (10), 6139-43.
94. Islinger, M.; Li, K. W.; Loos, M.; Liebler, S.; Angermuller, S.; Abdolzade, A.; Weber, G.; Eckerskorn, C.; Voelkl, A., Peroxisomes from the heavy mitochondrial fraction:

isolation by zonal free flow electrophoresis and quantitative mass spectrometrical characterization. *J Proteome Res* **2009**.
95. Hornig-Do, H. T.; Gunther, G.; Bust, M.; Lehnartz, P.; Bosio, A.; Wiesner, R. J., Isolation of functional pure mitochondria by superparamagnetic microbeads. *Anal Biochem* **2009,** 389, (1), 1-5.
96. Luers, G. H.; Hartig, R.; Mohr, H.; Hausmann, M.; Fahimi, H. D.; Cremer, C.; Volkl, A., Immuno-isolation of highly purified peroxisomes using magnetic beads and continuous immunomagnetic sorting. *Electrophoresis* **1998,** 19, (7), 1205-10.
97. Eistenthal, R.; Danson, M. J., *Enzyme assays*. Second ed.; Oxford University Press: New York, 2002; p 384.
98. Towbin, H.; Staehelin, T.; Gordon, J., Electrophoretic transfer of proteins from polyacrylamide gels to nitrocellulose sheets: procedure and some applications. *Proc Natl Acad Sci U S A* **1979,** 76, (9), 4350-4.
99. Storrie, B.; Madden, E. A., Isolation of subcellular organelles. *Methods Enzymol* **1990,** 182, 203-25.
100. Odgren, P. R.; Toukatly, G.; Bangs, P. L.; Gilmore, R.; Fey, E. G., Molecular characterization of mitofilin (HMP), a mitochondria-associated protein with predicted coiled coil and intermembrane space targeting domains. *J Cell Sci* **1996,** 109 (Pt 9), 2253-64.
101. Barrett, A. J.; Heath, M. F., *Lysosomes: A Laboratory Handbook*. Elsevier/North-Holland Biomedical Press: Amsterdam, 1977.
102. Manunta, M.; Izzo, L.; Duncan, R.; Jones, A. T., Establishment of subcellular fractionation techniques to monitor the intracellular fate of polymer therapeutics II. Identification of endosomal and lysosomal compartments in HepG2 cells combining single-step subcellular fractionation with fluorescent imaging. *J Drug Target* **2007,** 15, (1), 37-50.
103. Luers, G.; Hashimoto, T.; Fahimi, H. D.; Volkl, A., Biogenesis of peroxisomes: isolation and characterization of two distinct peroxisomal populations from normal and regenerating rat liver. *J Cell Biol* **1993,** 121, (6), 1271-80.
104. Anderson, A. B.; Gergen, J.; Arriaga, E. A., Detection of doxorubicin and metabolites in cell extracts and in single cells by capillary electrophoresis with laser-induced fluorescence detection. *J Chromatogr B Analyt Technol Biomed Life Sci* **2002,** 769, (1), 97-106.
105. Shrestha, B.; Vertes, A., In situ metabolic profiling of single cells by laser ablation electrospray ionization mass spectrometry. *Anal Chem* **2009,** 81, (20), 8265-71.
106. Reyzer, M. L.; Hsieh, Y.; Ng, K.; Korfmacher, W. A.; Caprioli, R. M., Direct analysis of drug candidates in tissue by matrix-assisted laser desorption/ionization mass spectrometry. *J. Mass. Spectrom.* **2003,** 38, (10), 1081-92.
107. Hsieh, Y.; Casale, R.; Fukuda, E.; Chen, J.; Knemeyer, I.; Wingate, J.; Morrison, R.; Korfmacher, W., Matrix-assisted laser desorption/ionization imaging mass spectrometry for direct measurement of clozapine in rat brain tissue. *Rapid Commun Mass Spectrom* **2006,** 20, (6), 965-72.
108. Walch, A.; Rauser, S.; Deininger, S. O.; Hofler, H., MALDI imaging mass spectrometry for direct tissue analysis: a new frontier for molecular histology. *Histochem Cell Biol* **2008,** 130, (3), 421-34.

109. Bonner, R. F.; Emmert-Buck, M.; Cole, K.; Pohida, T.; Chuaqui, R.; Goldstein, S.; Liotta, L. A., Laser capture microdissection: molecular analysis of tissue. *Science* **1997,** 278, (5342), 1481,1483.
110. Wang, H. Y., Laser capture microdissection in comparative proteomic analysis of hepatocellular carcinoma. *Methods Cell Biol.* **2007,** 82, 689-707.
111. Drexler, D. M.; Garrett, T. J.; Cantone, J. L.; Diters, R. W.; Mitroka, J. G.; Prieto Conaway, M. C.; Adams, S. P.; Yost, R. A.; Sanders, M., Utility of imaging mass spectrometry (IMS) by matrix-assisted laser desorption ionization (MALDI) on an ion trap mass spectrometer in the analysis of drugs and metabolites in biological tissues. *J. Pharmacol. Toxicol. Methods* **2007,** 55, (3), 279-88.
112. Oguri, S.; Nomura, M.; Fujita, Y., Site-specific sampling of taurine from rat brain followed by on-line sample pre-concentration, throughout in-capillary derivatization and capillary electrophoresis. *J. Chromatogr. B* **2006,** 843, (2), 194-201.
113. Coley, H. M.; Amos, W. B.; Twentyman, P. R.; Workman, P., Examination by laser scanning confocal fluorescence imaging microscopy of the subcellular localisation of anthracyclines in parent and multidrug resistant cell lines. *Br J Cancer* **1993,** 67, (6), 1316-23.
114. Beyer, U.; Rothern-Rutishauser, B.; Unger, C.; Wunderli-Allenspach, H.; Kratz, F., Differences in the intracellular distribution of acid-sensitive doxorubicin-protein conjugates in comparison to free and liposomal formulated doxorubicin as shown by confocal microscopy. *Pharm Res* **2001,** 18, (1), 29-38.
115. Molinari, A.; Cianfriglia, M.; Meschini, S.; Calcabrini, A.; Arancia, G., P-glycoprotein expression in the Golgi apparatus of multidrug-resistant cells. *Int J Cancer* **1994,** 59, (6), 789-95.
116. Dejong, J.; Vermorken, J. B.; Vandervijgh, W. J. F., Analysis and Pharmacokinetics of a New Prodrug N-L-Leucyldoxorubicin and Its Metabolites in Plasma Using Hplc with Fluorescence Detection. *Journal of Pharmaceutical and Biomedical Analysis* **1992,** 10, (4), 309-314.
117. Pierce, R. N.; Jatlow, P. I., Measurement of adriamycin (doxorubicin) and its metabolites in human plasma using reversed-phase high-performance liquid chromatography and fluorescence detection. *J Chromatogr* **1979,** 164, (4), 471-8.
118. Maessen, P. A.; Pinedo, H. M.; Mross, K. B.; van der Vijgh, W. J., New method for the determination of doxorubicin, 4'-epidoxorubicin and all known metabolites in cardiac tissue. *J Chromatogr* **1988,** 424, (1), 103-10.
119. Sakai-Kato, K.; Saito, E.; Ishikura, K.; Kawanishi, T., Analysis of intracellular doxorubicin and its metabolites by ultra-high-performance liquid chromatography. *J Chromatogr B Analyt Technol Biomed Life Sci* 878, (19), 1466-70.
120. Zenkevich, I. G.; Makarov, E. D., Chromatographic quantitation at losses of analyte during sample preparation. Application of the modified method of double internal standard. *J Chromatogr A* **2007,** 1150, (1-2), 117-23.
121. Anderson, A. B.; Ciriacks, C. M.; Fuller, K. M.; Arriaga, E. A., Distribution of zeptornole-abundant doxorubicin metabolites in subcellular fractions by capillary electrophoresis with laser-induced fluorescence detection. *Analytical Chemistry* **2003,** 75, (1), 8-15.
122. Landers, J. P., *Handbook of capillary electrophoresis*. 2nd ed.; CRC Press: Boca Raton, 1997.

123. Lin, C. E.; Chen, M. J.; Huang, H. C.; Chen, H. W., Capillary electrophoresis study on the micellization and critical micelle concentration of sodium dodecyl sulfate - Influence of solubilized solutes. *Journal of Chromatography A* **2001,** 924, (1-2), 83-91.
124. Collet, J.; Gareil, P., Micellar electrokinetic chromatography of long chain saturated and unsaturated free fatty acids with neutral micelles - Considerations regarding selectivity and resolution optimization. *Journal of Chromatography A* **1997,** 792, (1-2), 165-177.
125. Landers, J. P.; Oda, R. P.; Schuchard, M. D., Separation of Boron-Complexed Diol Compounds Using High-Performance Capillary Electrophoresis. *Analytical Chemistry* **1992,** 64, (22), 2846-2851.
126. Rathore, A. S., Joule heating and determination of temperature in capillary electrophoresis and capillary electrochromatography columns. *J Chromatogr A* **2004,** 1037, (1-2), 431-43.
127. Beckers, J. L.; Bocek, P., Multiple effect of surfactants used as additives in background electrolytes in capillary zone electrophoresis: cetyltrimethylammonium bromide as example of model surfactant. *Electrophoresis* **2002,** 23, (12), 1947-52.
128. Nishi, H.; Fukuyama, T.; Terabe, S., Chiral separation by cyclodextrin-modified micellar electrokinetic chromatography. *Journal of Chromatography A* **1991,** 553, 503.
129. Fanali, S., Enantioselective determination by capillary electrophoresis with cyclodextrins as chiral selectors. *J Chromatogr A* **2000,** 875, (1-2), 89-122.
130. Terabe, S.; Miyashita, Y.; Shibata, O.; Barnhart, E. R.; Alexander, L. R.; Patterson, D. G.; Karger, B. L.; Hosoya, K.; Tanaka, N., Separation of highly hydrophobic compounds by cyclodextrin-modified micellar electrokinetic chromatography. *Journal of Chromatography A* **1990,** 516, (1), 23.
131. Eder, A. R.; Chen, J. S.; Arriaga, E. A., Separation of doxorubicin and doxorubicinol by cyclodextrin-modified micellar electrokinetic capillary chromatography. *Electrophoresis* **2006,** 27, (16), 3263-3270.
132. Gavenda, A.; Sevcik, J.; Psotova, J.; Bednar, P.; Bartak, P.; Adamovsky, P.; Simanek, V., Determination of anthracycline antibiotics doxorubicin and daunorubicin by capillary electrophoresis with UV absorption detection. *Electrophoresis* **2001,** 22, (13), 2782-5.
133. Yang, L.; Lee, C. S., Micellar electrokinetic chromatography-mass spectrometry. *J Chromatogr A* **1997,** 780, (1-2), 207-18.
134. Cai, J. Y.; Henion, J., Capillary Electrophoresis Mass-Spectrometry. *Journal of Chromatography A* **1995,** 703, (1-2), 667-692.
135. Ewing, A. G.; Wallingford, R. A.; Olefirowicz, T. M., Capillary electrophoresis. *Anal Chem* **1989,** 61, (4), 292A-303A.
136. Wu, S.; Dovichi, N. J., High-sensitivity fluorescence detector fluorescein isothiocyanate derivatives of amino acids separated by capillary zone electrophoresis. *J Chromatogr* **1989,** 480, 141-55.
137. Li, X. F.; Ren, H.; Le, X.; Qi, M.; Ireland, I. D.; Dovichi, N. J., Migration time correction for the analysis of derivatized amino acids and oligosaccharides by micellar capillary electrochromatography. *J. Chromatogr. A* **2000,** 869, (1-2), 375-84.
138. Malarkey, D. E.; Johnson, K.; Ryan, L.; Boorman, G.; Maronpot, R. R., New insights into functional aspects of liver morphology. *Toxicol. Pathol.* **2005,** 33, (1), 27-34.

139. Vona, G.; Tuveri, R.; Delpuech, O.; Vallet, A.; Canioni, D.; Ballardini, G.; Baptiste Trabut, J.; Le Bail, B.; Nalpas, B.; Carnot, F.; Pol, S.; Brechot, C.; Thiers, V., Intrahepatic hepatitis C virus RNA quantification in microdissected hepatocytes. *J. Hepatol.* **2004,** 40, (4), 682-8.
140. Sobesky, R.; Feray, C.; Rimlinger, F.; Derian, N.; Dos Santos, A.; Roque-Afonso, A. M.; Samuel, D.; Brechot, C.; Thiers, V., Distinct hepatitis C virus core and F protein quasispecies in tumoral and nontumoral hepatocytes isolated via microdissection. *Hepatology* **2007,** 46, (6), 1704-12.
141. Anderson, A. B.; Gergen, J.; Arriaga, E. A., Detection of doxorubicin and metabolites in cell extracts and in single cells by capillary electrophoresis with laser-induced fluorescence detection. *J. Chromatogr. B* **2002,** 769, (1), 97-106.
142. de Jong, J.; Bast, A.; van der Vijgh, W. J. F., Analysis of anthracycline antitumour drugs in tissues and body fluids using liquid chromatography. *TrAC, Trends Anal. Chem.* **1993,** 12, (10), 422-8.
143. Krylov, S. N.; Starke, D. A.; Arriaga, E. A.; Zhang, Z.; Chan, N. W.; Palcic, M. M.; Dovichi, N. J., Instrumentation for chemical cytometry. *Anal Chem* **2000,** 72, (4), 872-7.
144. Eder, A. R.; Arriaga, E. A., Capillary electrophoresis monitors enhancement in subcellular reactive oxygen species production upon treatment with doxorubicin. *Chem. Res. Toxicol.* **2006,** 19, (9), 1151-9.
145. Anderson, A. B.; Xiong, G.; Arriaga, E. A., Doxorubicin accumulation in individually electrophoresed organelles. *J. Am. Chem. Soc.* **2004,** 126, (30), 9168-9.
146. Anderson, A. B.; Ciriacks, C. M.; Fuller, K. M.; Arriaga, E. A., Distribution of zeptomole-abundant doxorubicin metabolites in subcellular fractions by capillary electrophoresis with laser-induced fluorescence detection. *Anal. Chem.* **2003,** 75, (1), 8-15.
147. Lee, K. Y.; Mooney, D. J., Hydrogels for tissue engineering. *Chem Rev* **2001,** 101, (7), 1869-79.
148. Eder, A. R.; Arriaga, E. A., Micellar electrokinetic capillary chromatography reveals differences in intracellular metabolism between liposomal and free doxorubicin treatment of human leukemia cells. *J. Chromatogr. B* **2005,** 829, (1-2), 115-22.
149. Eder, A. R.; Chen, J. S.; Arriaga, E. A., Separation of doxorubicin and doxorubicinol by cyclodextrin-modified micellar electrokinetic capillary chromatography. *Electrophoresis* **2006,** 27, (16), 3263-70.
150. Gavelova, M.; Hladikova, J.; Vildova, L.; Novotna, R.; Vondracek, J.; Krcmar, P.; Machala, M.; Skalova, L., Reduction of doxorubicin and oracin and induction of carbonyl reductase in human breast carcinoma MCF-7 cells. *Chem. Biol. Interact.* **2008,** 176, (1), 9-18.
151. Imamura, H.; Kawasaki, S.; Shiga, J.; Bandai, Y.; Sanjo, K.; Idezuki, Y., Quantitative evaluation of parenchymal liver cell volume and total hepatocyte number in cirrhotic patients. *Hepatology* **1991,** 14, (3), 448-53.
152. Hu, K.; Ahmadzadeh, H.; Krylov, S. N., Asymmetry between sister cells in a cancer cell line revealed by chemical cytometry. *Anal. Chem.* **2004,** 76, (13), 3864-6.
153. Boardman, A. K.; McQuaide, S. C.; Zhu, C.; Whitmore, C. D.; Lidstrom, M. E.; Dovichi, N. J., Interface of an array of five capillaries with an array of one-nanoliter wells for high-resolution electrophoretic analysis as an approach to high-throughput chemical cytometry. *Anal. Chem.* **2008,** 80, (19), 7631-4.

154. Blum, R. H.; Carter, S. K., Adriamycin. A new anticancer drug with significant clinical activity. *Ann. Intern. Med.* **1974,** 80, (2), 249-59.
155. Young, R. C.; Ozols, R. F.; Myers, C. E., The anthracycline antineoplastic drugs. *New Engl. J. Med.* **1981,** 305, (3), 139-53.
156. Mathé, G.; Maral, R.; De Jager, R.; Fondation Simone et Cino Del Duca., *Anthracyclines: current status and future developments*. Masson Pub. USA: New York, 1983; p xviii, 214 p.
157. Zbinden, G.; DeCampeenere, D.; Baurain, R., Preclinical assessment of the cardiotoxic potential of anthracycline antibiotics: N-L-leucyl-doxorubicin. *Arch. Toxicol. Suppl.* **1991,** 14, 107-17.
158. Breistol, K.; Hendriks, H. R.; Berger, D. P.; Langdon, S. P.; Fiebig, H. H.; Fodstad, O., The antitumour activity of the prodrug N-L-leucyl-doxorubicin and its parent compound doxorubicin in human tumour xenografts. *Eur. J. Cancer* **1998,** 34, (10), 1602-1606.
159. Breistol, K.; Hendriks, H. R.; Fodstad, O., Superior therapeutic efficacy of N-L-leucyl-doxorubicin versus doxorubicin in human melanoma xenografts correlates with higher tumour concentrations of free drug. *Eur. J. Cancer* **1999,** 35, (7), 1143-1149.
160. de Jong, J.; Geijssen, G. J.; Munniksma, C. N.; Vermorken, J. B.; van der Vijgh, W. J., Plasma pharmacokinetics and pharmacodynamics of a new prodrug N-l-leucyldoxorubicin and its metabolites in a phase I clinical trial. *J Clin Oncol* **1992,** 10, (12), 1897-906.
161. Dejong, J.; Vermorken, J. B.; Vandervijgh, W. J. F., Analysis and Pharmacokinetics of a New Prodrug N-L-Leucyldoxorubicin and Its Metabolites in Plasma Using Hplc with Fluorescence Detection. *J. Pharm. Biomed. Anal.* **1992,** 10, (4), 309-314.
162. Wilstermann, A. M.; Osheroff, N., Stabilization of eukaryotic topoisomerase II-DNA cleavage complexes. *Curr. Top. Med. Chem.* **2003,** 3, (3), 321-38.
163. Gewirtz, D. A., A critical evaluation of the mechanisms of action proposed for the antitumor effects of the anthracycline antibiotics adriamycin and daunorubicin. *Biochem. Pharmacol.* **1999,** 57, (7), 727-41.
164. Reinhoud, N. J.; Tjaden, U. R.; Irth, H.; van der Greef, J., Bioanalysis of some anthracyclines in human plasma by capillary electrophoresis with laser-induced fluorescence detection. *J Chromatogr.* **1992,** 574, (2), 327-34.
165. Simeon, N.; Chatelut, E.; Canal, P.; Nertz, M.; Couderc, F., Anthracycline analysis by capillary electrophoresis. Application to the analysis of daunorubicine in Kaposi sarcoma tumor.*J. Chromatogr. A* **1999,** 853, (1-2), 449-54.
166. Gosland, M. P.; Lum, B. L.; Sikic, B. I., Reversal by cefoperazone of resistance to etoposide, doxorubicin, and vinblastine in multidrug resistant human sarcoma cells. *Cancer Res.* **1989,** 49, (24 Pt 1), 6901-5.
167. Chen, G.; Duran, G. E.; Steger, K. A.; Lacayo, N. J.; Jaffrezou, J. P.; Dumontet, C.; Sikic, B. I., Multidrug-resistant human sarcoma cells with a mutant P-glycoprotein, altered phenotype, and resistance to cyclosporins. *J. Biol. Chem.* **1997,** 272, (9), 5974-82.
168. Lau, D. H.; Duran, G. E.; Lewis, A. D.; Sikic, B. I., Metabolic conversion of methoxymorpholinyl doxorubicin: from a DNA strand breaker to a DNA cross-linker. *Br. J. Cancer* **1994,** 70, (1), 79-84.

169. Battisti, R. F.; Zhong, Y.; Fang, L.; Gibbs, S.; Shen, J.; Nadas, J.; Zhang, G.; Sun, D., Modifying the sugar moieties of daunorubicin overcomes P-gp-mediated multidrug resistance. *Mol. Pharm.* **2007,** 4, (1), 140-53.
170. Stelakatos, G. C., Theodoropoulos, D.M., Zervas, L, On the trityl method for peptide synthesis. *J. Am. Chem. Soc.* **1959,** 81, (11), 2884-2887.
171. Anderson, G. W., Zimmerman, J.E., Callahan, F.M., The use of easter of N-hydroxysuccinimide in peptide synthesis. *J. Am. Chem. Soc.* **1964,** 86, (9), 1839-1842.
172. Sobottka, S. B.; Berger, M. R., Assessment of Antineoplastic Agents by Mtt Assay - Partial Underestimation of Antiproliferative Properties. *Cancer Chemother. Pharmacol.* **1992,** 30, (5), 385-393.
173. Graham, J. M.; Rickwood, D., *Subcellular fractionaton: a practical approach*. IRL Press at Oxford University Press: Oxford, 1997; p xx, 339 p.
174. Duffy, C. F.; Gafoor, S.; Richards, D. P.; Admadzadeh, H.; O'Kennedy, R.; Arriaga, E. A., Determination of properties of individual liposomes by capillary electrophoresis with postcolumn laser-induced fluorescence detection. *Anal. Chem.* **2001,** 73, (8), 1855-1861.
175. Harker, W. G.; Sikic, B. I., Multidrug (pleiotropic) resistance in doxorubicin-selected variants of the human sarcoma cell line MES-SA. *Cancer Res.* **1985,** 45, (9), 4091-6.
176. Eder, A. R.; Arriaga, E. A., Micellar electrokinetic capillary chromatography reveals differences in intracellular metabolism between liposomal and free doxorubicin treatment of human leukemia cells. *J. Chromatogr. B* **2005,** 829, (1-2), 115-22.
177. Schindler, M.; Grabski, S.; Hoff, E.; Simon, S. M., Defective pH regulation of acidic compartments in human breast cancer cells (MCF-7) is normalized in adriamycin-resistant cells (MCF-7adr). *Biochemistry* **1996,** 35, (9), 2811-7.
178. Zijlstra, J. G.; de Vries, E. G.; Mulder, N. H., Multifactorial drug resistance in an adriamycin-resistant human small cell lung carcinoma cell line. *Cancer Res.* **1987,** 47, (7), 1780-4.
179. Maton, A. J. H., Charles William McLaughlin, Susan Johnson, Maryanna Quon Warner, David LaHart, Jill D. Wright, *Human Biology and Health*. Pearson Prentice Hall: Englewood Cliffs, NJ, USA, 1993.
180. Preiss, R.; Matthias, M.; Sohr, R.; Brockmann, B.; Huller, H., Pharmacokinetics of adriamycin, adriamycinol, and antipyrine in patients with moderate tumor involvement of the liver. *J Cancer Res Clin Oncol* **1987,** 113, (6), 593-8.
181. Schmucker, D. L., Aging and the liver: an update. *J Gerontol A Biol Sci Med Sci* **1998,** 53, (5), B315-20.
182. Anantharaju, A.; Feller, A.; Chedid, A., Aging Liver. A review. *Gerontology* **2002,** 48, (6), 343-53.
183. Le Couteur, D. G.; McLean, A. J., The aging liver. Drug clearance and an oxygen diffusion barrier hypothesis. *Clin Pharmacokinet* **1998,** 34, (5), 359-73.
184. Woodhouse, K. W.; James, O. F., Hepatic drug metabolism and ageing. *Br Med Bull* **1990,** 46, (1), 22-35.
185. Zhou, S.; Starkov, A.; Froberg, M. K.; Leino, R. L.; Wallace, K. B., Cumulative and irreversible cardiac mitochondrial dysfunction induced by doxorubicin. *Cancer Res* **2001,** 61, (2), 771-7.

186. McLean, A. J.; Le Couteur, D. G., Aging biology and geriatric clinical pharmacology. *Pharmacol Rev* **2004,** 56, (2), 163-84.
187. Cadenas, E.; Davies, K. J., Mitochondrial free radical generation, oxidative stress, and aging. *Free Radic Biol Med* **2000,** 29, (3-4), 222-30.
188. Wang, Y.; Hong, J.; Cressman, E. N.; Arriaga, E. A., Direct sampling from human liver tissue cross sections for electrophoretic analysis of doxorubicin. *Anal Chem* **2009,** 81, (9), 3321-8.
189. Anderson, A. B.; Ciriacks, C. M.; Fuller, K. M.; Arriaga, E. A., Distribution of zeptomole-abundant doxorubicin metabolites in subcellular fractions by capillary electrophoresis with laser-induced fluorescence detection. *Anal Chem* **2003,** 75, (1), 8-15.
190. Arnold, R. D.; Slack, J. E.; Straubinger, R. M., Quantification of Doxorubicin and metabolites in rat plasma and small volume tissue samples by liquid chromatography/electrospray tandem mass spectroscopy. *J Chromatogr B Analyt Technol Biomed Life Sci* **2004,** 808, (2), 141-52.
191. Takahashi, R.; Goto, S., Age-associated accumulation of heat-labile aminoacyl-tRNA synthetases in mice and rats. *Arch Gerontol Geriatr* **1987,** 6, (1), 73-82.
192. Takanashi, S.; Bachur, N. R., Adriamycin metabolism in man. Evidence from urinary metabolites. *Drug Metab Dispos* **1976,** 4, (1), 79-87.
193. Gewirtz, D. A.; Yanovich, S., Metabolism of adriamycin in hepatocytes isolated from the rat and the rabbit. *Biochem Pharmacol* **1987,** 36, (11), 1793-8.
194. Riaz, A.; Chung, D. S., Calibration of migration times of variable salinity samples with internal standards in capillary electrophoresis. *Electrophoresis* **2006,** 27, (3), 553-62.
195. Pollak, N.; Dolle, C.; Ziegler, M., The power to reduce: pyridine nucleotides--small molecules with a multitude of functions. *Biochem J* **2007,** 402, (2), 205-18.
196. Peters, M. A.; Fouts, J. R., A study of some possible mechanisms by which magnesium activates hepatic microsomal drug metabolism in vitro. *J Pharmacol Exp Ther* **1970,** 173, (2), 233-41.
197. Vrignaud, P.; Londos-Gagliardi, D.; Robert, J., Hepatic metabolism of doxorubicin in mice and rats. *Eur J Drug Metab Pharmacokinet* **1986,** 11, (2), 101-5.
198. King, C. D.; Rios, G. R.; Green, M. D.; Tephly, T. R., UDP-glucuronosyltransferases. *Curr Drug Metab* **2000,** 1, (2), 143-61.
199. Negishi, M.; Pedersen, L. G.; Petrotchenko, E.; Shevtsov, S.; Gorokhov, A.; Kakuta, Y.; Pedersen, L. C., Structure and function of sulfotransferases. *Arch Biochem Biophys* **2001,** 390, (2), 149-57.
200. Santa Maria, C.; Machado, A., Changes in some hepatic enzyme activities related to phase II drug metabolism in male and female rats as a function of age. *Mech Ageing Dev* **1988,** 44, (2), 115-25.
201. Galinsky, R. E.; Johnson, D. H.; Kane, R. E.; Franklin, M. R., Effect of aging on hepatic biotransformation in female Fischer 344 rats: changes in sulfotransferase activities are consistent with known gender-related changes in pituitary growth hormone secretion in aging animals. *J Pharmacol Exp Ther* **1990,** 255, (2), 577-83.
202. Schrader, M.; Fahimi, H. D., The peroxisome: still a mysterious organelle. *Histochem Cell Biol* **2008,** 129, (4), 421-40.
203. Wanders, R. J.; Vreken, P.; Ferdinandusse, S.; Jansen, G. A.; Waterham, H. R.; van Roermund, C. W.; Van Grunsven, E. G., Peroxisomal fatty acid alpha- and

beta-oxidation in humans: enzymology, peroxisomal metabolite transporters and peroxisomal diseases. *Biochem Soc Trans* **2001,** 29, (Pt 2), 250-67.
204. Wanders, R. J.; Waterham, H. R., Biochemistry of mammalian peroxisomes revisited. *Annu Rev Biochem* **2006,** 75, 295-332.
205. Wanders, R. J.; Waterham, H. R., Peroxisomal disorders: the single peroxisomal enzyme deficiencies. *Biochim Biophys Acta* **2006,** 1763, (12), 1707-20.
206. Masters, C. J., On the role of the peroxisome in the metabolism of drugs and xenobiotics. *Biochem Pharmacol* **1998,** 56, (6), 667-73.
207. Graham, J. M., Isolation of peroxisomes from tissues and cells by differential and density gradient centrifugation. *Curr Protoc Cell Biol* **2001,** Chapter 3, Unit 3 5.
208. Volkl, A.; Fahimi, H. D., Isolation and characterization of peroxisomes from the liver of normal untreated rats. *Eur J Biochem* **1985,** 149, (2), 257-65.
209. Kikuchi, M.; Hatano, N.; Yokota, S.; Shimozawa, N.; Imanaka, T.; Taniguchi, H., Proteomic analysis of rat liver peroxisome: presence of peroxisome-specific isozyme of Lon protease. *J Biol Chem* **2004,** 279, (1), 421-8.
210. Reddy, J. K.; Hashimoto, T., Peroxisomal beta-oxidation and peroxisome proliferator-activated receptor alpha: an adaptive metabolic system. *Annu Rev Nutr* **2001,** 21, 193-230.
211. Yamada, J.; Ogawa, S.; Horie, S.; Watanabe, T.; Suga, T., Participation of peroxisomes in the metabolism of xenobiotic acyl compounds: comparison between peroxisomal and mitochondrial beta-oxidation of omega-phenyl fatty acids in rat liver. *Biochim Biophys Acta* **1987,** 921, (2), 292-301.
212. Kasurinen, J., A novel fluorescent fatty acid, 5-methyl-BDY-3-dodecanoic acid, is a potential probe in lipid transport studies by incorporating selectively to lipid classes of BHK cells. *Biochem Biophys Res Commun* **1992,** 187, (3), 1594-601.
213. Naylor, B. L.; Picardo, M.; Homan, R.; Pownall, H. J., Effects of fluorophore structure and hydrophobicity on the uptake and metabolism of fluorescent lipid analogs. *Chem Phys Lipids* **1991,** 58, (1-2), 111-9.
214. Reinhoud, N. J.; Tjaden, U. R.; Irth, H.; van der Greef, J., Bioanalysis of some anthracyclines in human plasma by capillary electrophoresis with laser-induced fluorescence detection. *J Chromatogr* **1992,** 574, (2), 327-34.
215. Simeon, N.; Chatelut, E.; Canal, P.; Nertz, M.; Couderc, F., Anthracycline analysis by capillary electrophoresis. Application to the analysis of daunorubicine in Kaposi sarcoma tumor. *J Chromatogr A* **1999,** 853, (1-2), 449-54.
216. Brando, T.; Pardin, C.; Prandi, J.; Puzo, G., Analysis of aminofluorescein-fatty acid derivatives by capillary electrophoresis with laser-induced fluorescence detection at the attomole level: application to mycobacterial fatty acids. *J Chromatogr A* **2002,** 973, (1-2), 203-10.
217. Petit, J. M.; Maftah, A.; Ratinaud, M. H.; Julien, R., 10N-nonyl acridine orange interacts with cardiolipin and allows the quantification of this phospholipid in isolated mitochondria. *Eur J Biochem* **1992,** 209, (1), 267-73.
218. Mannaerts, G. P.; Debeer, L. J., Mitochondrial and peroxisomal beta-oxidation of fatty acids in rat liver. *Ann N Y Acad Sci* **1982,** 386, 30-9.
219. Mueller, S.; Weber, A.; Fritz, R.; Mutze, S.; Rost, D.; Walczak, H.; Volkl, A.; Stremmel, W., Sensitive and real-time determination of H2O2 release from intact peroxisomes. *Biochem J* **2002,** 363, (Pt 3), 483-91.

220. Wanders, R. J.; van Roermund, C. W.; de Vries, C. T.; van den Bosch, H.; Schrakamp, G.; Tager, J. M.; Schram, A. W.; Schutgens, R. B., Peroxisomal beta-oxidation of palmitoyl-CoA in human liver homogenates and its deficiency in the cerebro-hepato-renal (Zellweger) syndrome. *Clin Chim Acta* **1986,** 159, (1), 1-10.
221. Hows, M. E. P.; Perrett, D., Effects of buffer depletion in capillary electrophoresis: Development of a continuous flow cathode. *Chromatographia* **1998,** 48, (5-6), 355-359.
222. Wendeler, M.; Sandhoff, K., Hexosaminidase assays. *Glycoconj J* **2009,** 26, (8), 945-52.
223. Vallejo-Cordoba, B.; Mazorra-Manzano, M. A.; Gonzalez-Cordova, A. F., Determination of short-chain free fatty acids in lipolyzed milk fat by capillary electrophoresis. *J Capillary Electrophor* **1998,** 5, (3-4), 111-4.
224. Zhang, L.; Hu, S.; Cook, L.; Dovichi, N. J., Analysis of aminophospholipid molecular species by methyl-beta-cyclodextrin modified micellar electrokinetic capillary chromatography with laser-induced fluorescence detection. *Electrophoresis* **2002,** 23, (17), 3071-7.
225. Sauro, V. S.; Strickland, K. P., Changes in oleic acid oxidation and incorporation into lipids of differentiating L6 myoblasts cultured in normal or fatty acid-supplemented growth medium. *Biochem J* **1987,** 244, (3), 743-8.
226. Chu, X. P.; Zhao, T.; Zhang, Y. Y.; Zhao, A. H.; Zhou, M. M.; Zheng, X. J.; Dan, M.; Jia, W., Determination of 13 Free Fatty Acids in Pheretima Using Ultra-Performance LC-ESI-MS. *Chromatographia* **2009,** 69, (7-8), 645-652.
227. Haynes, C. A.; Allegood, J. C.; Sims, K.; Wang, E. W.; Sullards, M. C.; Merrill, A. H., Jr., Quantitation of fatty acyl-coenzyme As in mammalian cells by liquid chromatography-electrospray ionization tandem mass spectrometry. *J Lipid Res* **2008,** 49, (5), 1113-25.
228. Magnes, C.; Sinner, F. M.; Regittnig, W.; Pieber, T. R., LC/MS/MS method for quantitative determination of long-chain fatty acyl-CoAs. *Anal Chem* **2005,** 77, (9), 2889-94.
229. Zhou, M.; Diwu, Z.; Panchuk-Voloshina, N.; Haugland, R. P., A stable nonfluorescent derivative of resorufin for the fluorometric determination of trace hydrogen peroxide: applications in detecting the activity of phagocyte NADPH oxidase and other oxidases. *Anal Biochem* **1997,** 253, (2), 162-8.
230. Taatjes, D. J.; Gaudiano, G.; Resing, K.; Koch, T. H., Redox pathway leading to the alkylation of DNA by the anthracycline, antitumor drugs adriamycin and daunomycin. *J Med Chem* **1997,** 40, (8), 1276-86.
231. Cartoni, A.; Menna, P.; Salvatorelli, E.; Braghiroli, D.; Giampietro, R.; Animati, F.; Urbani, A.; Del Boccio, P.; Minotti, G., Oxidative degradation of cardiotoxic anticancer anthracyclines to phthalic acids. Novel function or ferrylmyoglobin. *J Biol Chem* **2004,** 279, (7), 5088-99.
232. Mueller, S., Sensitive and nonenzymatic measurement of hydrogen peroxide in biological systems. *Free Radic Biol Med* **2000,** 29, (5), 410-5.
233. Boardman, A. K.; McQuaide, S. C.; Zhu, C.; Whitmore, C. D.; Lidstrom, M. E.; Dovichi, N. J., Interface of an array of five capillaries with an array of one-nanoliter wells for high-resolution electrophoretic analysis as an approach to high-throughput chemical cytometry. *Anal Chem* **2008,** 80, (19), 7631-4.

234. Namur, J.; Wassef, M.; Millot, J. M.; Lewis, A. L.; Manfait, M.; Laurent, A., Drug-eluting beads for liver embolization: concentration of doxorubicin in tissue and in beads in a pig model. *J Vasc Interv Radiol* **2010,** 21, (2), 259-67.
235. Gerber, M. A.; Thung, S. N., Enzyme patterns in human hepatocellular carcinoma. *Am J Pathol* **1980,** 98, (2), 395-400.
236. Ismail, E.; Al-Mulla, F.; Tsuchida, S.; Suto, K.; Motley, P.; Harrison, P. R.; Birnie, G. D., Carbonyl reductase: a novel metastasis-modulating function. *Cancer Res* **2000,** 60, (5), 1173-6.
237. Pearce, R. E.; McIntyre, C. J.; Madan, A.; Sanzgiri, U.; Draper, A. J.; Bullock, P. L.; Cook, D. C.; Burton, L. A.; Latham, J.; Nevins, C.; Parkinson, A., Effects of freezing, thawing, and storing human liver microsomes on cytochrome P450 activity. *Arch Biochem Biophys* **1996,** 331, (2), 145-69.
238. Chen, H. W.; Medley, C. D.; Sefah, K.; Shangguan, D.; Tang, Z.; Meng, L.; Smith, J. E.; Tan, W., Molecular recognition of small-cell lung cancer cells using aptamers. *ChemMedChem* **2008,** 3, (6), 991-1001.
239. Wang, Y.; Chen, T.; Han, C.; He, D.; Liu, H.; An, H.; Cai, Z.; Cao, X., Lysosome-associated small Rab GTPase Rab7b negatively regulates TLR4 signaling in macrophages by promoting lysosomal degradation of TLR4. *Blood* **2007,** 110, (3), 962-71.
240. Whiting, C. E.; Dua, R. A.; Duffy, C. F.; Arriaga, E. A., Determining under- and oversampling of individual particle distributions in microfluidic electrophoresis with orthogonal laser-induced fluorescence detection. *Electrophoresis* **2008,** 29, (7), 1431-40.
241. Takada, Y.; Sakairi, M.; Koizumi, H., Online Combination of Micellar Electrokinetic Chromatography and Mass-Spectrometry Using an Electrospray Chemical-Ionization Interface. *Rapid Communications in Mass Spectrometry* **1995,** 9, (6), 488-490.
242. Lamoree, M. H.; Tjaden, U. R.; van der Greef, J., On-line coupling of micellar electrokinetic chromatography to electrospray mass spectrometry. *J Chromatogr A* **1995,** 712, (1), 219-25.
243. Luedtke, S.; Unger, K. K., Capillary electrochromatography - Challenges and opportunities for coupling with mass spectrometry. *Chimia* **1999,** 53, (10), 498-500.
244. Solomon, B.; Soulen, M. C.; Baum, R. A.; Haskal, Z. J.; Shlansky-Goldberg, R. D.; Cope, C., Chemoembolization of hepatocellular carcinoma with cisplatin, doxorubicin, mitomycin-C, ethiodol, and polyvinyl alcohol: prospective evaluation of response and survival in a U.S. population. *J Vasc Interv Radiol* **1999,** 10, (6), 793-8.
245. Murren, J. R.; Durivage, H. J.; Rosenberg, A. H.; Chen, Y.; Del Prete, S. A.; Murphy, G. J.; Buzaid, A. C.; Hait, W. N., Cisplatin, doxorubicin, mitomycin C, and 5-fluorouracil for the treatment of metastatic non-small cell lung cancer. Limited activity of an aggressive chemotherapy regimen. *Am J Clin Oncol* **1994,** 17, (3), 239-41.

Appendix A

Supplementary Material to Chapter 3

Direct Sampling from Human Liver Tissue Cross-sections for Electrophoretic Analysis of Doxorubicin

A1. Elastic moduli of gelatin tissue-mimics

We measured the elastic moduli of solidified 10%, 15% and 20% (w/v) gelatin (Figure A-1 and Table A-1). The elastic modulus of 10% gelatin and hepatocellular carcinoma (HCC) tissue were similar. Therefore, we used the 10% gelatin tissue mimic to investigate sampling reproducibility.

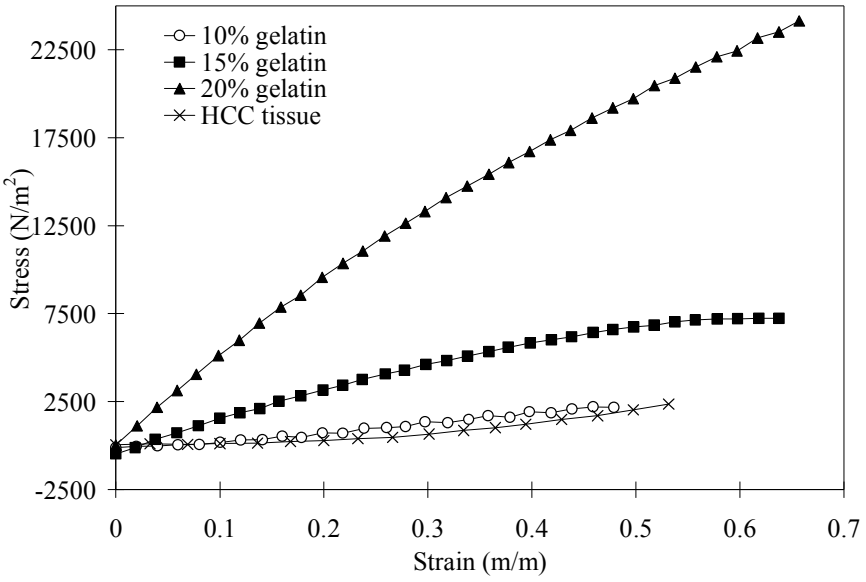

Figure A-1. Representative stress vs. strain plot of a 10% (-o-), 15% (-■-) or 20% (-▲-) gelatin and HCC tissue (-×-). Elastic modulus (*E*) was calculated from the slopes of the stress-strain plots.

Table A-1. Elastic moduli of gelatin tissue-mimics and HCC tissue. SD: standard deviation.

Sample	E (kPa) (average ± SD)	
10% gelatin	7.5±2.3	(n=7)
15% gelatin	14.2±2.1	(n=7)
20% gelatin	38.5±8.8	(n=5)
HCC tissue	6.8±1.5	(n=5)

A2. Fluorescence imaging of tissue cross-sections

Liver tissues from an untreated patients (Figure A-2A) display endogenous fluorescence, both green (Figure A-2Ai) and red (Figure A-2Aii). The red endogenous fluorescence especially interferes with the determination of DOX as the excitation and detection conditions are those used to image DOX localization (Figure A-2Bii). Thus, fluorescence microscopy cannot be used to locate and quantify DOX in tissue cross-sections. A method that incorporates both localization and separation, i.e., direct tissue sampling coupled with MEKC-LIF is necessary to determine the distribution of DOX in tissue cross-sections.

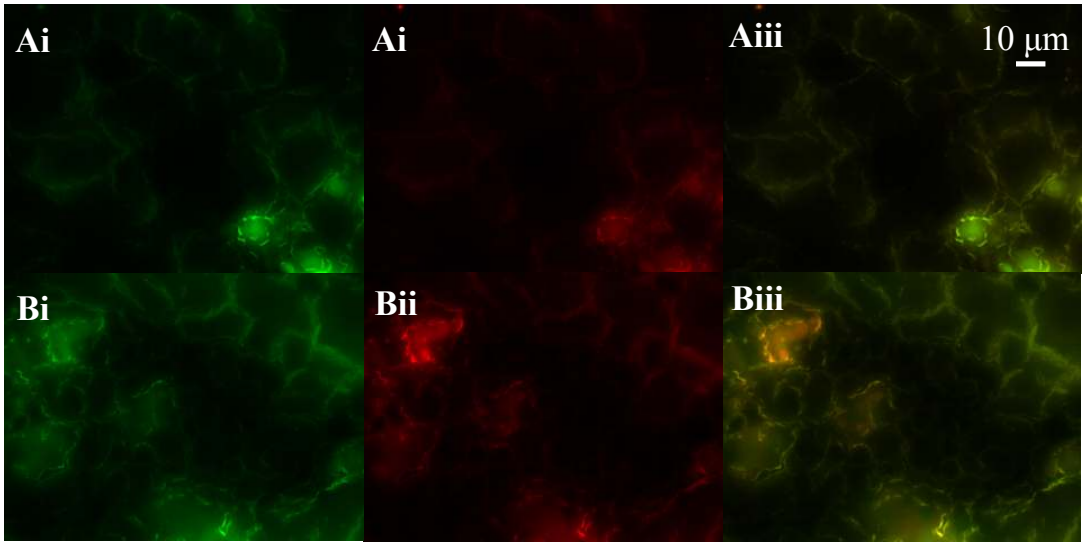

Figure A-2. Epifluorescence images of a non-chemoembolized and a chemoembolized tissue cross-sections. A and B are liver tissue cross-sections of patients without and with DOX (chemoembolization treatment), respectively. The images of the tissue cross-sections were taken with an Olympus IX-81 inverted fluorescence microscope (Olympus America Inc., Melville, NY) equipped with a 40× objective and FITC (excitation. 460-500 nm, 505 nm dichroic, emission. 510-560 nm) (Ai and Bi) and TRITC (excitation. 510-560 nm, 565 nm dichroic, emission. 570-650 nm) (Aii and Bii) filter cubes at 10 s exposure. Aiii and Biii are the overlays of Ai-Aii and Bi-Bii, respectively.

A3. MEKC-LIF analysis of tissue extract of a liver without chemoembolization

We optimized the MEKC separation conditions so that the endogenous fluorescent compounds in the liver (Figure A-3, Trace a) were resolved from DOX, as shown in the same preparation after spiking it with DOX standard. (Figure A-3, Trace b)

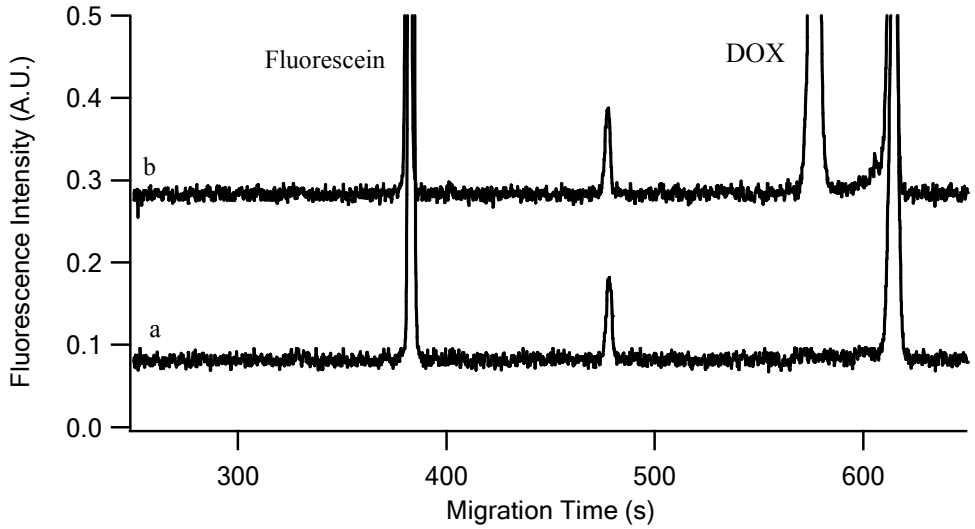

Figure A-3. MEKC separation of tissue extract without chemoembolization treatment. Trace a: tissue extract only. Trace b: tissue extract spiked with DOX. The y axis of trace b was offset 0.2 A.U. for clarity. The experimental conditions were same as Figure 3-6, except for the use of a 46.0-cm long capillary in the separation.

A4. Mobility corrections

We used Equation 3-4 to correct the migration times of the DOX peaks detected in samples taken from tissue cross-sections. The electrophoretic mobilities were then calculated using Equation 3-5. A comparison of the mobilities without and with correction for peaks detected in Figure A-4 is shown in Table A-2. The mobility reproducibility improved after correction. A Student's t test indicate that peaks detected in the analysis of tissue of chemoembolized livers are DOX peaks ($p = 0.82$ at 98% confidence level).

Table A-2. Comparison of calculated mobilities with and without correction.

	Without correction ($\times 10^{-4}$ cm^2/V·s)	With correction ($\times 10^{-4}$ cm^2/V·s)
Spot 1	2.106	2.143
Spot 2	2.089	2.157
Spot 3	2.144	2.150
Average ± SD	2.11±0.03	2.15±0.01
DOX standard (n=3)	2.16±0.03	2.15±0.01

Sampling was directly done from a 5-μm thick liver tissue cross-section at three separate spots. Mobility was corrected according to Equations 3-4 and 3-5

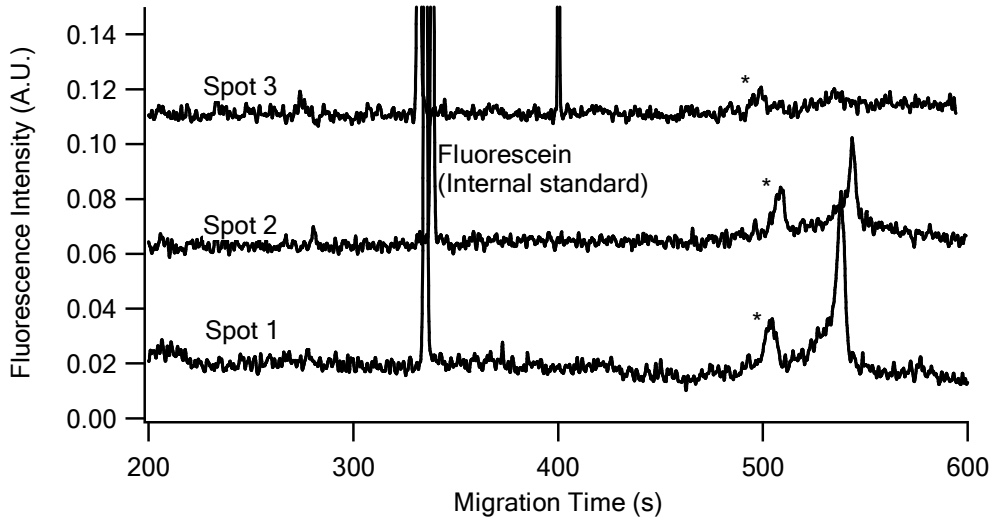

Figure A-4. MEKC separation of three samples taken from different spots in a 5 μm-thick tissue cross-section. Peaks marked with "*" are identified as DOX after carrying out mobility corrections (c.f. Equations 4 and 5). The y axes of electropherograms of regions 2 and 3 are offset for clarity. Experimental conditions were the same as in Figure 3-6 except for using a 42.5-cm long capillary.

A5. Hematoxylin and eosin (H&E) staining

H&E staining was done to confirm the identity of the morphological features of tumor and non-tumor regions. Procedure: (i) The tissue cross-section was washed in water (10 dips). (ii) Then, it was stained with hemotoxylin solution (Mayer's, Sigma-Aldrich, St. Louis, MO, USA) for 60 s. (iii) The stained tissue was again washed in water (10 dips). (iv) Hemotoxylin was then blued with 0.2% (v/v) NH_3-water (10 dips). (v) Then, the tissue

was stained by 1% (w/v) eosin (Sigma-Aldrich, St. Louis, MO, USA) solution for 10 min. (vi) After that, the tissue cross-section was dehydrated in subsequent treatments with 80% ethanol (10 dips), 95% ethanol (10 dips) and two changes (10 dips each) of 100% ethanol. (vii) Finally, it was cleared in two changes (10 dips each) of xylene (Mallinckrodt, Phillipsburg, NJ, USA) and mounted with Permount mounting media (Fisher Scientific, Fair Lawn, NJ, USA).

Images were taken on a Zeiss Axiovert 2 Upright Microscope (Carl Zeiss MicroImaging Inc., Thornwood, NY, US). The H&E staining of the non-tumor part showed fibrous septae and regenerative modules which are commonly seen in cirrhosis (Figure A-5, Part A). The tumor part showed extensively necrosis due to DOX treatment (Figure A-5, Part B).

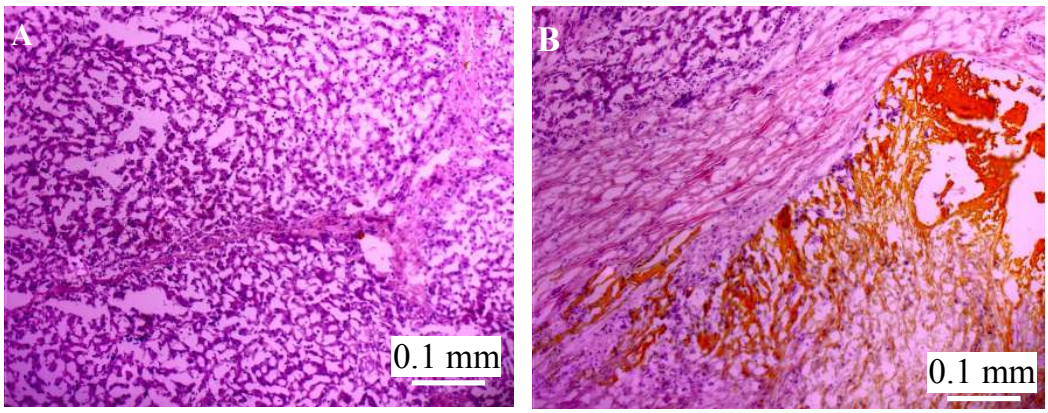

Figure A-5. Bright field images of H&E staining of liver tissue cross-sections. (A) Non-tumor region and (B) Tumor region.

Appendix B

Supplementary Material to Chapter 4

Monitoring Incorporation, Transformation and Subcellular Distribution of *N*-$_L$-leucyl-doxorubicin in Uterine Sarcoma Cells Using Capillary Electrophoretic Techniques

B1. Synthesis of *N*-L-leucyl-doxorubicin

N-hydroxysuccinimide, *N*-trityl leucine, *N*-hydrosuccinimide and trityl chloride were from Sigma Aldrich (St. Louis, MO, USA). Ethyl ether, petroleum ether, acetic acid and acetonitrile were from Mallinckrodt (Phillipsburg, NJ, USA).

LeuDOX was synthesized by coupling the *N*-hydroxysuccinimide ester of *N*-trityl leucine (Trt-Leu-Osu) with DOX. First *N*-trityl-leucine (Trt-Leu-OH), the derivative of L-leucine was obtained by coupling L-leucine with trityl chloride at room temperature for 24 h. Then Trt-Leu-Osu was derived from Trt-Leu-OH by reacting Trt-Leu-OH with *N*-hydrosuccinimide at 4°C for 24 h. The product was purified using home-made silica gel column and eluted with 30% ethyl ether and 70% petroleum ether (v/v). LeuDOX was obtained by coupling Trt-Leu-Osu with DOX in dark at room temperature for 24 h. The protection trityl group was removed by reacting in 75% acetic acid and 25% water (v/v) for 1 h. This synthesis procedure has a 33% yield of LeuDOX. The product was purified by HPLC using C18 column (VyDAC, 5 μm, 4.6 mm I.D., 250 mm length, Hesperia, CA, USA) with 0 to 100% gradient of acetonitrile in 100 min. The purified LeuDOX was examined by HPLC and electrosrpay ionization mass spectrometer (ESI-MS) (Bruker BioTOF II, Bruker Daltonics, Billerica, MA, USA), and determined that the purity is 98.4% (Figure B-1A) and molecular weight equals to 656.4 (Figure -1B).

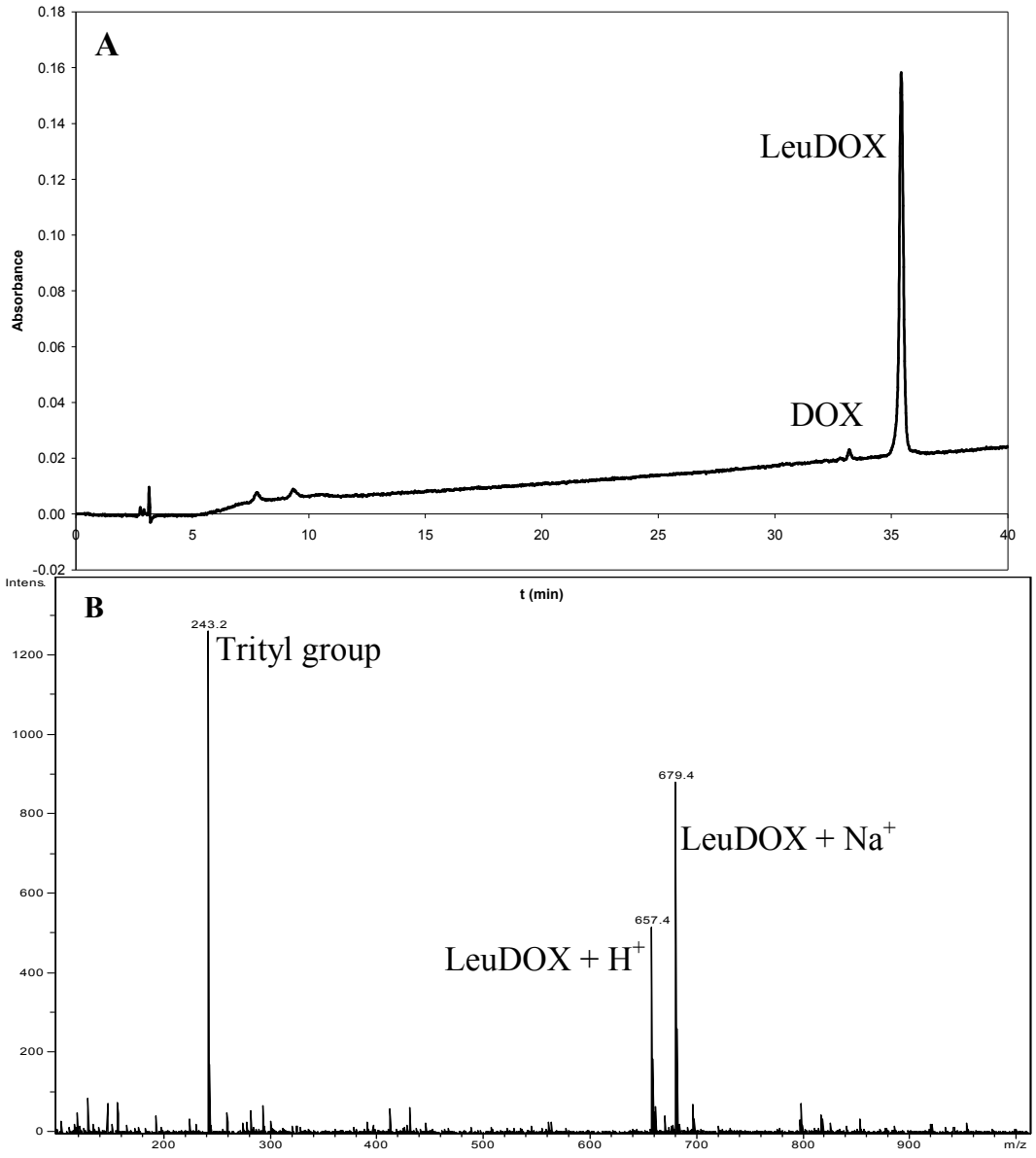

Figure B-1. Chromatogram and mass spectrum of LeuDOX. HPLC was performed using 0.1% trifluoroacetic acid (TFA) in water as solvent A and 0.1% TFA in acetonitrile as solvent B. Gradient: 0-40% of B in 40 min; Detection: 220 nm. Mass spectrum was obtained using a Bruker BioTOF II instrument using positive ion mode. The sample was dissolved in methanol and directly injected into the ionization source using a syringe.

B2. Viability of cells after DOX and LeuDOX treatments

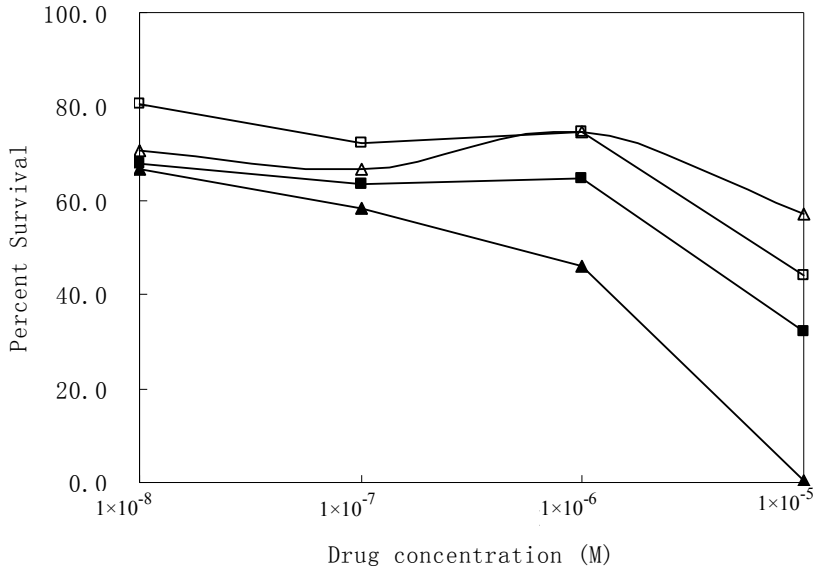

Figure B-2. Percent survival – drug concentration curve. DOX treated MES-SA cells (–▲–), LeuDOX treated MES-SA cells (–■–), DOX treated MES-SA /Dx5 cells (–△–) and LeuDOX treated MES-SA cells (–□–). Survival was determined by the MTT assay.

B3. Fluorescence spectra of DOX in borate-SDS and CTAB-tricine buffer

Emission spectra of 10^{-6} M DOX in 10 mM borate, 10 mM SDS buffer (pH = 9.3) and 4 mM CTAB-50 mM tricine buffer (pH = 8.5) were obtained with a FP-6200 spectro-fluorometer (Jasco, Tokyo, Japan). The sample was placed in a 1-cm path length polystyrene cuvette and excited at 488 nm.

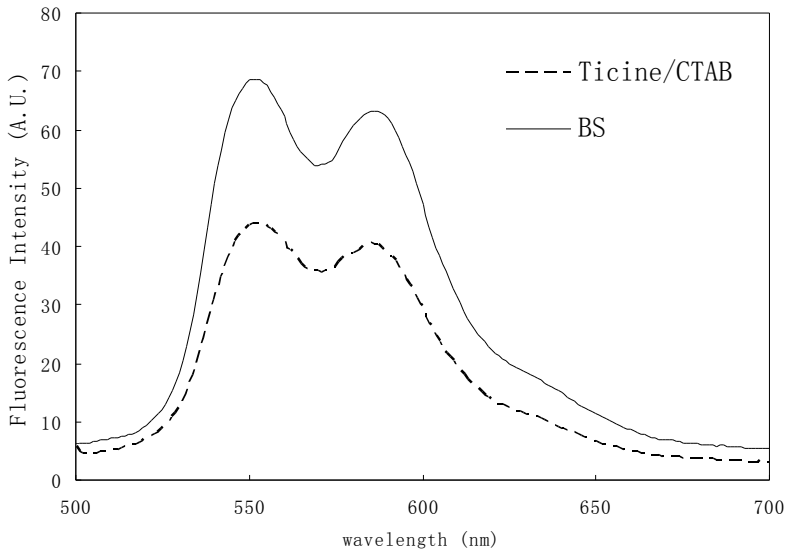

Figure B-3. Emission spectra of 1×10^{-6} M DOX. DOX was dissolved in 10 mM borate, 10 mM SDS buffer (——) or 50 mM tricine, 4 mM CTAB buffer (----). Spectra were obtained using 488 nm excitation.

B4. LeuDOX transformation in cell culture medium

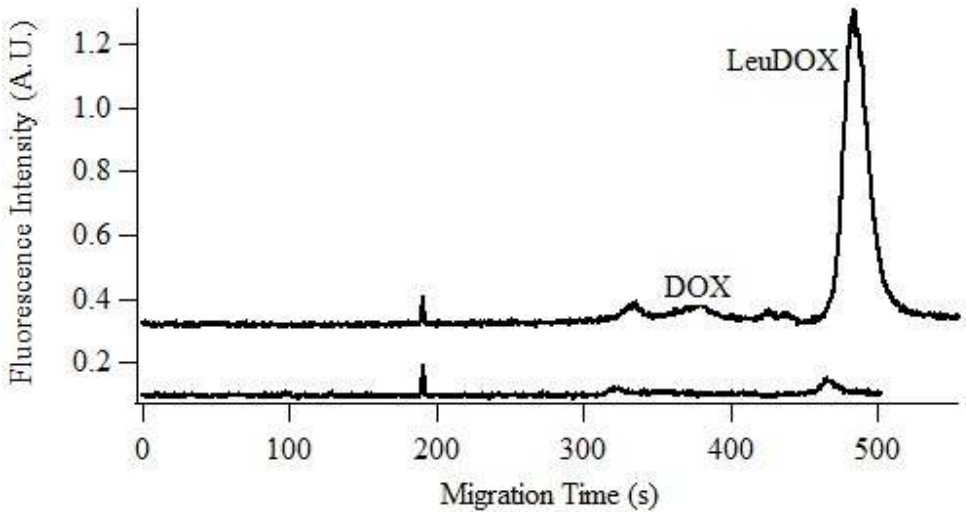

Figure B-4. Electropherogram of LeuDOX incubated in cell culture medium. Both cell culture medium (trace i) and medium with 10 μM LeuDOX (trace ii) were diluted 10 times with separation buffer before injection to capillary. Separation and detection conditions were same as in Figure 4-2. Fluorescence intensity of trace B was offset by 0.2 A.U. for clarify.

Appendix C

Supplementary Material to Chapter 5

Micellar Electrokinetic Chromatography Monitors Doxorubicin Metabolism in Subcellular Fractions of Young Adult and Old Fischer 344 Rat Livers

This unpublished work has been submitted to *Journal of Gerontology Series A: Biological Sciences*

HPLC-LIF-MS work was done by Joseph B. Katzenmeyer. The material is included with permission.

C1. Florescence spectrum of DOX and metabolites in BS50-γCD20 buffer

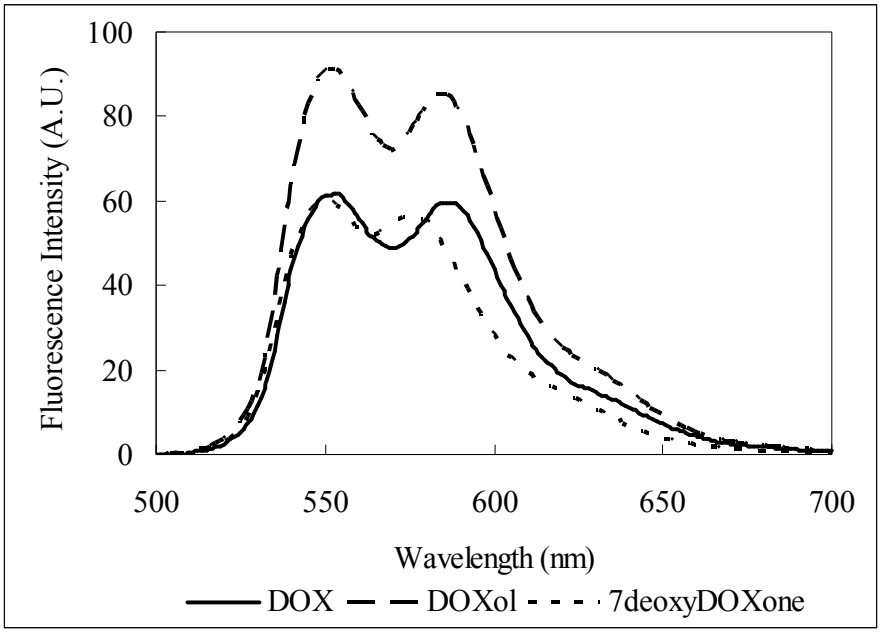

Figure C-1. Fluorescence spectra of DOX, DOXol and 7-deoxyDOXone. All samples were prepared in 50 mM borate, 50 mM SDS and 20 mM γ-cyclodextrin buffer to a final concentration of 5 μM. Excitation: 488 nm.

C2. Mobility correction and comparison

The electrophoretic mobility (μ_X) of DOX or metabolites was calculated by

$$\mu_X = \frac{L^2}{E \times t_m} \qquad \text{(Equation C-1)}$$

where L is the length of the capillary, E is the separation voltage and t_m is the migration time. The correction was done based on the peak of DOX and the corrected mobility ($\mu_{x,corrected}$) of a metabolite in a specific run was calculated as

$$\mu_{X,corrected} = \mu_X \times \frac{\mu_{Dox\ average}}{\mu_{Dox}} \qquad \text{(Equation C-2)}$$

where μ_{DOX} is the mobility of DOX in that run and $\mu_{DOX\,average}$ is the average mobility of

DOX in all runs. The corrected mobility of each metabolite was compared to that of DOXol and DOXone standards using Student's t-test for metabolite identification (Table S1). The null hypothesis "there is no significant difference in the mobility of metabolite X and that of the standard" was rejected when the p-value (p) <0.05 (95% confidence level).

Table C-1. Corrected mobilities and p-values of metabolites and standards

	Mobility[a]	M1	M2	M3
Mobility*	-	2.451±0.006	2.588±0.003	2.699±0.003
DOXol 1	2.487 ±0.005	1.1×10^{-3}	2.1×10^{-5}	3.4×10^{-6}
DOXol 2	2.427±0.004	4.8×10^{-3}	1.9×10^{-6}	6.2×10^{-7}
DOXone	2.61±0.03	7.9×10^{-3}	**0.29**[b]	0.030

a. Mobility corrected by Equation C-2. Variation is represented in standard deviation. Values are given as $\times10^{-4}$ $cm^2/(V\cdot s)$
b. Student's t-test showed no significant difference in the corrected mobility of M2 and DOXone. ($p > 0.05$)

C3. HPLC-LIF-MS analysis of *in vitro* DOX metabolism in PMF of rat livers

This work was done by Joseph B. Katzenmeyer.

PMF of young and old rat livers were used for the HPLC-LIF-MS experiments. For *in vitro* metabolism, DOX (50 μM) and NADPH generating system including $MgCl_2$ (5 mM), $NADP^+$ (0.25 mM), glucose-6-phosphate (2.5 mM) were added. The start of the reaction time was defined as the moment in which glucose-6-phosphate dehydrogenase (2.0 units) was added to the reaction mixture. The reaction mixture (final volume of 1.1 mL) was incubated at 37º C in a heated mixer and samples were removed at 10, 20, 30, and 40 min for analysis. DOX and metabolites were extracted use liquid-liquid extraction. The extraction solvent was prepared by mixing 14 μL of concentrated perchloric acid with 60 μL of HPLC mobile phase (67% water: 33% acetonitrile) in a 600 μL microcentrifuge tube. At a given reaction time, 40 μL of the reaction mixture were

removed and pipetted into the extraction mixture. The tube was vortexed for 30 seconds and the centrifuged at 3000×g for 3 minutes. The supernatant was used directly for analysis. An Agilent (Santa Clara, CA) 1100 capillary HPLC system was used in this analysis. A sample volume of 0.5 μL was injected into the HPLC apparatus and separated on a C18 column (0.3 x 150 mm, 3 μm particles, ACE11115003, Mac-Mod Analytical, Inc., Chadds Ford, PA). The mobile phase consisted of 67% water (0.1% formic acid) and 33% acetonitrile. The flow rate was set at 3.5 μL/min. For LIF detection, a 473 nm diode-pumped solid state laser (OnPoint Lasers, LTD, Eden Prairie, MN) was used for excitation. The HPLC column was connected to the electrospray ionization chamber of the mass spectrometer using 30 cm of 50 μm I.D. fused silica capillary. Dead volume was avoided by using Teflon sleeves (Upchurch, F-242X) to adapt the outer diameter of the capillary to fit standard size PEEK finger-tight fittings. An approximately 5 mm section of the polyimide coating of the fused-silica capillary was burned off creating a detection window. A fluorescence flow-through cell (SpectrAlliance, Inc., St Louis, MO) equipped with fiber optics to deliver incident light and collect fluorescent light was used as an on-column detector. The collected fluorescence was filtered with a 580BP45 filter (Omega Optics) and monitored using a photomultiplier tube (Hamamatsu, biased at 800 V). Data from the photomultiplier tube was digitized (10 Hz) using a National Instruments I/O board (PCI-6034E) run with a LabVIEW 5.1.1 (National Instruments, Austin, TX) program created in house. Using standards of DOX, the alignment of the fluorescence detection window was properly placed in the detection zone of the flow-through device to achieve the maximum signal. A 10 μM solution of doxorubicin in methanol was passed through the capillary using a syringe adapter and a 100 μL syringe

operated by a syringe pump at a flow rate of 3.5 μL/min. The capillary was secured with the nut on the flow-through device.

Mass spectral data were collected using a Bruker MicrOTOF$_Q$ mass spectrometer (Bruker Daltonics Inc., Billerica, MA) capable of high accuracy MS and MS/MS data collection (10,000 to 15,000 mass resolution for m/z 350-800). Helium was used as the collision gas because DOX was found to fragment extensively when using Argon. Positive ions were detected. The parameters (funnel 1 and 2 RF, hexapole RF and collision RF) were adjusted to achieve a maximum detection of DOX and metabolites.

Figure C-2 shows the MS chromatograms of DOX and metabolites after incubating 50 μM DOX with PMF of a rat liver for 10 min. 7-deoxyDOXone and 7-deoxyDOXolone metabolites from enzymatic reactions, while DOXone may form as a result of acid catalyzed cleavage of the daunosamine sugar during the sample extraction with perchloric acid. In fact, a control using only a doxorubicin standard in incubation buffer followed by perchloric acid extraction also resulted in DOXone detection.

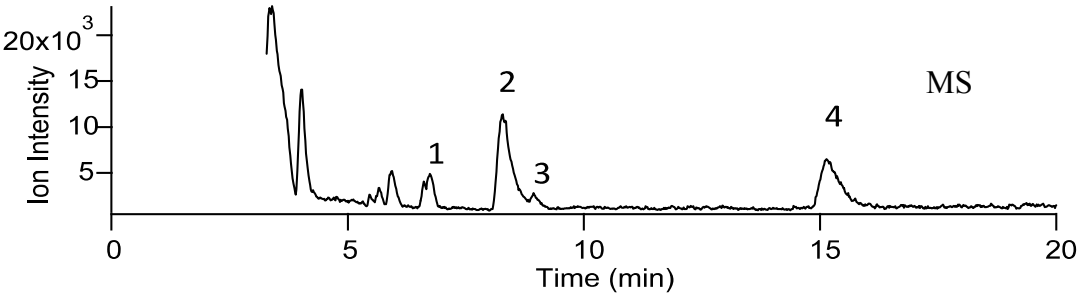

Figure C-2. Mass chromatogram of a liver PMF treated with doxorubicin. The PMF was treated with 50 μM doxorubicin, extracted after 10 min. A volume of 0.5 μL were was injected into the HPLC system. Separation proceeded was conducted in a 150×0.3 mm C18 column (ACE11115003, Mac-Mod) under isocratic conditions (67% water, 0.1% formic acid: 33% acetonitrile). The ESI-MS was done by Bruker MicrOTOFQ mass spectrometer. Peak 1: DOX, 2: 7-deoxyDOXolone, 3: Doxone, 4: 7-deoxyDOXone.

Figure C-3 is a representative figure of the change in mole fraction of DOX, 7-deoxyDOXone and 7-deoxyDOXolone during 40 min incubation in the PMF of a young rat liver.

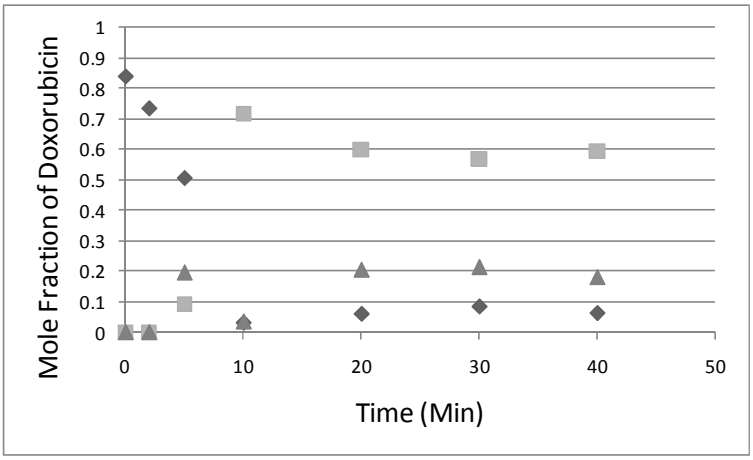

Figure C-3. DOX biotransformation dynamics in PMF of a young rat liver. Diamonds represent DOX (peak 1 in Figure C-2); squares represent 7-deoxyDOXolone (peak 2 in Figure C-2); and triangles represent 7-deoxyDOXone (peak 4 in Figure C-2).

C4. Percent of metabolites and DOX change over time

Table C-2. Percent of metabolites and DOX in PMF or MF at different incubation times[a]

Peak[b]	Fraction	15 min		30 min		60 min		120 min	
		Young	Old	Young	Old	Young	Old	Young	Old
DOX	PMF	45.9±0.1	90.5±0.4	3.2±0.1	68.1±0.7	3.9±0.2	54±3	3.9±0.5	47±2
	MF	86±2	100	81.0±0.6	94.7±0.5	77.2±0.4	92.3±0.6	72.5±0.7	93.2±0.8
7-deoxyDOXone	PMF	4.8±0.9	2.7±0.5	-[c]	2.3±0.2	-	2.3±0.2	-	3.2±0.9
	MF	5.0±0.7	-	4.8±0.2	3.5±0.4	6.0±0.7	3.2±0.8	6±1	2.1±0.4
7-deoxyDOXolone	PMF	49.3±0.8	6.7±0.2	87±2	29.6±0.9	71.4±0.3	44±3	66.2±0.7	50±1
	MF	7.3±0.9	-	11.4±0.5	1.8±0.2	13.3±0.6	4.5±0.2	17.4±0.3	4.7±0.4
M3	PMF	-	-	3.8±0.9	-	10.8±0.5	-	16.8±0.5	-
	MF	2.1±0.3	-	2.8±0.2	-	3.5±0.4	-	4.6±0.8	-
M4	PMF	-	-	6±1	-	14.0±0.3	-	13.1±0.5	-
	MF	-	-	-	-	-	-	-	-

a. Data correspond to the average of triplicate injections. Variation is represented in standard deviation (n = 3).
b. Percent of DOX or metabolite were calculated according to Equation 5-2
c. -: metabolite is not detected

Appendix D

Supplementary Material to Chapter 6

Biotransformation of Doxorubicin in Immunoisolated Peroxisomes

D1. Metabolism of B_{12}FA in cultured L6 myoblasts

L6 myoblasts were cultured with 5 μM B_{12}FA for different lengths of times (30 min, 2 h, 4 h and 6 h). After treatments, cell culture medium was removed and the cells were washed three times with 1×PBS. The cells were then lyzed in 10 mM borate and 10 mM SDS buffer (pH = 9.3) to a cell density of 2×10^6 cells/ml. The cell lysates were kept at -80 ºC until MEKC analysis.

The MEKC-LIF were performed in 30 mM borate, 30 mM SDS and 5 mM γ-cyclodextrin buffer (pH = 9.3) as described in Section 6.2.6. Figure D-1 shows the electropherograms of L6 cells after incubated with B_{12}FA for different lengths of times. Multiple peaks were observed after the B_{12}FA peak. These peaks have lower mobilities than B_{12}FA, which indicates that they are more hydrophobic. Based on the hydrophobicity, these peaks could be the triacylglycerol form of B_{12}FA. The intensities of these peaks increase with time because more B_{12}FA were taken up by the cells with longer incubation time.

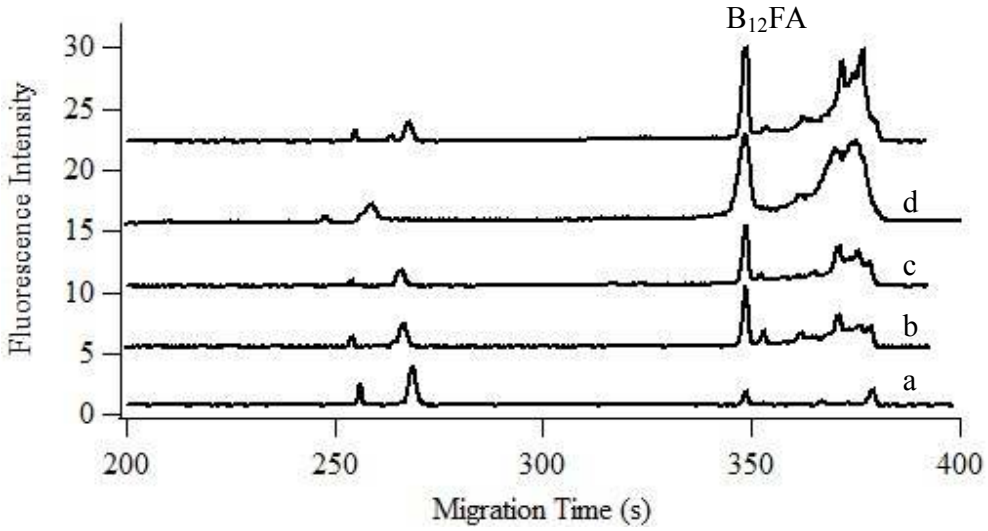

Figure D-1. Electropherograms of L6 cells incubated with $B_{12}FA$ for different lengths of times. The MEKC were performed in a 45.5 cm fused silica capillary. Trace a is L6 cell lysate alone, and trace b-e are L6 cells incubated with $B_{12}FA$ (5 μM) for 30 min, 2h, 4h and 6 h, respectively. The peaks after $B_{12}FA$ can be the triacylglycerol of $B_{12}FA$. Trace b to e were y-axis offset for clarity. Other conditions were the same as those described in Figure 6-3.